Memòria presentada per aspirar al Grau de Doctor per

Juan Manuel Ortiz Sánchez

Vist i plau,

Dr. Miquel Moreno Ferrer   Dr. Ricard Gelabert Peiri

Bellaterra, 30/09/09

Universitat Autònoma de Barcelona

Tesi doctoral

Excited state intramolecular proton transfer reactions
coupled with non adiabatic processes: electronic
structure and quantum dynamical approaches

Juan Manuel Ortiz Sánchez

Directors: Miquel Moreno Ferrer i Ricard Gelabert Peiri

Programa de doctorat: Química Teòrica i Computacional

Departament de Química, Facultat de Ciències

Universitat Autònoma de Barcelona

2009

A mi familia,
sin la que nada ni nadie sería.

Acknowledgements

The first person I should thank, in a chronological order, is my uncle Sebastián. He had also studied Chemistry at the *Universitat Autònoma de Barcelona*, and right before I began my studies, he took me for a tour to our faculty. After a while, he told me he wanted to greet his former Ph. D. advisor, Prof. J. M. Lluch; and that is how I met the Physical Chemistry deparment. At J. M. Lluch's office, he said "Well Sebas, what have we got here? A new recruit!" "Oh no"–Sebas replied–"I think he is most interested in Biochemistry." "It's OK Sebas, it's OK."–Josep Maria said–"You brought him here. Let us make the rest." Thanks Sebas for that tour!

I did not know then, that I would later meet such nice people in the "Chemical and biochemical reactions dynamics and mechanisms" research group. From the senior staff, I will always appreciate the help and kindness (and the delight to have attented some of their lessons) that Josep Maria, Àngels, Mireia and Laura have showed to me. I reserve a special gratitude to my advisors, Miquel and Ricard, because they have always been there anytime I needed them (even those days I turned up by their offices four or five times within half an hour!). Last but not least, because after these four years of working together, I know I can consider them (with no fear) friends of mine, besides as my advisors.

During this time, there have been different partners at the office. Some of them are still there, some others left to continue with their careers. I am very grateful to the absent ones, because even from far away they offered

me their support: many thanks Núria and Oriol! However, I am even more grateful with my present partners; for the great time spent together (I will never forget those Mario Kart championships!), but also for periods of time with bad temper they had to endure during the writing of this thesis. So Edgar, Edu, Juanma, Lea, Manuel. . . there are not enough thanks for you!

I shouldn't forget everyone else at the Physical Chemistry Unit, seniors and Ph. D. students. All the time we have spent together was worthwhile: attendance at lessons, conversations at the corridors, technical support, lunchs at the canteen, casual football matches. . . You probably did not realize it then, but any comment from you that contribute to improve my work here (teaching and research) or even this thesis, was always taken into account. I do not dare to name you all, because I do not want to miss any of you. You know who you are, and for you I can only say: many and many thanks! However, I must give a special thank to Carles, who helped me a lot during the post-production stages of this thesis.

By attending these Ph. D. studies, I have been able to meet a lot of people at the Theoretical and Computational Chemistry courses. I am very lucky to still keep in touch with some of them. Your support, but specially your friendship, also helped me to go on. Thank you very much to all of you for being there!

A very special and warmful thank to Lady L. Many and many thanks to make those weekends at the office more bearable.

And last, but not least, thanks to my family. Anything I could say would not do justice to what they represent to me.

Preface

What is this about? Chemistry? Physics? Computer sciences. . . ?

It was February 2000 when I first heard about physical chemistry. It was my first year as a chemistry undergraduate student at the *Universitat Autònoma de Barcelona*, and I remember I felt a little bit shocked. The only physics I knew at that time were the classical Newtonian laws of motion, the energy conservation principle. . . and all those basics we learn at high school. I could not manage to imagine how that physics could fit with atoms and molecules. My first physical chemistry lessons dealt with thermodynamics, but those lessons did not solve my incompatibility problem between physics and chemistry. However, I realized for the first time that chemistry was beyond the experimental and empirical study, and it could be beautifully described with the language of mathematics. Later on, I would attend lessons like chemical kinetics, spectroscopy, quantum chemistry, statistical thermodynamics and chemical dynamics; which showed me that the boundaries between physics and chemistry were so thin that it was impossible (at least for me) to figure out when one finished and the other started.

Let me say it in this way: If I were a Medieval monk, I would have probably written this thesis with a quill and a pot of ink. People would see that ink as a liquid consisting of the mixture of various pigments, each one obtained from different natural sources, like beans or cuttlefish. It would

be clear to see chemistry in the composition of that ink. However, I am not a Medieval monk, and I typed the lines you are reading right now with my 21st century laptop. Is that chemistry too? Well, someone could say that I am able to type these lines because they are the result of a beam of electrons which refreshes my screen fifty times every second, and that could be seen as physics. But are not those electrons generated from the emission of a conglomerate of small liquid crystals inserted in a silicon matrix? That would be chemistry again. As I said, the boundaries are very thin.

Nevertheless, if somebody who still wanted to establish a clear division between physics and chemistry asked me today to place such a frontier, my answer would be Democritus. In the 4th century B.C., the Greek philosopher Democritus and his master Leucippus gave birth to a new way of understanding matter. Through exclusively philosophic thoughts, what Greeks called the Pure Reason, they described matter as being formed uniquely by invisible entities called $\alpha\tau o\mu o\zeta$ (atoms), which literally means "uncuttable". Nowadays a lot of scientists (not to say all of them) are very skeptical of this way of thinking, without any experimental contrast. However, we cannot deny that Democritus was extremely advanced for his time, because twenty-five centuries later our microscopic description of the physical sciences lies completely on the existence of these atoms. Today, we all know that Democritus' $\alpha\tau o\mu o\zeta$ is not the atoms we learned in our chemistry lessons (hydrogen, carbon, nitrogen, oxygen. . .). Thanks to J. J. Thompson and his cathode rays experiments, it is clear now that the atom is far from being uncuttable, being in fact the host of smaller entities. While physicists are still working to find the Democritus' $\alpha\tau o\mu o\zeta$, the very first brick of matter beyond the actual standard model of elementary particles, all the phenomena studied by chemists lie at the level of the chemical atom, and the major challenge of modern chemistry consists of understanding the interactions between the different chemical atoms.

As chemists, we must have always in mind that the chemical atom is an entity that does not follow the laws of classic mechanics, but behaves

according to quantum mechanics. Hence, in order to get a quantitative description of a chemical reaction at a molecular level, we need to apply the formulism of quantum mechanics to chemical systems, which brings us to physics again. Such interaction between physics and chemistry led to the discipline of quantum or theoretical chemistry in the early 1930s, after the contributions of important personalities such as Planck, Schrödinger, Heisenberg, Born, Dirac... Even though theoretical chemistry has experienced a fast growth with the continous development of algorithms and methodologies, the basics established at the begining are still completely valid nowadays, and the book by Linus Pauling and E. Bright Wilson "Introduction to Quantum Mechanics with applications to Chemistry", is a good example of that.

Despite the mathematical elegance of theoretical chemistry, its practical insertion within the scientific community did not arrive until the final years of the 1950s. The development of the first integrated circuit-based computers allowed to perform the complex mathematical operations that theoretical chemistry calculations demanded, within a reasonable time. At this point of my discourse, a new discipline has appeared: computer sciences. Indeed, the implementation of the mathematical description of chemistry on a computer experienced a very fast evolution, since the number of transistors that can be placed inexpensively on an integrated circuit increased exponentially, doubling approximately every two years, according to Moore's Law. The application of theoretical chemistry on computers rose as a new discipline: Computational chemistry. This evolution was so fast, that the first scientific journal devoted to this discipline, "The Journal of Computational Chemistry", was first published only thirty years later. As stated in the preface of the first volume of the Reviews in Computational Chemistry, "During the 1970s, widely different methods began to be seen as part of a new emerging discipline of computational chemistry".[1] Hence, theoretical chemistry may be defined as a mathematical description of chemistry, whereas computational chemistry can be regarded as the application of chemical, mathematical and computing skills to the solutions of chemical problems. However, despite of

the eficiency of computers, we should never forget that computers do not solve problems, only people do.

In conclusion, this thesis is about chemistry, but also about physics and computer sciences. . . and what's wrong with that? The more, the merrier!

Juan Manuel Ortiz Sánchez

Bellaterra, September 30, 2009

List of abbreviations

The following list contains the abbreviations most used through the present thesis, displayed in alphabetical order. The table also shows the number of the page where each abbreviation is first introduced.

BO	Born-Oppenheimer	17
BP(NH$_2$)$_2$	[2,2'-bipyridyl]-3,3'-diamine	18
BP(OH)$_2$	[2,2'-bipyridyl]-3,3'-diol	18
BP(OH)(NH$_2$)	[2,2'-bipyridyl]-3-amine-3'-ol	18
CASPT2	Complete Active Space Perturbation Theory up to 2nd order	39
CASSCF	Complete Active Space Self Consistent Field	39
CI	Conical Intersection	15
CIS	Configuration Interaction with Single excitations	38
DC	Derivative Coupling	46
DFT	Density Functional Theory	38
ESIDPT	Excited-State Intramolecular Double Proton Transfer	12
ESIPT	Excited-State Intramolecular Proton Transfer	11
FC	Franck-Condon	5
GD	Gradient Derivative	46
HAN	1-hydroxy-2-acetonaphthone	18
HF	Hartree-Fock	38
IC	Internal Conversion	5
MCTDH	Multi-Configuration Time-Dependent Hartree	50
MECP	Minimum Energy Crossing Point	86
PES	Potential Energy Surface	12
QY	Quantum Yield	14
SA	Salicylideneaniline	18
SMA	Salicylidene Methylamine	17
TDDFT	Time-Dependent Density Functional Theory	38
TDSCF	Time-Dependent Self-Consistent Field	52

Contents

1

General introduction

"A beginning is the time for taking the most delicate care that the balances are correct."

Frank Herbert, *Dune* (1965)

1.1 The chemical problem

Chemistry has always shown a compromise between the generation of new knowledge that allows us to understand the nature of our world, and the development of new materials and technologies that provide us with a higher quality of life. For many years, the most basic essence of chemistry involved only processes where the formation and dissociation of chemical bonds took place in the lowest electronic state (ground state). However, the study of chemical phenomena is not limited to this situation. Each atom and molecule presents different electronic states with different electronic distributions. In those electronic states, the chemical processes do not take place like in the ground state. In this sense, one of the most prolific and challenging natural phenomena (both in fundamental and applied research) which is observed in a wide spectrum of electronic states, is organic photochromism.

1.1.1 Organic photochromism

Words like photocopy or photograph are very popular among the general public, and people inmediately know what they refer to. However, many people are not aware of "photochromism" even though many of them wear "light adjusting" ophthalmic glasses, a very common object which darkens in the sunlight and bleaches in dim light, as shown in Figure 1.1.

We can trace the phenomenon of photochromism back to 1867,[2] when J. Fritzsche noticed that an orange-colored solution of tetracene became colorless in daylight, and recovered its original colour later at night. A very important feature of photochromism was then observed: reversibility. Since that early work, a similar behaviour has been observed in a huge variety of organic compounds, both in solution or in solid state.[3] The term photochromism, from the greek $\phi\omega\varsigma$ (light) and $\chi\rho\omega\mu\alpha$ (colour), was introduced from these observations to refer to any physical or chemical process where a reversible change of color is induced by light. The development of the field experienced an important expansion during the 1950–1960 period, along-

Figure 1.1: *A pair of ophthalmic glasses made with a photochromic organic compound. The darkest part of the lenses is directly exposed to an intense beam of light.*

side the development of physical molecular analysis methods (IR, NMR, X-ray, UV, time-resolved and flash spectroscopies), and organic synthesis studies. The works of Fischer and Hirshberg[4–9] (whom suggested the term photochromism) are considered as pioneering in the field. Along the years, the original definition of photochromism has been extended in order to include from colored compounds to any molecular system capable of absorbing electromagnetic radiation (deep UV to far IR). Nowadays, when we talk about photochromism, we refer to any physical or chemical process where a reversible change of color, and by extension, any other physical property, is induced by electromagnetic radiation.[2]

In the ground electronic state, a typical photochromic process is usually endoergic, and also presents a characteristic high energy barrier (~ 20 kcal mol^{-1}). These two factors prevent the reactants from evolving towards products. However, in the excited state the energetics of the reaction is reversed and becomes exoergic. Besides, the energy barrier decreases or even vanishes. In such conditions, the chemical reaction can take place very fast, sometimes within times in the order of 10^{-15} s. In general terms, the mechanism of a photochromic process starts with the photoexcitation of a thermodynam-
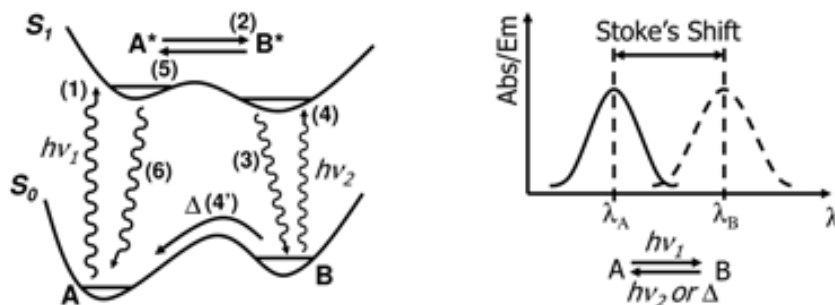
Figure 1.2: *Energy diagram of a simple unimolecular photochromic process between two singlet states (left), and a schematic representation of the corresponding absorption/emission spectrum (right). $h\nu_1$ and $h\nu_2$ refer to the energies that trigger the direct and reverse photochromic process, respectively; while Δ denotes the thermal transformation $B \rightarrow A$. The numbering of event follows the sequential order of the photochromic cyclic process. The solid line and the dashed line in the spectrum represent the absoption band of A (1) and the emission band of B^* (3), respectively.*

ically stable chemical species (let us call it A) from its ground electronic state, to an electronic excited state. According to the spin conservation rule, only those electronic transitions which keep the same spin multiplicity are allowed (besides, depending on molecular symmetry other additional transition rules might apply). Given that almost every organic compound is found a singlet state on its ground state (S_0), the electronic excited state also corresponds to a singlet state (S_n, $n > 0$). However, there exist few cases in which a molecule can undergo an internal conversion (IC) from a singlet excited state to a triplet state (T_n) before the photochromic reaction takes place.[10,11] From the Franck-Condon (FC) excitation point of this excited state, the A molecule evolves very fast to a second chemical species (we shall call it B) with very different physical and chemical properties in comparison with A. The transformation $A \rightarrow B$ usually takes place through one transition state (or even without energy barrier), but there are some cases where the process is not direct and proceeds through a metastable intermediate, like some dinaphthopyran derivatives.[12] The reverse reaction from B to A is also possible, and it can be thermally or photochemically induced. This general description of a photochromic process is summarized in Figure 1.2.

It is inferred from the figure that $h\nu_1 > h\nu_2$. Hence, the emission band of B corresponds to an electronic transition which is less energetic compared with the transition corresponding to the absorption band of A. Should the excited A especies not evolve towards a different chemical entity but only fluoresce to the ground state, the difference between the maxima of the absorption and emission bands (either in wavelength or frequency units), which is known as Stokes shift, is usually of the order of several hundreds of cm^{-1}. In contrast, in a photochromic process this difference is abnormally large (> 10000 cm^{-1}), due to the fact that the final photochromic especies (B) is no longer the same chemical entity originally photoexcited (A).

Even though this introductory explanation about the general mechanism of photochromism is limited to unimolecular reactions, there exist some cases in which the process is bimolecular, such as photocycloaddition reactions.[13]

1.1.2   Technological applications of photochromism

The excitation process of a photochromic molecule physically fixed at a specific position in a given material environment can be seen as a writing process. Analogously, the emission process of the "written" molecules can be seen as a reading process. Given the reversible nature of organic photochromism, this switch on–switch off sequence can be repeated many times due to the fact that photochromism is a nondestructive process.

One of the most fundamental problems of mankind, specially since human society reached its most complex stages of civilization, is the storage of the huge amount of information that is generated everyday. Organic photochromism presents a great technological potential to overcome that problem, which is the reason why organic photochromism lies in the spotlight of academic and technological development. However, it should not be forgotten that within a photochromic cycle side reactions can occur, which lead to the loss of perfomance over time due to chemical degradation (called fatigue). Usually, the major cause of damage to photochromic substances is oxidation.[14]

The possibility of using photochromic compounds for data storage was first suggested in 1956 by Yehuda Hirshberg.[8] Since then, a large number of works by both academic and commercial groups have been published on the subject. Of particular interest is the area of 3D optical data storage, where the surface of the disc comprises the usual two dimensions of storage, and the thickness of the disc represents the third dimension. This technology promises discs that can hold up to several terabytes (Tb) of data per disc. One of the most recent and promising photochromic compounds suggested to be used in 3D data storage is the fluorescent protein asFP595.[15]

In the academic field, the studies compiled in the relatively recent special issue devoted to Optical Memories and Switches, published on the journal *Chemical Reviews* in the year 2000,[16] should be mentioned as an ilustrative example of the the field's state of the art. In the bibliography of the last ten years in organic photochromism,the works of Masahiro Irie and collaborators, who developed one of the first families of photochromic materials (diarylethenes),[17–19] have to be highlighted. It is also worth mentioning the works of Seth Marder and collaborators, who performed the development of logical approaches to the molecular design of high 2-photon cross-section chromophores,[20–22] and Min Gu and Yoshimasa Kawata, who developed methods for the enhancement of the writing – reading process in data storage devices.[23, 24]

In addition to the academic research, several corporations like *Colossal Storage*[25] from the USA, or *Microholas*[26] from Berlin (just to mention two examples), have begun to commercialize 3D optical data storage devices. However, it is not yet clear whether this technology will ever come to market in strong competition from other quarters such as hard drives, flash storage, holographic storage (CD, DVD, HD-DVD, Blue-Ray...) and internet-based storage. Regardless of whether 3D optical data storage becomes widely used or not, the very first attempts of five-dimensional optical recording can already be found in the most recent scientific publications.[27]

Even though the storage of data is the most developed application of photochromic compounds, they can be also applied to the transport of ions through a membrane or the design of stimulated emission devices; but their presence is also ubiquitous in our dayly experience: sunglasses, toys, cosmetics... If necessary, to maximize the properties of these compounds, many of them are incorporated into polimeric structures, liquid crystals or other matrices; or they can be forced to change between desired colors by combination with a permanent pigment. After all, since photochromic chromophores are dyes and operate according to well-known reactions, molecular engineering to fine-tune their properties can be achieved relatively easily using known design models, theoretical chemistry and experimentation. At this point, it is convenient to highlight that there exist few lines of research in chemistry where the synergy experiment-theory is so beneficial as in the study of photochromic processes.

1.1.3   Photochromic compounds and reactions

The variety of organic compounds that exhibit photochromic properties is huge, due to the fact that the development of organic photochromism has been parallel to the development of organic synthesis, as previously explained. Figure 1.3 shows the most significant families of photochromic compounds cited in the specialized literature.[2]

There exist also photochromic compounds in biological systems, but only a few of them are able to keep their photochromic properties after being isolated from their cellular environment. Some examples are the retinal proteins,[28, 29] which participate in the mechanism of vision in animals, and phytochromes,[30, 31] which control the photomorphogenesis process in plants.

Nevertheless, photochromism is not limited to organic compounds. Many inorganic substances also exhibit photochromic properties, as for example silver and zinc halides (usually the corresponding chloride). Actually, one of the very first applications of photochromism, ophthalmic glasses, was first based in inorganic compounds. Even though the inorganic crystals are stronger
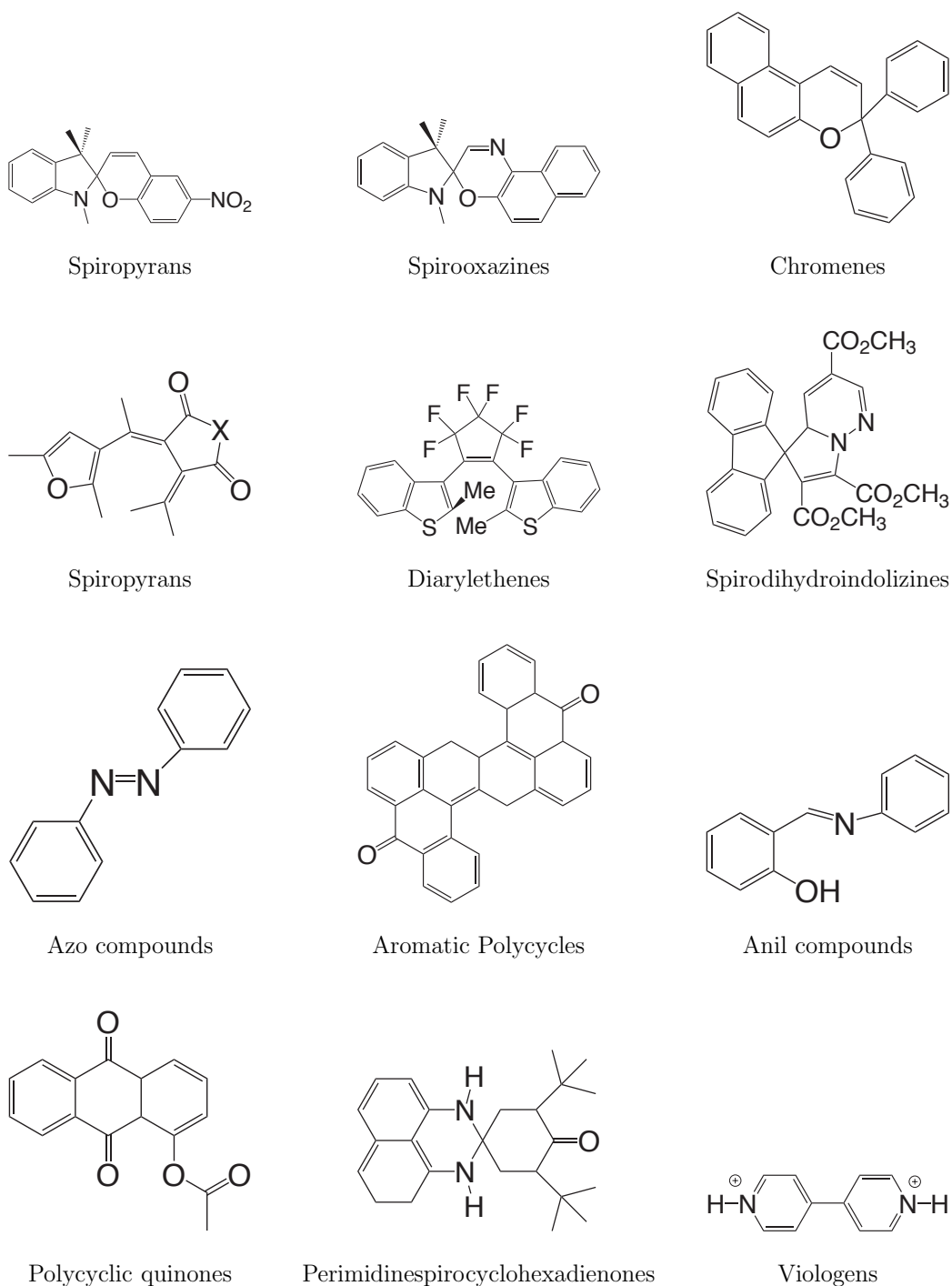
Figure 1.3: *The families of organic photochromic compounds most cited in the specialized literature (see Ref. 2).*

Heterolytic dissociation   Intramolecular functional group transfer

Intramolecular hydrogen/proton transfer   Reduction-oxidation process

Pericyclic reactions   *Cis-Trans* (E/Z) isomerization
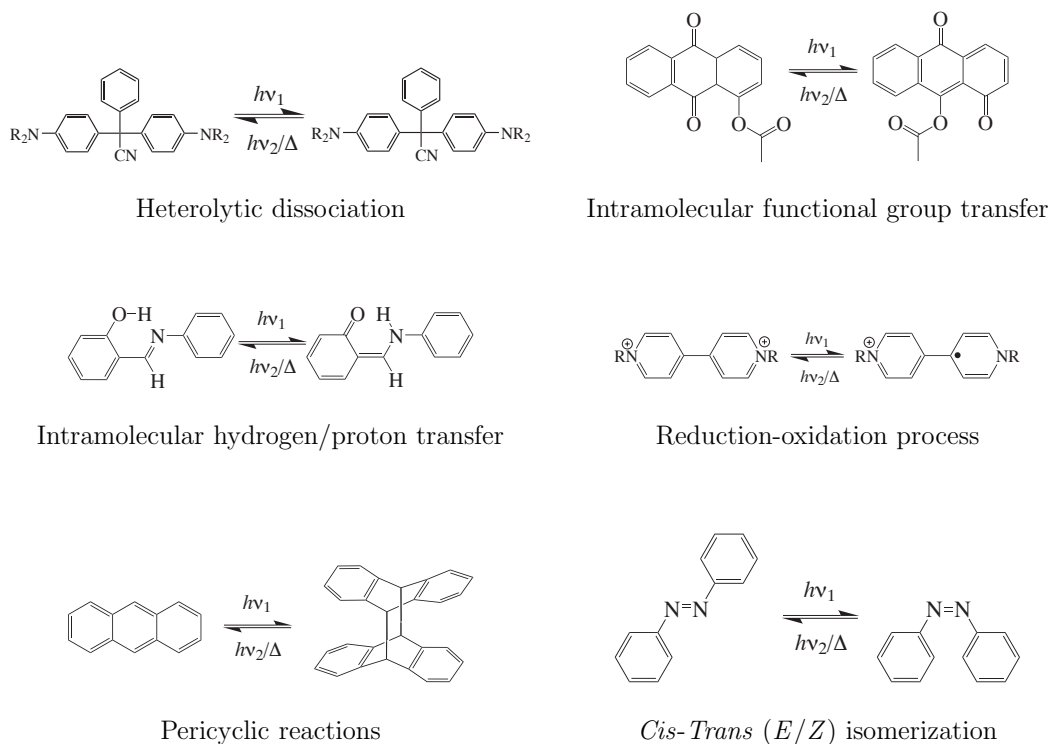
Figure 1.4: *Examples of the six photochromical reactions found in the specialized literature.*

and have a better resistance to grating or scratching than organic crystals, it is well known among the glass-wearing public that organic crystals are much lighter and resistant to falling than inorganic ones. For that reason nowadays the photochromic inorganic substances are less used in the manufacture of glasses.

The chemical reactions these photochromic compounds may undergo after photoexcitation is very varied. The actual classification of photochromic reactions, according to the literature, is as follows:[2] electrocyclation, intramolecular proton transfer, *cis-trans* isomerization (usually preceded by a proton transfer process), intramolecular functional group transfer, dissociations (homolytic or heterolytic) and oxido-reductions. Figure 1.4 shows a particular example of each reaction. Several of these reactions range among the fastest chemical reactions known to date.

Nowadays there are better resources to study photochromic reactions than 20 years ago, mainly due to two reasons: (*i*) the experimental techniques which allow to follow ultrafast phenomena, with time resolutions of a few femtoseconds, are more common in standard laboratories, and (*ii*) the availability of advanced theoretical methods which allow to study bigger systems with a good accuracy at reasonable calculation cost.

1.1.4   Excited state intramolecular proton transfer processes

Among the different types of photochromical reactions, the excited state intramolecular proton transfer (ESIPT) processes are of very special interest. Hydrogen is a very particular element at the interface between physics, chemistry, biology and technology. It forms covalent bonds and hydrogen bonds in inorganic, organic and biochemical systems. It has four isotopes (which leads to the main kinetic isotope effects knwon), and it can exist as free or solvated proton, hydrogen atom, hydride anion and always as a quantummechanical material wave. Hence, it is not surprising that hydrogen transfer has been a hot topic for experiments and theory for decades.[32,33] It is wellknown that photoinduced proton-transfer reactions play a fundamental role in many chemical and biological processes. However, given the characteristic high rate of such reactions, they can only be followed using femtochemistry techniques. From the theoretical point of view, ESIPT processes are specially suited for consideration as the relatively low number of atoms implied in the process allows for quite sophisticated and accurate quantum-electronic calculations. Also the dynamics of the whole process can be followed using molecular dynamics techniques that would be too time consuming were it not for the ultrafast nature of the process.

ESIPT processes generally occur in chemical compounds which present, in their molecular structure, a delocalized π–electron system and one or several regions where acidic and basic functional groups are relatively close. Despite of the large diversity of molecules known to undergo ESIPT, it is

well-accepted that ESIPT processes are usually initiated by the absorption of electromagnetic radiation (by the π electronic system) which promotes the molecule towards an electronic excited state. In such excited state, usually characterized by the HOMO (π) $\rightarrow$ LUMO (π^*) electronic transition, the enhancement of the acidity and basicity of these functional groups occurs, thus favoring the proton transfer process. In other words, the potential energy surfaces (PES) of the ground and excited states are so different, that the more stable tautomer in the ground state becomes less stable (or even unstable) in the excited state. The most commonly observed examples are when the acid and basic groups share a hydrogen bond, *e.g.* between hydroxil and imine groups, respectively.

The vast majority of studies have dealt with single ESIPT processes. Excited-state intramolecular double proton transfer (ESIDPT), in contrast, is far less well-known. In ESIDPT, the reaction is expected to be more complicated, since two possible limiting mechanisms can be envisaged. In the first limiting mechanism, the two protons transfer in a single step (concerted mechanism), whereas in the second, one proton transfer precedes the other so that the mechanism involves a zwitterionic intermediate (stepwise mechanism). The possibility of two or more proton transfer processes opens the door to several reaction paths so that the possibility of obtaining a stable structure upon photoexcitation at a given wavelength largely increases, enabling the design of fine molecular photomemories.[34] Water molecules or other substrates can mediate the ESIPT process, via a "proton relay" mechanism, which eventually results in a formal intramolecular proton transfer.[35–37] However, these systems are even less common and are restricted to only a few molecular compounds.

The reversible ultrafast transfer process of a very light particle (such as the proton) enables (for example) the design of molecular switches *i.e.* molecular devices which can oscillate very quickly between two positions. This application sets the basis for optic photomemories.[38] The importance of ESIPT processes in technological applications is thus undeniable. However,

its importance goes beyond the field of lifeless environments. Photoinduced intramolecular proton transfer is also an ubiquitous process in biology.[39] A large number of biomolecules, from small cofactors to large proteins, owe their tridimensional structure (and thus its biological function) to ESIPT procceses. In addition to this, such molecular structures play a very important role in many biochemical processes like electron transfers, energy production, ion transport...In other words, the study of ESIPT processes is also relevant from the fundamental point of view, in order to get a deeper understanding of all these biochemical processes acting in nature. Some examples of such processes are the photorelease with near – UV light of biologically relevant compounds (ATP, amino acids...),[40] the mutation processes that can take place during the DNA replication process (both source of evolution and illnesses),[41,42] or the protein – ligand binding processes.[43] Even more recently, the biological and biomedical applications of ESIPT processes have recevied attention with the 2008 Nobel Prize in Chemistry, awarded to Osamu Shimomura, Martin Chalfie and Roger Y. Tsien for the discovery and the development of applications of the green fluorescent protein.[44–46]

1.1.5 Presence of competitive processes in ESIPT reactions

In many chemical reactions that take place in the electronic ground state, the possibility that the reactants participate in side reactions towards different final products exists. Temperature, pressure or the presence of certain chemical species may cause the appearance of different mechanisms. In contrast, there are many classes of electronic excited states, each one described by a different PES, which can present a large number of minima, transition states, but also interacting regions between different electronic states. Hence, in ESIPT reactions, as in every reaction in excited states, the presence of side reactions that compete with the main photochemical process is more ubiquitous than in the ground state.

Immediately after the photoexcitation process, also known as photophysics as no changes in the electronic bond structure take place,[47] the quantum of energy contained in the absorved photons is rapidly distributed among the traslational, rotational, vibrational and electronic degrees of freedom of the molecule. The energy distribution among certain degrees of freedom will set off the main photochemical mechanism, and thus the reactant will evolve towards a final photoproduct along a given PES. Eventually, the final photoproduct will relax to the ground state. This scheme of events is referred as adiabatic photochemistry.[47] However, the distribution of energy among different degrees of freedom might trigger secondary mechanisms which can compete with the main process. It is then compulsory to monitor the evolution along the different PESs in order to get a full understanding of the photoinduced chemical reaction.

In experimental photochemistry, the most used marker for that purpose is the quantum yield (QY, usually denoted as Φ). The QY of a radiation-induced process is the number of times that a defined event occurs per photon absorbed by the system. Hence, either a QY for the absorption process or for the ulterior emission process can be defined. Concretely, those molecular systems that exhibit an intense emission of radiation, present a value of Φ close to 1, *i.e.* practically every absorbed photon leads to the emission of a concrete final photoproduct. However, any reduction in the emission QY means that a fraction of the total energy has activated a relaxation channel different from the emission of radiation. This new channel represents a competitive process of the main photochromic process. In such cases, the molecule has experienced a deactivation process, or quenching in the photochemical terminology. The most usual quenching mechanism is the radiationless decay, which takes place when the molecule reaches a crossing channel, also known as funnel, between the two PESs corresponding to the excited and ground electronic states. In the regions where two electronic states are very close in energy, molecular energy transfer processes between the two states are very likely to occur. Thus, such deactivation processes are very efficient. These processes
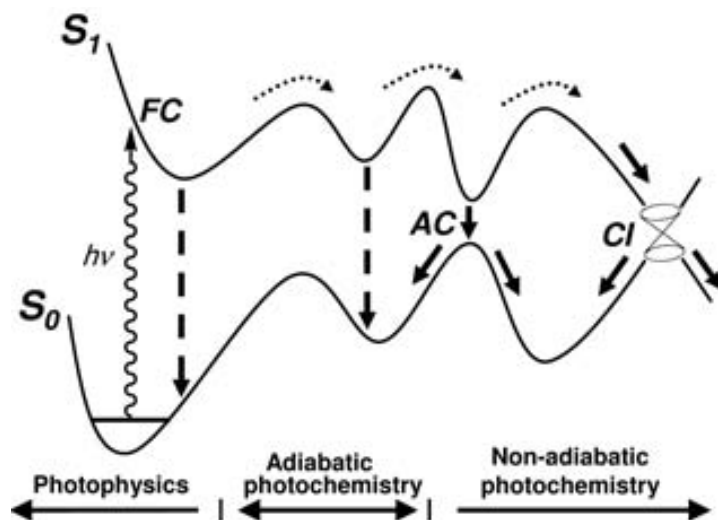
Figure 1.5: *Hypothetical potential energy profiles of the singlet ground state and first singlet excited state of a given molecular system. The most singular points are denoted as FC, AC and CI for Franck-Condon, Avoided Crossing and Conical Intersection, respectively. The curly, dotted, dashed and solid arrows represent absorption, photoadiabatic reaction, emission and non adiabatic processes, respectively (Figure inspired on Figure 1 in Ref. 47).*

are called internal conversions or intersystem crossings, if the energy transfer takes place between states of the same or different multiplicity, respectively. In terms of PES topology, the regions where these processes take place are called conical intersections (CI) or avoided crossings, to differentiate if such an effective crossing between two electronic states does or does not really exist, respectively. Those processes constitute the non-adiabatic photochemical processes, as during the chemical reactions a change of PES has taken place.[47] A graphical summary of these processes can be seen in Figure 1.5

Nowadays there is no doubt about the key role CIs play in non-radiative de-excitation transitions from excited electronic states to the ground electronic state of molecules in many chemical and biological reactions,[48] and ESIPT processes are not an exception. However, even though the use of femtosecond laser experiments show direct evidences of their existence, the concept of a CI is strictly theoretical, and as such is not directly accessible to experimental observation. Given that a general mathematical procedure

to predict the presence of a CI in a molecular system does not seem to exist, the work of many theoreticians during the last decade, remarkably Robb, Olivucci, Bernardi and collaborators,[49] consisted in the sistematic determination of CI in a large number of photochemical reactions.

1.2   Molecular systems of interest

The variety of organic compounds that exhibit ESIPT processes is so wide that a four-year research term suffices only to scratch the surface of this vast field. After saying so, the most logic question that you may be thinking right now is: which molecular systems are interesting enough to be studied in such a short period of time? As researchers, our interests should be placed in those problems of general relevance for which a clear and definitive explanation has not been found yet. Besides, our attention should be also focused on these unsolved problems for which our traditional approaches to the solution become inappropriate, and a revision of our methodology is needed.

Proton transfer reactions, and more concretely ESIPT processes, meet our criteria for what we consider research of interest. As it has been commented, ESIPT processes are with no doubt among the most basic chemical reactions by excellence, as they are present in gas phase, solution and even in solid state, both in inert or biological systems. The apparent simplicity of the process should not be overrated, because defining a general ESIPT reaction as the ultrafast displacement of a proton from one location to another within a molecule is far from complete. Actually, the transfer of the proton between the donor and acceptor atoms is not usually free from the influence of other chemical or physical processes, like *cis-trans* isomerization or internal vibrational energy redistribution. These additional processes make the study of ESIPT processes a daunting task. Besides, the complexity of the study can even increase if we consider not one but multiple proton transfer processes.

In theory, we can determine the temporal evolution of the system through all these possible paths, by means of the Schrödinger equation, if we can compute the energetics of each parallel process. Quantum chemistry provides a solid framework to achieve this: the Born-Oppenheimer (BO) approximation, probably the most central approximation in theoretical chemistry. However, it is possible that the different electronic states where the ESIPT process takes place intersect at certain molecular geometries. At these special regions of the PES, the BO approximation is, by definition, no longer valid. Hence, the traditional treatment of the energetics and the dynamics of the system based on the separation of the electronic and nuclear coordinates breaks down. In order to obtain correct results for this situations, a new formulation of the BO approximation must be adopted.

With this aim in mind, the molecular systems whose studies are collected in the present thesis[50–55] represent direct examples of the different orders of complexity that the study of ESIPT processes can present; from the comprehension of (sometimes) controversial experimental data to the need of adoption of efficient theoretical strategies that fit best to solve each problem.

First of all, we focus on determine the basics of ESIPT reactions, isolated from competitive processes. To this end, it is necessary to study molecular systems that undergo standalone ESIPT processes. No other parallel processes should be present or, at least, should not interfere with the proton transfer reaction. The derivatives of the anil compounds (see Figure 1.3), best known as aromatic Schiff bases, represent a large family of photochromic compounds that has attracted much attention over the last years.[56–60] The simplest member of this family, the salicylidene methylamine (SMA) molecule, is far from being a well-studied system. Very little has been published about its photochemical properties and behavior, but more important, no other competitive processes to the ESIPT have been reported for SMA to date. Besides, the derivatives of the 2-(2'-hydroxyphenyl) benzoxazole compound represent another well-known and most simple molecular

families that follow ESIPT process.[61–63] The dynamics of the ESIPT process of the 1-hydroxy-2-acetonaphtone (HAN) molecule, one of its family members, has been recently described as the sole ultrafast transfer of the proton.[64] Hence, these two actual molecular systems, SMA and HAN, are of great interest to stablish the basic features of ESIPT, but also as a first step in the study of larger members of their correspondig photochromic families.

Secondly, the study of ESIPT processes must be brought one step beyond. We are interested in determining the effect that possible competitive processes may have on the ESIPT reaction. For this study, we have revisited the aromatic Schiff bases. Undoubtedly, the salicylideneaniline (SA) system is the most thoroughly studied aromatic Schiff base.[57,58] However, the results are not fully consistent and much controversy is still present regarding the full photochemical behavior of SA. Several studies point out to the presence of non radiative processes that directly compete with the proton transfer process. The SA system fits with our purposes in this second step of our study.

Finally, we take a careful look to the study of molecular systems which present multiple ESIPT processes. In contrast to their single homologues, multiple ESIPT processes exhibit alternative reaction paths for the proton transfer process, which makes their study more complicated. But more important, systems that present multiple ESIPT and competitive non adiabatic processes together are being thoroughly studied for their potential application as molecular photochromic devices. A few years ago, the advisors of the present thesis reported a quantum dynamical theoretical report on the ESIDPT process in [2,2'-bipyridyl]-3,3'-diol (BP(OH)$_2$),[65] one of the best studied multiple-ESIPT systems.[66–70] Here, we have extended this previous study to the isoelectronic bipyridyl derivative [2,2'-bipyridyl]-3,3'-diamie (BP(NH$_2$)$_2$), and the hipothetical hybrid derivative of the former two, the [2,2'-bipyridyl]-3-amine-3'-ol (BP(OH)(NH$_2$)) compound. We analyze and compare the viability of these bipyridyl derivatives as molecular optical devices.

In this way, this thesis presents a progressive and systematic approach to the enormously complicated, and at the same time fascinating, set of systems that present ESIPT. The study evolves from the simplest (without competitive processes) single ESIPT, to the most complex and realistic systems, in which competitive processes take part. The final chapter presents a humble proposal for a technical use of some of these systems.

2

Experimental techniques in chemical kinetics

"A chemical physicist makes precise measurements on impure compounds. A theoretical physical chemist makes imprecise measurements on pure compounds. An experimental physical chemist makes imprecise measurements on impure compounds."

From GAUSSIAN 03's quotes.

At this point of reading, you might have got surprised to find a section about experimental techniques in a thesis which is clearly devoted to theoretical and computational chemistry. This is so because I cannot conceive Chemistry separated from the experimental study. It is necessary for the theoretician to understand how the experimentalists work, in order to take the first glance at the chemical problem. This is usually the starting point for his/her theoretical contribution to the solution. In our case, it should be necessary to understand how a chemical reaction can be followed, not only in its electronic ground state, but also in any electronic excited state. With this aim in mind, this section serves as a basic introduction for you (and also for myself too) to the most common experimental techniques used in chemical kinetics, with a special focus in femtochemistry. Please note that the following presentation on experimental techniques does not by any means attempt to be exhaustive, and the references therein have been chosen with the intention of pointing you to further material, rather than honoring all the work that has been made in this field.

We call chemical kinetics, also known as reaction kinetics, the study of rates of chemical processes. The first work on reaction kinetics is considered to be the one of Peter Waage and Cato Maximilian Guldberg, who stablished in 1864 the law of mass action, which states that the speed of a chemical reaction is proportional to the quantity of the reacting substances. Thirteen years later, Jacobus Henricus van't Hoff would arrive at a similar relationship and would demonstrate experimentally its validity. In addition to this, in 1889 Svante Arrhenius provided one of the most simple, but remarkably accurate, empirical relationships known in chemistry:

$$k(T) = Ae^{-E_a/RT} \tag{2.1}$$

which gives the dependence of the rate constant k of a chemical reaction (that is, a value which quantifies the speed of a chemical reaction) on the absolute temperature T. Such formula would be given a theoretical ground with the arrival of the Transition State Theory developed by Eyring, Evans

and Polanyi in 1935. Nevertheless, these two major contributions essentially established the mathematical models that describe the characteristics of a chemical reaction and how different experimental conditions could influence their rate. What was left was only a matter of designing experimental set ups with which the rate of a reaction could be measured.

The very first kinetic experimental techniques used, and also the first every scholar learns, were chemistry-based methods. They consist in taking samples of a chemical reaction in solution at regular times, stopping the reaction with the use of a proper inhibitor or decreasing the temperature, and directly measuring the quantity of product formed or reactant consumed by titration. This methods are only suitable for slow reactions (in the second and minute time scale), but are cheap and easy to use. However, they generate residues and the overall process is very aggressive with the sample. These disadvantages were overcome when physical methods were introduced *i.e.* to follow the time evolution of a physical property of the reaction, which depends on the concentration of one or more chemical species involved in the reaction. This new branch of methods, which are cleaner and less aggressive than the chemistry-based methods, can be coupled with spectroscopic techniques in order to study faster chemical reactions. The main disadvantage is that the faster the reaction we want to follow is, the more expensive and more complicated the experimental set up becomes.

Flux methods were the first attempt to combine physical kinetic methods with spectroscopic detection techniques. This technique was originally developed by Hartridge and Roughton in the 1920s,[71] and allowed to study reactions in solution which took place in the milisecond time scale (10^{-3} s). A simple sketch of the array is depicted in Figure 2.1. Basically, the reactants are physically separated in different and thermostated compartments at a concrete pressure. At a certain time the plungers of each compartment are simultaniously activated, releasing the reactants at a constant flux rate. At the point where all the pipes converge, the pressure of the reactants allow the mixture to take place within 10^{-4} s, and it is assumed that the reaction
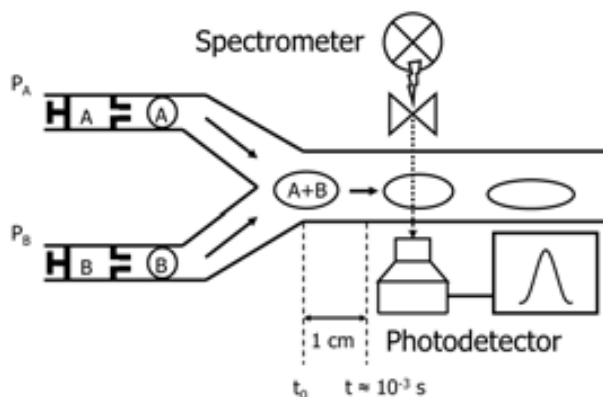
Figure 2.1: *Schematic diagram of a kinetic flux method experimental setup.*

starts when the mixture begins to advance through the central tube. Let us suppose the array was set in a way that the mixture takes 10^{-3} s for advancing 1 cm. Hence, if we want to take a measure of the kinetics after 10^{-3} s, we should place our spectrometer 1 cm away from the mixture region, and so on. It is essential to obtain a complete mixture between reactants before taking any measure. Because the mixture usually takes at least $\sim 10^{-4}$ s to be complete, this technique is limited to reactions within the milisecond time scale.

Thirty years later, Manfred Eigen and collaborators developed a new kind of techniques which overcame the limitation of the flux based methods, the so called relaxation methods.[71] Instead of mixing the separate reactants, the main idea consists in starting from a mixture which is in chemical equilibrium. If a little but sudden perturbation is applied over this system, for example a temperature change, then according to van't Hoff's equation:

$$\frac{d\,lnK}{dT} = \frac{\Delta H^0}{RT^2} \tag{2.2}$$

a temperature change must suppose some change in the equilibrium constant K, then the equilibrium state is lost and the system evolves to a new equilibrium. The transition from one equilibrium state to another takes place within the kinetics of the reactions, which can be measured. As an illustrative

example, we will assume a first order reversible process:

$$A \quad \underset{k_{-1}}{\overset{k_1}{\rightleftharpoons}} \quad B \tag{2.3}$$

with k_1 and k_{-1} for the direct and reverse rate constant processes, respectively. Being a and b the equilibrium concentrations, and $(a+x)$ and $(b-x)$ the concentrations at a certain time t for the species A and B, respectively, the corresponding rate equation is:

$$\begin{aligned} -\frac{dx}{dt} &= k_1(a+x) - k_{-1}(b-x) = \\ &= k_1 a - k_{-1} b + (k_1 + k_{-1})x = (k_1 + k_{-1})x \end{aligned} \tag{2.4}$$

where the relationship $k_1 a = k_{-1} b$ has been used. By integrating (2.4) we arrive at:

$$x = x_0 e^{-(k_1 + k_{-1})t} \tag{2.5}$$

where x_0 is the initial perturbation applied on the system. From this equation, we can define a relaxation time τ as:

$$\tau = (k_1 + k_{-1})^{-1} \tag{2.6}$$

and thus, if the equilibrium constant $K = \frac{k_1}{k_{-1}}$ at the final temperature is known, both k_1 and k_{-1} can be determined from τ.

Within these techniques, the kinetics of chemical reactions in solution could be measured up to the range of 10^{-4} s - 10^{-5} s. However, the study of gas phase reactions was behind the studies of reactions in solutions, which was still limited to very slow reactions. In 1949, and simultaneously to the development of relaxation methods, Manfred Eigen, Ronald George Wreyford Norrish and George Porter performed the first experiments of a new technique which would awarded the Nobel Prize of Chemistry in 1967, the flash
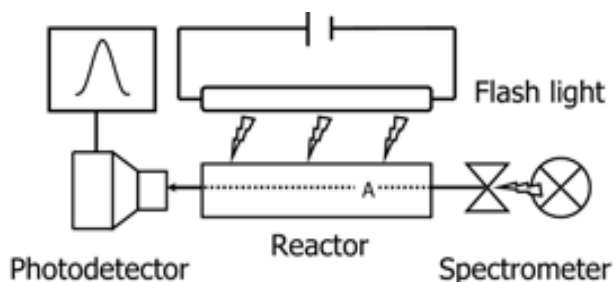
Figure 2.2: *Schematic diagram of a flash photolysis experimental setup.*

photolysis.[72] The corresponding experimental array is roughly presented in Figure 2.2.

As we can see, the main element is a reactor containing the reactants to be studied, which can be either in gas phase or in solution. This reactor needs to be built up with a transparent material. The array is completed with two light sources, one close to the reactor (called the flash) and the other more separated (the spectrometer). The flash serves as the activator of the reaction (hence the need of transparent walls), and because of this, only reactions that can be photoactivated can be studied with this technique. In this sense, flash photolysis was the first major contribution to the development of modern photochemistry. The second light source, the spectrometer, is used to take the measure. Adjusting the distance between the spectrometer and the reactor, which determines the time the beam takes to reach the photodetector, allows for obtaining measures at different times. The experiment can be performed activating both light sources at the same time or not, but either way, the experimentalist had absolute control of the initial time of the reaction. In 1949, the most common light sources available were Xenon flash lamps, with which Eigen, Norrish and Porter succeeded in taking kinetic measures of a chemical reaction 10^{-6} s after it was initiated.

The time limit of 10^{-6} s was the shortest time an experimentalist could measure in a kinetic chemical process in the decade of 1950. It was not until the arrival of another keypiece in the development of photochemistry that this

limit could not be beaten; the laser. Laser stands for Light Amplification by Stimulated Emission of Radiation, and was first developed in 1958 by Townes and Schawlow. In a nutshell, a laser is an optical device which produces a highly intense, directional and monochromatic beam of radiation. With such a radiation, it is possible to obtain time measures well under 10^{-6} s. Actually, the limit of detection in chemical reactions decreased nearly 3 orders of magnitude during the next twenty years, since the laser was developed (10^{-9} s in 1960 and 10^{-12} s in 1970). 1970 set the inflection point in the history of chemical kinetics. At room temperature, the speed of an atomic nucleus is about 10^4 cm s^{-1} - 10^5 cm s^{-1}. At this speed, the time it takes for two nuclei to collide is in the order of 10^{-11} s - 10^{-12} s. It means that before 1970, it was not possible to take a time measure right after a collision between nuclei had taken place. That year marked the transition between chemical kinetics and chemical dynamics *i.e.* the study of rates of chemical processes at a molecular level.

Needless to say, the main contributor to the development of the modern experimental techniques in the field of photochemistry is the Egyptian-American chemist Ahmed Zewail. Using a rapid ultrafast laser technique (consisting of ultrashort laser pulses delayed by mirrors), Zewail studied reactions on very short time scales (10^{-15} s) in 1987. Such times were short enough to analyze "transition states" in selected chemical reactions. Allowing to study chemical reactions in the femtosecond time scale, this new branch of techniques were named femtochemistry, for which Zewail obtained the Noble Prize of Chemistry in 1999.[73] In Figure 2.3 we can see the sketch of a classical femtochemistry experimental array.

One of the main requisites (and also one of the hardest to obtain) of a femtochemistry experiment is the formation of a fine beam of molecules from the sample, in order to take measures at the single molecule level. This can be achieved first by jet cooled techniques, which descend the temperature of the sample and slow down the speed of the molecules. Then, the molecules are directed to a filter containing a gap on the order of the molecular diameter,
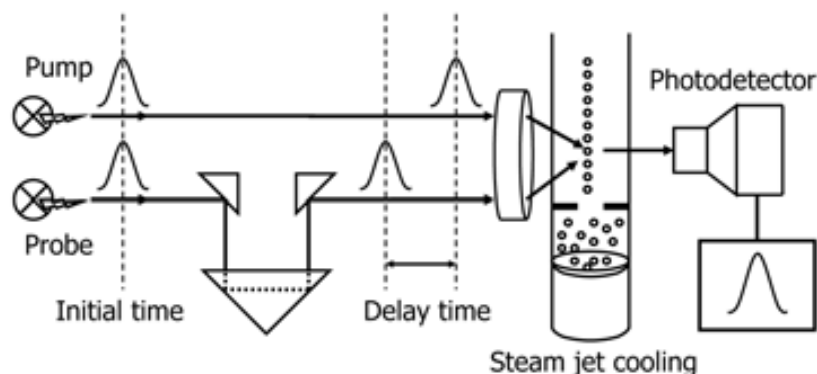
Figure 2.3: *Schematic diagram of a femtochemistry experimental setup.*

thus obtaining a beam of single molecules. As in a flash photolysis array, two light sources are also used, which are generated by a pulsed laser. A first beam, called pump, is sent to excite each molecule. The second beam, called probe, is delayed with respect the pump beam with the aid of a set of calibrated mirrors, which alter the course of the origial beam and set a delay time between both beams. Depending on the chemical nature of the sample, the probe beam may cause an induced emission of the excited molecules (thus obtaining an emission measure) or may cause a second absorption via a two-photon absorption process. The calibration of the mirrors, which in the end determines the time of the measure, can take several months, an a little deviation of some nanometers in only one mirror can cause a time delay of several picoseconds, a time for which the reaction under study is beyond completeness.

Many variations of this basic array exist, such as the most modern femto-chemistry techniques called transient-absorption spectroscopy, time-resolved infrared spectroscopy or time-resolved fluorescence spectroscopy; but all of them belong to the family of the so-called "pump-probe" methodologies, which has proved to be the most efficient in the study of ultrafast processes, being the lowest measured time around 50 fs.[74]

In the concrete case of ESIPT processes, the emission of the excited photochromic products can be induced by sending a probe beam at different times, thus obtaining its experimental emission spectrum. As the photoreaction advances, the emission signal of the photoproduct tends to increase. Otherwise, the decay of the photoproduct's fluorescence can be also measured as the reaction goes on. These characteristic raise and decay times, which are the main experimental data that a theoretician can be interested in, can be obtained by fitting these signals with mono-exponential functions (assuming a first order kinetics). However, if the signals are better fitted with a multi-exponential function, this can be indicative of the presence of several mechanisms involved in the postESIPT process.

3

Theoretical and computational chemistry

- "What're quantum mechanics?"
- "I don't know. People who repair quantums, I suppose."

Terry Pratchett, *Eric* (1990)

3.1 Basics of quantum mechanics

The study of ESIPT processes in small organic compounds is particulary attractive from the theoretical point of view. These systems usually present a well defined reactive starting geometry which can be easily modelled, in contrast to large biomolecules. In addition, the time the proton transfer lasts can be measured precisely, so that the comparison between experimental and theoretical data is more direct. The involvement of light nuclei (hydrogen atoms) in chemical reactions causes the quantum nature of matter to arise, in the form of tunnel or interference effects. In that case, the laws of quantum mechanics have to be applied in order to get a quantitative description of these processes.

According to the formulism of quantum mechanics, the most suitable mathematical object to describe the quantum state of a physical system is the state vector $|\psi\rangle$, which in Dirac's notation is called *ket* vector. Nowadays, the academic formation of a general chemist might include several gaps on the fundamentals of quantum mechanics, which can represent a serious handicap when dealing with abstract objects as *ket* vectors. However, the most important feature we should consider about *ket* vectors is that they represent the system, and thus they contain all the information about it (position, momentum, energy...), which in turn can be obtained by proper mathematical manipulation.

Ket vectors can be used to define a single quantum state, or the combination of different quantum states (also known as wave packet), for a concrete system. However, concepts such as vector state or wave packet come from the physical formulation of quantum mechanics, and trying to adapt them into chemical problems can be tough. It would be of great help if we could represent the *ket* vector of a system over a concrete set of coordinates *e.g.* the electronic or nuclear positions in a molecule. This is possible since the state vector of a system can be projected (by dot prodcut operation) over a given configurational space $\vec{q}$:

$$\langle \vec{q} \mid \psi \rangle = \psi(\vec{q}) \tag{3.1}$$

where $\langle \vec{q} \mid$ and $\psi(\vec{q})$ are two new mathematical entities known as *bra* vector (of the configurational space $\vec{q}$) and wave function, respectively.

The advantage of dealing with the wave function is that it still contains all the information of the system (as does the vector state) and it is also a function of a given set of coordinates $\vec{q}$. Hence, any important physical magnitude of the system can be expressed as a function of these coordinates. That is the reason why theoretical chemists have adopted the wave function concept as the most suitable way to describe a chemical system.

In order to study the behaviour of any system, it is not enough to define a state vector or a wave function. It is also necessary to observe how this system evolves with time. Newton's laws of motion are no longer valid to describe the systems we are interested in. Its quantum equivalent is represented by the time-dependent Schrödinger equation:

$$i\hbar \frac{\partial}{\partial t} \psi(\vec{q}, t) = \hat{H} \psi(\vec{q}, t) \tag{3.2}$$

where $\hat{H}$ is the Hamiltonian operator, and the wave function depends also on time. It has to be noted that, as written, Eq. 3.2 could be applied to every imaginable physical system, as only a wave function and a Hamiltonian have to be provided. If we set $\vec{q}$ as the collective coordinate to represent the position of both the nuclei and electrons on a molecule as $\vec{q} = \{\vec{q}_{nuclei}, \vec{q}_{electrons}\}$, and do not consider any relativistic effect on the system, the molecular Hamiltonian becomes (expressed in atomic units with $e = m_e = \hbar = 1$):

$$\hat{H} = \hat{T}_N + \hat{T}_{e^-} + \hat{V}_{NN} + \hat{V}_{e^- - e^-} + \hat{V}_{e^- - N} =$$

(Continues on next page.)

$$
= \sum_{i=1}^{N} -\frac{\nabla_i^2}{2} + \sum_{\alpha=1}^{M} -\frac{\nabla_\alpha^2}{2m_\alpha} + \sum_{\alpha>\beta}^{M} \frac{Z_\alpha Z_\beta}{|\vec{R}_\alpha - \vec{R}_\beta|}
$$

$$
+ \sum_{i>j}^{N} \frac{1}{|\vec{r}_i - \vec{r}_j|} + \sum_{i=1}^{N}\sum_{\alpha=1}^{M} \frac{-Z_\alpha}{|\vec{r}_i - \vec{R}_\alpha|}
\tag{3.3}
$$

According to Eq. 3.2, the wave function $\psi(\vec{q}, t)$ depends on the time and both on the electronic and nuclear coordinates, and these variables are *a priori* non-separable. However, certain special conditions exist in which a separation of the variables can be possible. In the case that the molecular Hamiltonian has no time dependence and the system is described with an eigenstate of the Hamiltonian, $\psi(\vec{q}, t)$ can be rewritten as a product of two functions in which the space and temporal coordinates can be separated:

$$
\psi(\vec{q}, t) = \Psi(\vec{q})\Phi(t)
\tag{3.4}
$$

since we have imposed that $\hat{H} \neq \hat{H}(t)$, replacing Eq. 3.4 into Eq. 3.2 leads to:

$$
i\hbar\frac{\partial}{\partial t}\left[\Psi(\vec{q})\Phi(t)\right] = \hat{H}\left[\Psi(\vec{q})\Phi(t)\right] \Rightarrow
$$

$$
\Rightarrow i\hbar\frac{1}{\Phi(t)}\frac{\partial\Phi(t)}{\partial t} = \frac{\hat{H}\Psi(\vec{q})}{\Psi(\vec{q})}
\tag{3.5}
$$

this relationship of equality can only be true if Eq. 3.5 does neither depend on t or $\vec{q}$, *i.e.* it is a constant. Given that the Hamiltonian $\hat{H}$ is the operator corresponding to the total energy of the system, that constant has to be the molecular energy E. Hence, from the left term of Eq. 3.5 we can easily see that:

$$
i\hbar\frac{1}{\Phi(t)}\frac{\partial\Phi(t)}{\partial t} = E \Rightarrow \Phi(t) = e^{-iEt/\hbar}
\tag{3.6}
$$

and from the right term:

$$\frac{\hat{H}\Psi(\vec{q})}{\Psi(\vec{q})} = E \Rightarrow \hat{H}\Psi(\vec{q}) = E\Psi(\vec{q}) \tag{3.7}$$

where Eq. 3.7 is known as the time-independent Schrödinger equation, given that the time-dependence has been removed from Eq. 3.2. Since the early development of quantum chemistry, most of the efforts of theoretical chemists have been placed in solving Eq. 3.7 in order to obtain the total energy of a molecular system within a stationary state. However, this description does not take into account the time evolution and hence the motion of the molecules; and no chemical reaction can occur in such conditions. Thus, the time-independent Schrödinger equation must be seen as a first step to the real problem that is needed to solve the time-dependent scheme.

3.2 The Born-Oppenheimer approximation

3.2.1 Description of the approximation

Even after the simplification achieved by the time-space separation in Eqs. 3.6 and 3.7, the resolution of the time-independent Schrödinger equation still becomes unfeasible for virtually every chemical system. The electrons–nuclei interaction term $\hat{V}_{e-N}$ in Eq. 3.3 does not allow the separation of the electronic and nuclear coordinates, which results in a problem of serious mathematical complexity. However, this limitation can be overcome with the introduction of the BO approximation.

According to this approximation, given the mass difference between nuclei and electrons ($M_{nuclei} \gtrsim 1{,}800 \ m_{electron}$), it is reasonable to expect that the fast electrons will adjust instantly to the more inertial nuclei. This is mathematically traduced by rejecting the nuclear kinetic energy operator term $\hat{T}_N$ when compared with the electronic kinetic energy operator term $\hat{T}_{e^-}$ in Eq. 3.3. In that way, the nuclear–nuclear potential energy operator term $\hat{V}_{NN}$ becomes a constant, and the nuclear and electronic coordinates

become uncoupled. Hence, we can separate the molecular Hamiltonian into pure electronic and nuclear contributions and Eq. 3.7 can be split into:

$$\hat{H}_e \Psi_e(\vec{q}; \vec{Q}) = U(\vec{Q}) \Psi_e(\vec{q}; \vec{Q}) \tag{3.8}$$

$$\left[\hat{T}_N(\vec{Q}) + U(\vec{Q}) \right] \Psi_N(\vec{Q}) = E \Psi_N(\vec{Q}) \tag{3.9}$$

where $\hat{H}_e = \hat{T}_{e^-} + \hat{V}_{e^- - e^-} + \hat{V}_{e^- - N} + \hat{V}_{NN}$ is the electronic Hamiltonian, $\Psi_e(\vec{q}; \vec{Q})$ is the electronic wave function, $U(\vec{Q})$ is the total potential energy of the molecule assuming the nuclei fixed in the coordinates $(\vec{Q})$, $\Psi_N(\vec{Q})$ is the nuclear wave function, and E is the total molecular energy. Eqs. 3.8 and 3.9 are known as the electronic and nuclear time-independent Schrödinger equations, respectively. Within the BO approximation, the original time-independent Schrödinger equation is divided into two different (and less complex) parts. However, the validity of the BO approximation may be compromised under certain special circumstances, as will be discussed in Section 3.3.

3.2.2 Electronic-structure methods

The resolution of the electronic time-independent Schrödinger equation (Eq. 3.8) allows the evaluation of molecular properties, such as electronic charges or dipolar moments. But more important, in order to perform a time evolution calculation of the nuclei, a previous knowledge about the energy of the chemical process is needed, in other words, some information about the shape of the PES must be provided. By solving the electronic time-independent Schrödinger equation on selected fixed geometries (thus assuming the validity of the BO approximation), it is possible to obtain information about the topology of a concrete electronic state. In this sense, the electronic calculations are not considered the goal, but the way to treat the dynamical problem.

The exact solution of the electronic time-independent Schrödinger equation can be obtained for one electron systems. However, as the number of

electrons within a molecule increases, the resulting electron-electron repulsion makes the quantum mechanical calculations much heavier and rapidly unfeasible. In this case, the only realistic alternative is to obtain approximate solutions of the electronic Schrödinger equation. To this end, three major approaches have been developed in quantum chemistry: (*i*) semiempirical methods, (*ii*) *ab initio* methods and (*iii*) electronic density functional based methods.

In a nutshell, semiempirical methods make use of an approximate Hamiltonian, which is simpler than the exact molecular Hamiltonian, and use parameters whose values are adjusted to agree with experimental data or with the results of a higher-level calculation. A very first example of semiempirical method is the Hückel approximation for the treatment of conjugated hydrocarbon derivatives. More modern contributions are the NDDO, CNDO, INDO, MNDO, AM1 or PM3 methods. In contrast, *ab initio* methods (from Latin "from first principles") use the correct molecular Hamiltonian and no other experimental values than the fundamental physical constants (like Planck's constant or the speed of light) and the atomic numbers of the atoms present in the molecule. On the other side, density functional based methods do not attempt to evaluate the molecular wave function, but the molecular electronic density ρ, from which the molecular electronic energy (among other properties) can be directly obtained by virtue of the Hohenberg-Khon theorem.[75]

In our studies we have not only dealt with chemical processes in the electronic ground state, but in electronic excited states. Hence, the careful choice of the best suited method for the system and the electronic state to compute is a very important step in the study. In our calculations, we have employed *ab initio* and electronic density functional based methods. Concretely, the Hartree-Fock (HF) and Density Functional Theory (DFT) methods have been used for ground state calculations, while Configuration Interaction with Single excitations (CIS), and Time-Dependent DFT (TDDFT) methods have been employed for excited electronic states calculations. Also, Complete

Active Space Self-Consistent Field (CASSCF) and CASSCF to second order perturbation theory (CASPT2) have been used for ground and excited electronic states.

It is not the aim of this chapter to introduce the theory and basics of such well-known electronic methods in theoretical chemistry. The interested reader may find all the desired information in a plethora of specialized text books.[75–77] However, a brief (and by no means self-consistent) description of the electronic methods employed in this thesis can be found in the Appendix B.

3.3 Beyond the Born-Oppenheimer approximation

The separation of the electronic and nuclear motion sets the correct theoretical background for the detailed analysis of the different energetic contributions within a molecule. Let us focus on the total potential energy ($U(\vec{Q})$ in Eq. 3.9). Given the multidimensional character of the nuclear coordinates $\vec{Q}$ and the fact that the total potential energy corresponds to a concrete electronic state ($U(\vec{Q}) = \hat{V}_{NN} + E_e$), $U(\vec{Q})$ is also called adiabatic hyper-PES, or just adiabatic PES. Hence, $U(\vec{Q})$ provides direct information of all the potential interactions a molecule can experience in an electronic state. This is probably one of the major achievements of the BO approximation, because many chemical processes can be rationalized in terms of the dynamics of the nuclei on a single BO adiabatic PES. However, chemical processes of nonadiabatic nature are ubiquitous in chemistry, specially in photochemistry and photobiology. Even though these processes can be understood in terms of the BO approximation, they cannot be studied from it. This forces the revision of the BO approximation in order to obtain a correct description of the dynamics of such phenomena.

3.3.1   Breakdown of the approximation

As we have explained in Section 3.2, the BO approximation is based in the difference of masses between nuclei and electrons. In other words, we make the assumption that nuclei are more inertial than electrons, and hence a small change in the nuclear distribution of a molecule should not significantly affect its electronic distribution. However, some additional requirements must be fulfilled to validate this assumption. In what follows, we present a very short adaptation of the excellent review of G. A. Worth and L. S. Cederbaum on the BO approximation,[78] in order to elucidate under which circumstances the BO approximation fails.

As we have previously seen, the time-independent Schrödinger equation (Eq. 3.7) presents a high degree of mathematical complexity for practically all the existing molecular systems. One of the most extended strategies to tackle this difficulty is known as the orbital aproximation. Let us supose a system depending on two coordinates, $\vec{x}_1$ and $\vec{x}_2$. The corresponding time-independent Schrödinger equation can be written as:

$$\hat{H}(\vec{x}_1, \vec{x}_2)\Psi(\vec{x}_1, \vec{x}_2) = E\Psi(\vec{x}_1, \vec{x}_2) \tag{3.10}$$

According to the orbital approximation, we start from the assumption that the different coordinates are not coupled. If $\vec{x}_1$ and $\vec{x}_2$ are independent, $\Psi(\vec{x}_1, \vec{x}_2)$ and $\hat{H}(\vec{x}_1, \vec{x}_2)$ can be expressed as a combination of two terms, each one depending on only one coordinate:

$$\Psi(\vec{x}_1, \vec{x}_2) = \psi_1(\vec{x}_1)\psi_2(\vec{x}_2) \tag{3.11}$$

$$\hat{H}(\vec{x}_1, \vec{x}_2) = \hat{H}_1(\vec{x}_1) + \hat{H}_2(\vec{x}_2) \tag{3.12}$$

Then, if we apply the Hamiltonian of Eq. 3.12 on the wave function in Eq. 3.11, having into account that each independent Hamiltonian will only act on its corresponding coordinate, we arrive at:

$$\hat{H}(\vec{x}_1, \vec{x}_2)\Psi(\vec{x}_1, \vec{x}_2) = (\hat{H}_1(\vec{x}_1) + \hat{H}_2(\vec{x}_2))(\psi_1(\vec{x}_1)\psi_2(\vec{x}_2)) =$$
$$= \hat{H}_1(\vec{x}_1)\psi_1(\vec{x}_1) + \hat{H}_2(\vec{x}_2)\psi_2(\vec{x}_2) = E_1\psi_1(\vec{x}_1) + E_2\psi_1(\vec{x}_2) \qquad (3.13)$$

The conclussion reached in Eq. 3.13 indicates that we can approximate the total energy of the system as the sum of two individual contributions:

$$E = E_1 + E_2 \qquad (3.14)$$

which are easier to obtain than the total energy E directly from Eq. 3.10.

With the orbital aproximation above in mind, let us focus now on the time-independent Schrödinger equation (Eq. 3.7), rewritten with the explicit contributions of the Hamiltonian operator:

$$\left[\hat{T}_N(\vec{Q}) + \hat{H}_e(\vec{q}; \vec{Q})\right]\Psi(\vec{q}, \vec{Q}) = E\Psi(\vec{q}, \vec{Q}) \qquad (3.15)$$

As we can see in Eq. 3.15, the molecular Hamiltonian is expressed as the sum of two terms, $\hat{T}_N(\vec{Q})$ and $\hat{H}_e(\vec{q}; \vec{Q})$, that act on the nuclear and electronic coordinates, respectively. This situation is partially reminiscent of the condition required in Eq. 3.12 for the orbital approximation, but not exactly the same as the electronic Hamiltonian has a parametrical dependence on the nuclear coordinates. However, a similar procedure as in the example above can be temptatively applied to solve Eq. 3.15.

We will focus first on the electronic Hamiltonian $\hat{H}_e(\vec{q}; \vec{Q})$. Given that the nuclear coordinates act as a parameter in the electronic Hamiltonian, for any value of $\vec{Q}$, its eigenvalues $\{V_i\}$ and eigenfunctions $\{\Phi_i\}$ can be found from:

$$\hat{H}_e(\vec{q}; \vec{Q})\Phi_i(\vec{q}; \vec{Q}) = V_i(\vec{Q})\Phi_i(\vec{q}; \vec{Q}) \qquad (3.16)$$

where the set of eigenfunctions $\{\Phi_i\}$ is complete and orthonormal. We can use these functions as a basis set to expand the wave function of the system

in order to solve Eq. 3.15. Then:

$$\Psi(\vec{q}, \vec{Q}) = \sum_i \chi_i(\vec{Q}) \Phi_i(\vec{q}; \vec{Q}) \tag{3.17}$$

where the $\chi_i(\vec{Q})$ functions are nuclear functions that act as the expansion coefficients. Note that Eq. 3.17 is reminiscent of Eq. 3.11. This expansion, known as the Born representation, is exact as long as the expansion is complete. It has been proved that the Born representation is valid for both bound and continuum states.[78] In order to obtain a solution for the expansion coefficients $\chi_i(\vec{Q})$, we replace Eq. 3.17 into Eq. 3.15 and multiply by one particular electronic function $\langle \Phi_j |$. This leads to:[†]

$$\sum_i \left[\delta_{ij} \hat{T}_N(\vec{Q}) + U_{ji}(\vec{Q}) - G_{ji}(\vec{Q}) - 2\vec{F}_{ji}(\vec{Q}) \hat{\vec{\nabla}}_N \right] \chi_i(\vec{Q}) = E\chi_j(\vec{Q}) \tag{3.18}$$

where the following shorthand matrix notation has been introduced:

$$U_{ji}(\vec{Q}) \; = \; \langle \Phi_j \mid \hat{H}_e \mid \Phi_i \rangle \tag{3.19}$$

$$G_{ji}(\vec{Q}) \; = \; \sum_\alpha \frac{1}{2m_\alpha} \frac{\langle \Phi_j \mid (\hat{\vec{\nabla}}_\alpha^2 \hat{H}_e) \mid \Phi_i \rangle}{U_{ii}(\vec{Q}) - U_{jj}(\vec{Q})} \tag{3.20}$$

$$\vec{F}_{ji}(\vec{Q}) \; = \; \sum_\alpha \frac{1}{2m_\alpha} \frac{\langle \Phi_j \mid (\hat{\vec{\nabla}}_\alpha \hat{H}_e) \mid \Phi_i \rangle}{U_{ii}(\vec{Q}) - U_{jj}(\vec{Q})} \tag{3.21}$$

where $U_{ji}(\vec{Q})$ is the total potential energy (as previously seen), and $G_{ji}(\vec{Q})$ and $\vec{F}_{ji}(\vec{Q})$ are known as the scalar coupling and derivative coupling, respectively.

[†]The full and rigorous derivation of the Born-Oppenhimer approximation is beyond the scope of this section. The interested reader can find a deeper and more complete discussion in Ref. 78.

The solution for the expansion coefficients $\chi_i(\vec{Q})$ in Eq. 3.18 is rigorously valid, as long as the expansion is complete and orthonormal for any given electronic basis set in electronic space. However, which basis to use is just a matter of convenience. In the concrete case that the choice is the basis set which diagonalizes $\hat{H}_e$, that is, the solutions of the electronic Schrödinger equation $\{\Phi_i\}$, then the coupling terms $U_{ji}(\vec{Q})$ $(i \neq j)$ vanish and Eq. 3.18 is reduced to:

$$\left[\hat{T}_N(\vec{Q}) + U_{jj}(\vec{Q})\right]\chi_j(\vec{Q}) - \sum_i \left[2\vec{F}_{ji}(\vec{Q})\hat{\vec{\nabla}}_N + G_{ji}(\vec{Q})\right]\chi_i(\vec{Q}) = E\chi_j(\vec{Q})$$

(3.22)

Eq. 3.22 is called the "adiabatic representation", and is mathematically exact as no approximation have been introduced. Besides, it is the standard procedure in most quantum chemistry applications. Note that Eq. 3.22 is equivalent to Eq. 3.15, but in a different representation.

If we now replace the multiconfigurational *ansatz* (Eq. 3.17) of the adiabatic representation, by a monoconfigurational wave function:

$$\Psi(\vec{q}, \vec{Q}) = \chi(\vec{Q})\Phi(\vec{q}; \vec{Q})$$

(3.23)

the adiabatic representation of the Schrödinger equation turns into:

$$\left[\hat{T}_N(\vec{Q}) + U_{ii}(\vec{Q}) - G_{ii}(\vec{Q}) - 2\vec{F}_{ii}(\vec{Q})\hat{\vec{\nabla}}_\alpha\right]\chi_i(\vec{Q}) = E\chi_i(\vec{Q})$$

(3.24)

Eq. 3.24 is known as the "Born-Oppenheimer Approximation", and it is the one we all learn in our quantum chemistry lessons. Moreover, if the derivative and scalar couplings are small, Eq. 3.24 can be even reduced further to:

$$\left[\hat{T}_N(\vec{Q}) + U_{ii}(\vec{Q})\right]\chi_i(\vec{Q}) = E\chi_i(\vec{Q})$$

(3.25)

which is called the "Born-Oppenheimer Adiabatic Approximation" or just the "Adiabatic Approximation" for short. As we can see, several BO approx-

imations exist, and proclaming that Eq. 3.24 is the only one is not totally true.

We can say that the Born-Oppenheimer approximation in Eq. 3.24 is expected to be accurate if the off-diagonal elements of the coupling are negligible, whereas the Adiabatic Born-Oppenheimer approximation in Eq. 3.25 will be valid if all coupling elements are negligible. In view of the m_α^{-1} dependence in $G_{ji}(\vec{R})$ and $\vec{F}_{ji}(\vec{R})$ in Eqs. 3.20 and 3.21, respectively, this seems to be always the case. However, this also depends on whether the numerator remains moderate in value. The mass relationship between nuclei and electrons is not the only justification for the adiabatic approximations. The nonadiabatic coupling also depends inversely on the energy gap between surfaces $U_{ii}(\vec{Q}) - U_{jj}(\vec{Q})$. Thus, when two adiabatic electronic states become totally degenerate, the derivative coupling becomes singular. Under such circumstances, the adiabatic representation exposed in Eq. 3.22) becomes meaningless, and the BO approximation is no longer valid. Nevertheless, some of these difficulties could be overcome if the original adiabatic electronic basis set could be transformed into a new representation for which the coupling terms in the kinetic energy operator ($\vec{F}_{ji}(\vec{Q})$ and $G_{ji}(\vec{Q})$ in Eq. 3.22) vanish:

$$\Phi' = \mathbf{S}\Phi \qquad (3.26)$$

where $\mathbf{S}$ is an unitary transformation matrix, and Φ' and Φ are the diabatic and adiabatic electronic basis sets, respectively. This is a so-called diabatic picture of the Schrödinger equation, in which the kinetic couplings are not present. However, in these representation the potential energy operator is no longer diagonal, but the potential energy coupling terms are at least smooth and well-behaved.

As we have explained in the Introduction, the degeneracy of two adiabatic electronic states is an ubiquitous phenomena in electronic excited states. It is a clear situation in which the BO approximation fails, and a quantum dynamical approach based in a diabatic picture is necessary. However, it is

necessary to obtain an accurate description of the topographical features of these special regions of the PES before any dynamical treatment could be performed.

3.3.2 Theoretical treatment of conical intersections

Undoubtedly, the computation of PESs is a much more difficult task for excited states as compared with the ground state. One has to deal with many types of excited states, each one requiring different amounts of electronic correlation and flexible one-electron basis functions able to describe all effects simultaneously. Also, the PESs of excited states involve a large number of minima, transition states, but specially, surface crossings and state couplings. Among these topographical features, CIs suppose an excellent subject for theoretical study, as very little information can be inferred from experimental data, and full characterization can only be achieved by accurate theoretical descriptions of the PESs. This is one of the few areas where apparently only theory can provide answers and explanations to real chemical problems.

From a mathematical point of view, a CI is defined as the set of molecular geometries (given a spatial and spin symmetries) where two special conditions meet: (i) the energy of two different electronic states are degenerate, and (ii) there is no interaction between these states. Hence, in a molecular system of N nuclear degrees of freedom, we say that we have a CI between two electronic states if the representation of the energy with respect to the N coordinates leads to an intersection along a "hyperline" of N-2 dimensions. The set of degenerate points that lie in this hyperline is called the intersection space, or seam. The remaining two dimensions that lift the energetic degeneracy of the system are known as the branching space, and are defined as:

$$\vec{g} = \frac{\partial(E_1 - E_2)}{\partial Q} \tag{3.27}$$

$$\vec{h} = \langle \Psi_1 \mid \frac{\partial \Psi_2}{\partial Q} \rangle \tag{3.28}$$

where the $\vec{g}$ and $\vec{h}$ vectors are also knwon as the gradient derivative (GD) and derivative coupling (DC) vectors, respectively. If the PESs are plotted as functions of these two coordinates, they form locally a cone centered at the degeneracy point. The name "conical intersection" comes precisely from this observation. D. R. Yarkony also proposed the name "diabolical conical intersections",[79] perhaps for its ressemblance to the diabolo toy or for the high degree of mathematical complexity they supossed in the chemical panorama.

Given the importance of CIs in photochemistry and photobiology, a lot of interest has been placed in the computation of geometries at the critical points within such crossings. The algorithms developed so far can be roughly grouped into three families: (i) techniques that minimize a Lagrangian including the constraints to maintain the degeneracy of the crossing states,[80–82] (ii) gradient projection based techniques,[83–85] and (iii) methods using a penalty function.[86] Very recently, a comparison of these three techniques has been published,[87] in which it is stated that the Lagrange-Newton technique needs the smallest number of iterations to converge to the minimum energy point of the CI. The gradient projection technique needs usually more iterations but converges to the same result, whereas the penalty function method frequently converges to a slightly different geometry and energy. Therefore, based on the convergence performance, the Lagrange-Newton method should be the first choice. However, it has been observed that the common Newton-Raphson algorithms employed in the most used quantum chemical packages cannot be easily adapted to this technique,[88] whereas modifications required by the projection technique are more straightforward.

Regardless which algorithm is used, it has to be implemented within a quantum electronic method, in order to solve the electronic Schrödinger equation and to obtain the energies of the two intersecting surfaces. At present, the most used electronic technique for such calculations is the CASSCF

method, given that the CASSCF wave function takes into account the multiconfigurational nature of CIs (see Appendix B). Nevertheless, it has been recently proposed that TDDFT methodologies, even though they do not properly describe the branching space, give a qualitative good description of the degeneracy points of the seam.[89] Being so, TDDFT would provide a much more economical alternative in the early search of CI, compared with the high-cost and less black-box character of multireferential methodologies.

In our calculations, the TDDFT method, implemented in the TURBO-MOLE 5.4 package,[90,91] has been chosen in order to search for CIs; while CASSCF and CASPT2 calculations (using the Newton-Raphson algorithm implemented in the quantum chemistry package MOLCAS 6.2[92]) have been employed to confirm the TDDFT results, as well as to provide accurate hints of $\vec{g}$ and $\vec{h}$.

3.4   Quantum nuclear dynamics

As previously said, the electronic aspect of a chemical problem provides the topology of the electronic state in which the nuclei will evolve, but it is the passage of time what provides the change of state of a system. The nuclear motion involved in many chemical processes (reactions in solution, biomolecular systems, solid state...) takes place in a range of nuclear masses large enough to adopt a classical physics treatment. In that case, the nuclei are treated as point masses which are governed by the Newton's equations of motion, and the state of the system (position, rate and acceleration of each nucleus) can be determined at any time. This kind of dynamical treatment is known as classical molecular dynamics. Besides, if the electronic energy of the system is calculated using parametrized force fields but not obtained from solving the electronic Schrödinger equation on the fly, the molecular mechanics method[93] is derived, which is widely used in theoretical chemistry for the treatment of large biological systems.

What happens if light nuclei play a relevant role in the process? It is a consequence of quantum mechanics that the concept of trajectories is meaningless in a quantum system, and a different treatment must be applied. The time evolution operator $(e^{-i\hat{H}t/\hbar})$ provides the correct description of the time evolution of a quantum system, which is the basis of quantum dynamics:[94]

$$|\Psi(t)\rangle = e^{-i\hat{H}t/\hbar}|\Psi_0\rangle \qquad (3.29)$$

where Ψ_0 is the initial *ket* vector of the system. Note that Eq. 3.29 is an equivalent way to rewrite Eq. 3.2. If the Hamiltonian is time-independent, the time evolution operator can be expressed in terms of its corresponding eigenvectors, and thus (3.29) can be rewritten as:

$$|\Psi(t)\rangle = \sum_E |E\rangle\, e^{-iEt/\hbar}\,\langle E|\Psi_0\rangle \qquad (3.30)$$

where the summation runs over all the eigenvectors $\{|E\rangle\}$ with eigenvalues $\{E\}$, which correspond to the energies associated to the Hamiltonian. Again, we can switch into a description of quantum mechanics based on wave functions rather than *ket* vectors. If we project our *ket* vectors into the space of nuclear coordinates $\vec{Q}$, Eq. 3.30 is rewritten as:

$$\Psi(\vec{Q},t) = \sum_E \Psi_E(\vec{Q})e^{-iEt/\hbar}\,\langle E \mid \Psi_0\rangle \qquad (3.31)$$

and hence, the dynamics of the nuclei will be described by the time-dependent nuclear Schrödinger equation:

$$i\hbar\frac{\partial\Psi(\vec{Q},\,t)}{\partial t} = \left[\hat{T}_N(\vec{Q}) + U(\vec{Q})\right]\Psi(\vec{Q},\,t) \qquad (3.32)$$

Given that we study chemical reactions in which the lightest atom of the Periodic Table is involved, the quantum nature of matter cannot be ignored, and a quantum treatment of the dynamics of the system is compulsory. This leads to the development of methods that solve approximately Eq. 3.32.

3.4.1 Theoretical methods for quantum nuclear dynamics

Once the topology of the PES is known at a reasonable good level of (electronic) calculation, including special critical points as CIs, it is time to perform the time evolution of the system.

The first numerical methods developed to solve (3.32) were based in an exact time propagation scheme. The wave function of the system is expanded in a time-independent primitive basis set, according to the expression:

$$\Psi(Q_1, \ldots, Q_f, t) = \sum_{j_1=1}^{N_1} \cdots \sum_{j_f=1}^{N_f} C_{j_1,\ldots,j_f}(t) \prod_{\kappa=1}^{f} \chi_{j_\kappa}^{(\kappa)}(Q_\kappa) \tag{3.33}$$

where f specifies the number of degrees of freedom, $Q_1, \ldots, Q_f$ are the nuclear coordinates, $C_{j_1,\ldots,j_f}(t)$ denote the time-dependent expansion coefficients, and $\chi_{j_\kappa}^{(\kappa)}$ are the orthogonal time-independent primitive functions for the degree of freedom κ. Each product of primitive functions, actually a Hartree product, is known as a configuration. The set of primitive functions $\{\chi_{j_\kappa}^{(\kappa)}\}$ conforms the primitive space *i.e.* the grid of points in which the problem of the time propagation will be numerically solved. The primitive space has to be large enough to contain the wave function during all the temporal evolution of the system, otherwise, the wave packet could explore regions of the space for which there is no definition, and the description of the system would be inaccurate.

The equations of motion for the coefficients $C_{j_1,\ldots j_f}(t)$ can be derived from the Dirac-Frenkel variational principle:

$$\left\langle \partial\Psi \left| \hat{H} - i\hbar\frac{\partial}{\partial t} \right| \Psi \right\rangle = 0 \tag{3.34}$$

Placing Eq. 3.34 in Eq. 3.33 leads to a system of N equations:

$$i\hbar\dot{C}_j = \sum_{f}^{N} \left\langle \chi_j \left| \hat{H} \right| \chi_f \right\rangle C_f \tag{3.35}$$

The advantage of applying a variational principle to the equations of motion is that the temporal derivative of the wave packet at each time, evaluated by the Hamiltonian, will be the one that will aproach variationally the solution of the time-dependent Schrödinger equation. The mathematical problem is that solving Eq. 3.32 involves a system of N (where $N = N_1 \times \cdots \times N_f$) first order coupled linear differential equations. Several specific integrators have been developed to solve this kind of equations, and deserve a special attention the Chebyshev[95] and Lanczos[96] algorithms. However, the main disadvantage of the exact temporal propagation is that the computational cost scales exponentially with the number of degrees of freedom f, which limits the treatment to no more of about 4 degrees of freedom at a time. The use of these methods in wave packet propagation are feasible if the dimensionality of the system is very reduced. If not, approximate methods have to be applied. In this thesis, we have employed three different approximate methodos in order to solve the time propagation of the wave packet: (i) the split-time propagator scheme, (ii) the spectral expansion and (iii) the MultiConfigurational Time-Dependent Hartree (MCTDH) method.

The split-time propagator scheme

Given a time-independent Hamiltonian defined as:

$$\hat{H} = \hat{T} + \hat{V}(\vec{Q}) \tag{3.36}$$

where $\vec{Q}$ is the set of coordinates upon which the PES of the corresponding electronic state is defined, the time evolution operator in Eq. 3.29 can be rewritten as:

$$e^{-i\hat{H}t/\hbar} = e^{-i(\hat{T}+\hat{V}(\vec{Q}))t/\hbar} \tag{3.37}$$

Hence, the temporal propagation of the system can be obtained by:

$$\Psi(t + \Delta t) = e^{-i(\hat{T}+\hat{V}(\vec{Q}))\Delta t/\hbar}\Psi(t) \tag{3.38}$$

Perhaps mimicking the properties of the exponential functions, it is tempting to rewrite Eq. 3.38 as:

$$\Psi(t + \Delta t) = e^{-i\hat{T}\Delta t/\hbar} \, e^{-i\hat{V}(\vec{Q})\Delta t/\hbar} \, \Psi(t) \tag{3.39}$$

which would make time evolution computation easier (note that the entities in the exponents are operators –matrices– and not scalars). However, because of the kinetic and potential energy operators do not commute, the time propagation of the system using Eq. 3.39 would cause propagation errors at each step. In order to minimize such errors, a split-operator propagator[97,98] can be applied over a short time interval Δt:

$$e^{-i\hat{H}\Delta t/\hbar} \approx e^{-i\hat{V}(\vec{Q})\Delta t/2\hbar} \, e^{-i\hat{T}\Delta t/\hbar} \, e^{-i\hat{V}(\vec{Q})\Delta t/2\hbar} \tag{3.40}$$

That is, during each time step the potential energy propagator is initially applied for half a time step; this is then followed by the kinetic energy propagator, which is applied a full time step, and finally, the potential energy propagator is applied for another half a time step. Since the potential energy operator depends directly on the position coordinates $\vec{Q}$ and the kinetic energy operator depends on its second derivatives, a direct evaluation of Eq. 3.40 with the wave packet expressed in a position representation would be fast for the $e^{-i\hat{V}(\vec{Q})\Delta t/2\hbar}$ term, but very time-consuming for the $e^{-i\hat{T}\Delta t/\hbar}$ term. However, if the wave packet can be expressed in a momentum representation, the time evaluation of $e^{-i\hat{T}\Delta t/\hbar}$ is as fast as applying the potential propagator on the wave packet in the position representation. In order to achieve this, a fast Fourier transform[99] can be applied to transform the wave packet from position to momentum representation (and vice versa) in between any two propagators in Eq. 3.37.

The spectral expansion

The resolution of Eq. 3.29 can be also carried out in a numerically exact manner. If the matrix representation of the nuclear Hamiltonian operator in

a concrete electronic excited state is diagonalized, its corresponding energies $\{E_i\}_{i=1,...,N}$ and eigenvectors $\{|\varphi_i\rangle\}_{i=1,...,N}$ can be obtained. Then, if completeness is assumed for the set of states (in practice, $N \rightarrow \infty$), the following spectral representation of the time evolution operator in the excited state can be accepted as exact:[100]

$$e^{-i\hat{H}t/\hbar} = \sum_{i=1}^{N} |\varphi_i\rangle e^{-iE_i t/\hbar} \langle \varphi_i| \tag{3.41}$$

Time evolution is obtained then in a straightforward manner by computing the wave packet at different t values with the following equation, which gives directly the amplitude of the wave function at time t:

$$\begin{aligned}\Psi(\vec{Q},t) = \langle \vec{Q} \mid \Psi(t)\rangle &= \sum_{i}^{N} \langle \vec{Q} \mid \varphi_i\rangle e^{-iE_i t/\hbar} \langle \varphi_i \mid \Psi_0\rangle \\ &= \sum_{i}^{N} \varphi_i(\vec{Q}) e^{-iE_i t/\hbar} \langle \varphi_i \mid \Psi_0\rangle\end{aligned} \tag{3.42}$$

The MCTDH method

The two previous methods for wave packet propagation are specially efficient when it is possible to reduce the dimensionality of our dynamical model to only one or two degrees of freedom. However, very often it is necessary to take into account the high dimensionality of a molecular system in order to get a very accurate description of the nuclear motion. As we have previously seen, Eq. 3.32 can be solved numerically, but the computational cost scales exponentially with the number of degrees of freedom. For the last years, different general algorithms have been developed, in order to overcome the size limitation imposed by the standard methods. Nowadays, the most used family of algorithms are based on the Time-Dependent Self-Consistent Field aproximation (TDSCF), also known as time-dependent Hartree.[101] In the TDSCF aproximation, the wave function of the system is expressed with one single time-dependent configuration, which is in fact a Hartree product:

$$\Psi(Q_1, \ldots, Q_f, t) = A(t) \prod_{\kappa=1}^{f} \varphi_{j_\kappa}^{(\kappa)}(Q_\kappa, t) \qquad (3.43)$$

where $A(t)$ is a complex number of modulus 1 (time dependent) which gives phase to the functions $\varphi_{j_\kappa}^{(\kappa)}$.

A multiconfigurational extension of the TDSCF aproximation has been found to provide a much improved description.[101] Among the algorithms derived from this multiconfigurational scheme, we should highlight the MCTDH method,[102, 103] developed at the University of Heidelberg by Prof. Hans-Dieter Meyer and collaborators. The MCTDH method has been computationally implemented in the MCTDH package,[104] which has been widely accepted in the quantum dynamic community, and it has also been successfully applied in multidimensional intramolecular proton transfer processes.[105, 106]

In the MCTDH method, the wave function is built as a linear combination of time-dependent configurations that adapt to the wave packet according to the Dirac-Frenkel variational principle. Thus, the number of configurations needed to achieve convergence is smaller with respect to the standard methods. The MCTDH wave function *ansatz* is:

$$\Psi(Q_1, \ldots, Q_f, t) = \sum_{j_1}^{n_1} \cdots \sum_{j_f}^{n_f} A_{j_1, \ldots, j_f}(t) \prod_{\kappa=1}^{f} \varphi_{j_\kappa}^{(\kappa)}(Q_\kappa, t) \qquad (3.44)$$

where $Q_1, \ldots, Q_f$ are the nuclear coordinates, $A_{j_1, \ldots, j_f}$ denote the MCTDH expansion coefficients, and $\varphi_{j_\kappa}^{(\kappa)}$ are the n_κ expansion functions for each degree of freedom κ, known as single particle functions. At a deeper level, each single particle function is expanded into a linear combination of time-independent base functions.

The main difference between the standard methods and the MCTDH method is that we do not have one, but two sets of equations of motion, corresponding to the $A_{j_1, \ldots, j_f}(t)$ coefficients and $\varphi_{j_\kappa}^{(\kappa)}(Q_\kappa, t)$ functions, called the A and φ vectors respectively. The dependence with time lies in these two

vectors. Once the Dirac-Frenkel variational principle (Eq. 3.34) has been applied onto Eq. 3.44, we obtain the MCTDH equations of motion:

$$i\hbar \dot{A}_J = \sum_L \langle \Phi_J | H | \Phi_L \rangle A_L \tag{3.45}$$

$$i\hbar \dot{\varphi}^{(\kappa)} = \left(1 - P^{(\kappa)}\right) \left(\rho^{(\kappa)}\right)^{-1} \left\langle \hat{H} \right\rangle^{(\kappa)} \varphi^{(\kappa)} \tag{3.46}$$

where the vectorial notation $\varphi^{(\kappa)} = (\varphi_1^{(\kappa)}, \ldots, \varphi_{n_\kappa}^{(\kappa)})^T$ has been introduced. For the interested reader, the definitions of the mean-fields $\langle \hat{H} \rangle^\kappa$, the density $\rho^{(\kappa)}$ and the projector P^κ can be found in Ref. 103, along with the detailed derivation of Eqs. 3.45 and 3.46.

This system of $2n$ coupled equations is clearly more complex than the system of N equations presented in (3.35). However, as it has been said, the MCTDH time-dependent base functions follow the wave function according to a variational principle at each time step, so much less basis functions are needed to reach convergence. Thus, the total number of $2n$ coupled equations to be evaluated is lower than the required N equations in Eq. 3.35. This is the key point on the efficiency of the MCTDH method, and it is possible to deal with processes involving more than 10 degrees of freedom.[107–109]

Among the different integrators developed to solve (3.45) and (3.46) efficiently, it is worth mentioning the constant mean field integrator,[110] which reduces the number of evaluations by a factor of 10. However, this integrator only works in an optimal way if the Hamiltonian can be expressed as a summation of products of one-dimensional operators:

$$\hat{H} = \sum_{r=1}^s c_r \prod_{\kappa=1}^p \hat{h}_r^{(\kappa)} \tag{3.47}$$

where $\hat{h}_r^{(\kappa)}$ operates only on the κth particle, and c_r represents the coefficient of the linear combination. Current implementations of the MCTDH method restrict the Hamiltonian of the system to be of the form of Eq. 3.47, which in fact means that the potential energy operator has to be of the same form.

3.5   Simulation of photoexcitation processes

A very important step in every dynamical simulation is the definition of the initial state *i.e.* the physical situation of the system from which the simulation starts. To overlook the careful choice of the initial conditions can lead to erroneous results. Usually, the availability of experimental data about the system helps in the design of the initial state. Given that ESIPT processes take place in excited electronic states, we need to determine which quantum state or ensemble of quantum states describe the system after it has been promoted to the excited electronic state.

Inmediately after the electronic excitation, by virtue of the FC principle, the electrons will be distributed according to the new electronic state but the nuclei would still keep the ground state nuclear configuration. Assuming that only the ground roto-vibrational state is populated right before the electronic excitation, the starting nuclear configuration at the excited state will hence correspond to this lowest roto-vibrational state.

It is possible to obtain the lowest roto-vibrational state of a system, by means of a relaxation calculation over the potential energy surface of the electronic ground state. The relaxation process is a procedure analogous to the time propagation. The only difference is that the time propagator operator $(e^{-i\hat{H}t/\hbar})$ is subtituted by the relaxation operator $(e^{-\beta\hat{H}})$, also known as Boltzmann's operator. This exchange of operators is possible, since an isomorfism between both operators exists. If we consider the following formal comparison:

$$\beta = \frac{1}{k_B T} \leftrightarrow \frac{it}{\hbar} \tag{3.48}$$

we can see that if we want to converge a ground state, we have to get the situation where only one state is populated *i.e.* $T \to 0 \equiv \beta \to \infty$, which is formally equivalent to:

$$\mid \Psi_0 \rangle = \lim_{t \to -\infty \cdot i} e^{-i\hat{H}t/\hbar} \mid \phi_0 \rangle \tag{3.49}$$
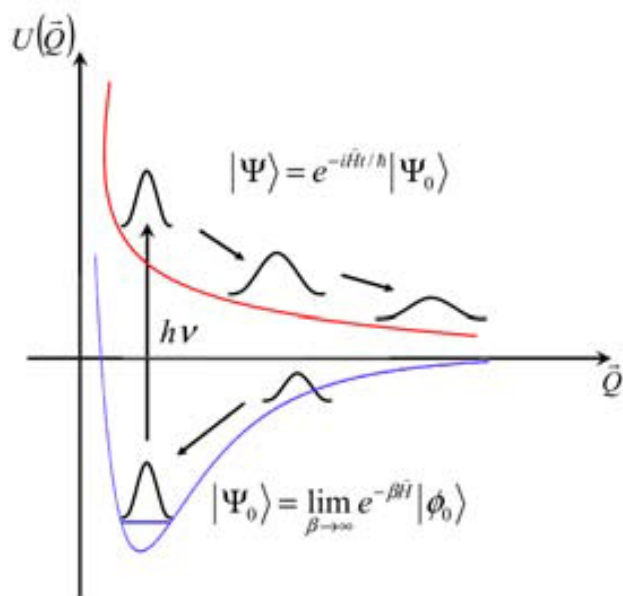
Figure 3.1: *Schematic representation of the simulation of a photoexcitation process from the quantum dynamical point of view.*

where $|\phi_0\rangle$ is an arbitrary state, and $|\Psi_0\rangle$ is the lowest ground roto-vibrational state. Hence, starting from an arbitrary wave packet and using the time propagator integrator, but making the time to be negative, imaginary and large, we will converge eventually to the lowest ground roto-vibrational state.

Given that the relaxed wave packet, obtained from Eq. 3.49, does not represent a stationary state of the excited state, it will spontaneously evolve after being placed in the FC arrival point, This evolution can be followed by means of the nuclear time-dependent Schrödinger equation, as depicted in Figure 3.1.

4

Objectives

"One never notices what has been done; one can only see what remains to be done."

Maria Skłodowska-Curie

ESIPT reactions are ubiquitous in nature, as we have emphasized in the Introduction, and are seldom found as standalone processes, but rather coupled to competitive processes or presenting multiple proton transfer paths. The careful study of such reactions is of great importance for the understanding of a wide variety of processes in chemistry, molecular biology and optical technologics. The most modern kinetic experimental techniques available today, allow the monitoring of ESIPT processes up to the order of the femtosecond. However, the experimental results are usually difficult to analyze, specially when multiple processes are involved. Those additional processes suppose an extra challenge in the study of this topic. In this sense, theoretical and computational chemistry represents a powerful tool of interpretation, given the absolute control that researchers can impose on modelized isolated systems.

The title of this thesis briefly summarizes its twofold nature. It could be said that this thesis will try to shed some light into the ESIPT subject, from a theoretical point of view. Besides, the methodological aspects of the electronic and dynamical approach to the problem are also considered.

We present a theoretical study encompassing from standalone ESIPT processes (for which a dynamical approach has been developed) to ESIPT coupled with non adiabatic processes. Hence, with the aim of exploring all these phenomena, the objectives proposed in this thesis can be regarded from two different perspectives. On one hand, the goals concerning the ESIPT as a chemical process are:

1. To verify the basic features that nowadays make ESIPT reactions some of the fastest chemical processes ever observed. For that purpose, the theoretical analysis of two molecular systems, HAN and SMA, that exhibit ESIPT isolated from competitive processes will be done.

2. To understand the effect that the presence of non adiabatic processes may cause, both in the energetics and dynamics of a typical ESIPT reaction. To do so, the electronic-structure and quantum dynamical study of the aromatic Schiff base SA will be performed.

3. To characterize the different pathways that multiple ESIPT systems may undergo after photoexcitation, and compare the basic features of these processes to those performed by their single homologues. This exploration will be performed on the three bipyridyl derivatives $BP(OH)_2$, $BP(NH_2)_2$ and $BP(OH)(NH_2)$.

4. To obtain, through quantum dynamical calculations, proton transfer times accurate enough to be compared with the experimental results. In a first stage, we will only consider the single proton transfer systems for such calculations.

5. To determine the characteristic time of a competitive non adiabatic channel to an ESIPT process, isolated from it. For this discussion, the SA system will be considered.

6. To analyze the feasibility, from a theoretical point of view, of molecules showing multiple proton transfers coupled to non adiabatic channels, as potential candidates for the design of bistable optical devices. This analysis will be based on the topological study of the ESIPT in the three bipyridyl derivatives $BP(OH)_2$, $BP(NH_2)_2$ and $BP(OH)(NH_2)$.

On the other hand, the objectives mentioned above would not be accomplished without the use of the proper methodology. Given the different degrees of chemical complexity we have to deal with, we have to employ a wide variety of theoretical methods that best fit for each situation. Hence, the proposed goals concerning the methodology employed are:

1. To compare the accuracy of reduced dynamical models of different dimensionalities, when employed in the calculation of ESIPT times. This comparison will be performed confronting a one-dimensional and a three-dimensional dynamical models for the HAN and SMA systems, respectively.

2. To test the suitability of cheap monoreferential electronic methods, in contrast to the more expensive multireferential methods, in the

study of ESIPT reactions coupled with non adiabatic processes. A comparative study on the photochemistry of SA using TDDFT and CASSCF/CASPT2 methods will be performed. In particular, we will check the efficiency of monoreferential electronic methods in the localization and characterization of conical intersections. To do so, the results obtained from the TDDFT study of the conical intersections presented in the SA system, will be compared with those at the CASSCF level of theory.

5

General results and discussion

- "Where shall I begin, please your Majesty?" She asked.
- "Begin at the beginning," the King said gravely, "and go on till you come to the end: then stop."

Lewis Carrol, *Alice's Adventures in Wonderland* (1865)

5.1 Standalone ESIPT processes: Papers I and II

In the first section of our general discussion, we will present the basic features that characterize a proton transfer reaction in an electronic excited state, and how to treat it from a theoretical point of view. In order to obtain accurate results and solid conclusions concerning only the ESIPT process, it is necessary to study those molecular systems for which, after photoexcitation and subsequent ESIPT, no evidences of competitive processes had been reported. In our studies, we have selected two systems which fulfill these requisites: 1-hydroxy-2-acetonaphthone (HAN) and salicylidene methylamine (SMA). Actually, it is not strictly true that these two molecules do not present any other chemical or physical process in the excited state, as functional groups rotations have been observed[64] for HAN and *cis-trans* isomerizations[111] for SMA. However, these additional processes usually present larger potential energy barriers than ESIPT, and they cannot take place until the proton transfer reaction is complete.

5.1.1 Molecular structural aspects of ESIPT

In many of the best known and most simple molecular systems that undergo ESIPT after photoexcitation, the hydrogen belonging to a (usually) hydroxyl group transfers to a neighboring nitrogen or oxygen atom. 2-(2'-hydroxyphenyl) benzoxazole derivatives (like HAN) and aromatic Schiff bases (like SMA) are some of the most extensively studied molecular systems that belong to this category, mainly due to the contributions of Prof. Lochbrunner[61–63] and Prof. Grabowska,,[57,59,111–115] respectively. For all these systems it has been shown that proton transfer does not occur in ground state. Nevertheless, after photoexcitation, ESIPT process proceeds within 50 fs and high fluorescent QY. As it has been said, these reactions present an endoergic profile and a high energy barrier in the ground electronic state, but this situation gets totally reversed in the excited electronic state. It is then natural
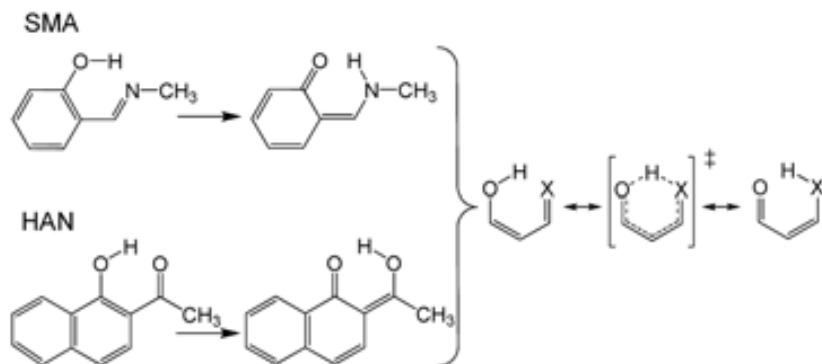
Figure 5.1: *Schematic representation of the ESIPT process in SMA and HAN, compared with the hydrogen transfer reaction in malonaldehyde.*

to wonder which changes take place with the electronic molecular structure of these systems after photoexcitation to produce such a fast phenomenon.

The ESIPT process proceeds in both systems from a a enol structure (for the alcohol group fixed to a double bond) to a keto tautomer (for the remaining ketone group), as depicted in Figure 5.1. If we compare the σ and π bond structure of HAN and SMA along the process, we will observe that the molecular region where the proton transfer takes place can be reduced to a malonaldehyde-like structure. This organic compound is well known in physical chemistry, as it has served as one of the simplest models for the study of hydrogen transfer reactions through tunnel effect in the ground state.[116,117]

It would be reasonable to assume that some of the chemical properties of malonaldehyde could play a role in the ESIPT process. We could also expect the ESIPT reaction to be fast, as for malonaldehyde the transition-state structure for the hydrogen transfer presents a six-membered cyclic structure and a high degree of electronic delocalization, as seen in Figure 5.1. In addition to this, the possibility of delocalization of the double bond would allow the keto form to revert to the original enol structure, thus, establishing a enol-keto equilibrium, or tautomerization. However, all these reasonings would lead us to a common mistake when studying processes in excited elec-
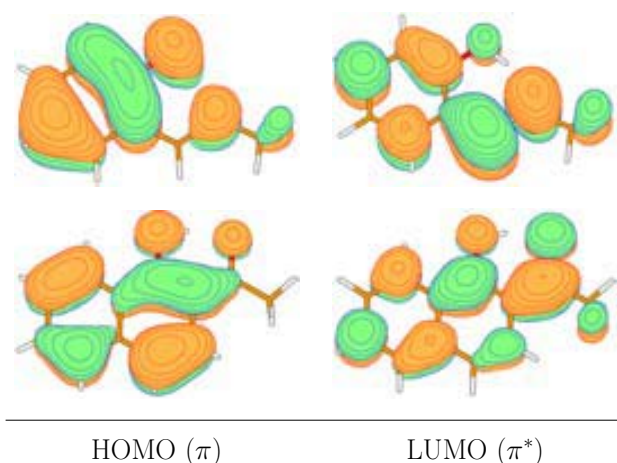
HOMO (π)   LUMO (π^*)

Figure 5.2: *Probability isodensity surfaces representation of the HOMO (left) and LUMO (right) for the SMA (top) and HAN (bottom) systems, obtained at the DFT/B3-LYP/6-31G(d,p) level of theory.*

tronic states. A discussion based on Lewis structures, as the one presented here, is meaningless in excited states, as the electronic distribution changes after the photoexcitation process. In other words, the chemistry of excited electronic states barely resembles the one on the ground electronic state. In fact, the hydrogen transfer reaction in malonaldehyde can take place in the ground electronic state, but it becomes disabled at the first electronic excited states;[118] in contrast to the ESIPT process in SMA and HAN. In light of this information, doubts arise when trying to explain the typical global reduction of the energy barrier in a ESIPT process, which is around 20 kcal mol^{-1}, in terms of just a malonaldehyde transition-state structure. It is then necessary to take one step beyond and observe the consequences of the photoexcitation process in the reactive and product species.

As we have previously commented, the ESIPT process is usually preceded by an HOMO (π) $\rightarrow$ LUMO (π^*) excitation between the ground (S_0) and first singlet excited states (S_1). Figure 5.2 shows the HOMO and LUMO molecular orbitals of the reactants species of SMA and HAN. If we compare both orbitals, we can see that the molecular orbital contribution over the donor atom decreases during the HOMO $\rightarrow$ LUMO transition, whereas it
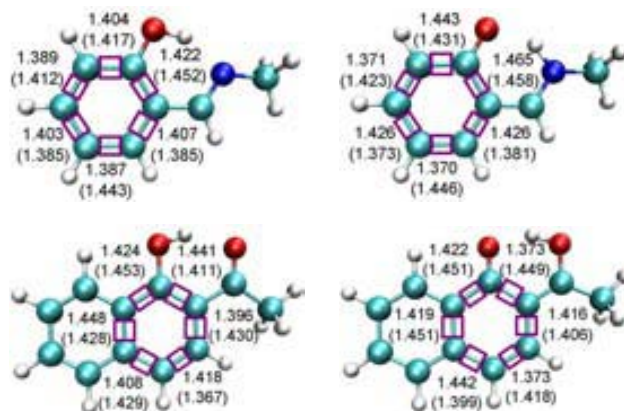
Figure 5.3: *Comparison of the S_0 and S_1, the latter in parentheses, interatomic distances corresponding to the phenolic ring (marked in lilac squares) for the enol (left) and keto (right) tautomers of SMA (top) and HAN (bottom). All values are expressed in Å. The optimized geometries in S_0 and S_1 have been obtained at the DFT/B3-LYP/6-31G(d,p) and TDDFT/B3-LYP/6-31G(d,p) levels of theory, respectively.*

increases for the acceptor atom. This fact points to a qualitative increase of the acid and basic characters of the donor and acceptor groups, respectively, thus favoring the proton transfer process and considerably decreasing the energy barrier.

Up to now, we have focused on a reduced representation of the molecular systems (malonaldehyde like-structure) to discuss the energetics of the ESIPT process in S_1. However, it is not possible to obtain a complete explanation for the inversion of the energetics in ESIPT processes without taking into account the whole molecular structure of our systems, *i.e.* the aromatic π system attached to the malonaldehyde like-structure.

If we observe again the schematic representation of the ESIPT process in Figure 5.1, we will see that the formation of the product species involves a substantial loss of aromaticity along the process, thus explaining the high energy barrier in S_0. We can check that from the values of the interatomic distances corresponding to the phenolic ring for the reactant and product species of SMA and HAN, depicted in Figure 5.3. More details are provided in Papers I and II about the localization of these structures. However, an explanatory comment is necessary here. The reactant species of SMA in S_1

and the product species of HAN in S_0, do not exist as energy minima. For this comparative discussion on the interatomic distances, we obtained the reactant species of SMA and the product species of HAN fixing the O–H distance and the hydroxy-methil dihedral angle, respectively (more details are provided in Papers I and II).

As we can see from Figure 5.3, the rank of the C–C bond distances increase from reactants to products in S_0, from 0.035 Å to 0.095 Å and from 0.052 Å to 0.069 Å in SMA and HAN, respectively. This is a clear indication of aromaticity loss. However, we should not forget that the chemistry of the ground state barely ressembles the chemistry of the electronic excited states. Indeed, the molecular orbital representation depicted in Figure 5.2 indicates an increase in the number of nodal planes from HOMO to LUMO. The reactant species have already lost a certain aromatic character after photoexcitation to S_1. If we calculate the range of the C–C bond distances in the reactant species between S_0 and S_1, we will observe an increase from 0.035 Å to 0.067 Å and from 0.052 Å to 0.086 Å in SMA and HAN, respectively. This effect is notably weaker in the product species, as they have already lost the aromatic character in S_0. The highest destabilization of the reactants in S_1 when compared to products leads to an inversion of the energy profile in S_1, which seems to be characteristic of ESIPT process.

5.1.2   Comparison of reduced dynamical models

We should not forget that one of the main goals of the present thesis is to obtain quantitative values of transfer times for proton transfer processes. To this end, after the electronic structure study of the systems is finished, one can proceed with the dynamical simulation of nuclear motion. However, for some reasons dynamical calculations are not so straightforward as electronic calculations. First, the potential energy operator included in the electronic Hamiltonian presents a well-defined analytic expression, which can be efficiently coded and hence the plethora of quantum chemistry software package. Thus, the electronic Schrödinger equation can be easily solved with

black-box procedures. In contrast, the nuclear energy operator depends on the internal coordinates, and the nuclear potential energy has to be calculated for every system. Second, the energy difference between ground and excited electronic states can be up to the order of several eV, whereas nuclear states are separated by energies of the order of a few cm^{-1}. Thus dynamical calculations are in essence multiconfigurational. And last but not least, we would like to focus on the fact that the nuclear kinetic energy operator strongly depends on the set of dynamical coordinates chosen to describe the dynamics of the system. There may exists few general sets of coordinates for which the expression of $\hat{T}_N$ has been derived *e.g.* Jacobi coordinates for 3-atom systems.[94] However, the most convenient set of coordinates, the one that better fits the dynamics of a given chemical reaction, rarely coincide with an already fixed set of coordinates. Hence the nuclear kinetic energy operator must be derived for that specific set of coordinates from scratch.

It is important to describe the system with a dynamical model simple enough to derive (if possible) an expression for the corresponding kinetic energy operator, but at the same time retaining the most basic features of the chemical process we want to simulate. In order to give some concrete examples, we will show in detail the dynamical model employed in our dynamical calculations on SMA.

Ideally, in order to perform a rigorous quantum dynamical study, every molecular coordinate should be taken into account (see the SMA molecular structure in Figure 5.4 (a) and (b)). However, this suposes a daunting task, even for small systems. The experimental data collected for a concrete chemical reaction can be used in order to decide which molecular coordinates should be relevant and which ones not to describe the physical representation of a reaction. By the time of our study on SMA, no experimental information about the dynamics of the ESIPT process was available. However, the dynamics of related aromatic Schiff bases *e.g.* salicylideneaniline (SA)[57] described the process as ultrafast. Therefore, it seems a reasonable assumption to restrict the motion of the proton to the molecular plane containing, at
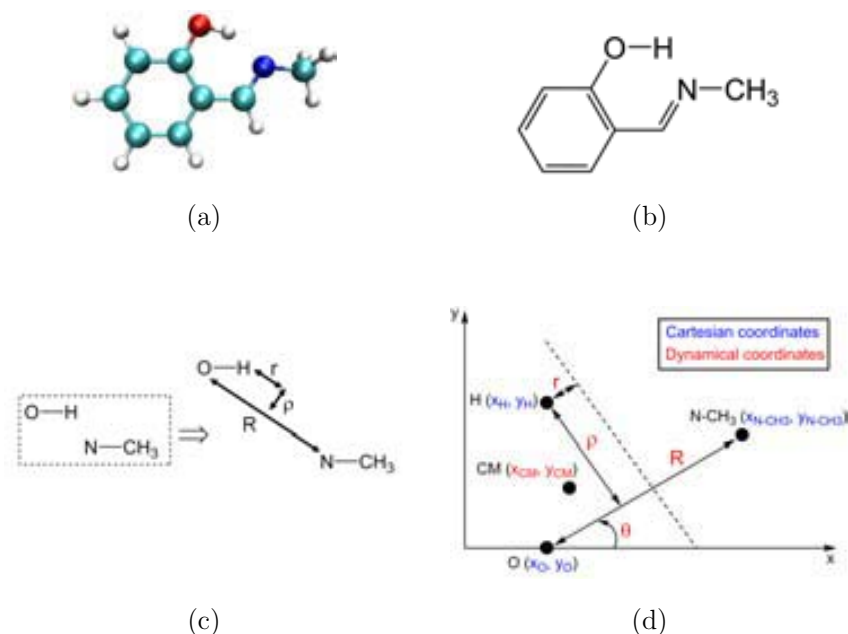
Figure 5.4: *Modelling process of the dynamics of SMA: abstraction of the ESIPT process from the molecular structure (a) to the Cartesian representation of the dynamical coordinates (d).*

least, the donor and acceptor atoms. In addition, it has been known that besides the position of the transferring proton, the distance between the donor and acceptor atoms is of great importance for the ESIPT, and should be included in the simulation.[119, 120] With all this information, we designed a set of three coordinates relevant for the proton transfer process: (i) the distance between the oxygen and nitrogen atoms R, (ii) the distance between position of the hydrogen atom and the mediatrix of the O–N segment r, and (iii) the distance between the position of the hydrogen atom and the straight line linking the donor and acceptor atoms at any time ρ. This set of dynamical coordinates are depicted in Figure 5.4 (c). Given the approximations introduced in this set of coordinates (see Paper II for more details), the SMA molecule is broken-up in three structureless fragments as for the ESIPT is concerned: the proton, the oxygen atom (attached to the aromatic ring) and the nitrogen-methyl segment.

The next step is the derivation of the mathematical expression for the nuclear kinetic energy operator. The strategy to achieve this is to start from the expression of the nuclear kinetic energy operator in Cartesian coordinates, and then to establish the mathematical relationships between the dynamical and Cartesian set of coordinates. In the SMA case, only two Cartesian coordinates (x, y) are necessary to locate each of the three fragments of the model in a plane. Given that both sets of coordinates define the same subspace, we included three additional dynamical coordinates: the Cartesian coordinates of the center of mass (x_{CM}, y_{CM}) and the in-plane global rotation angle θ. The Cartesian representation of both coordinates systems is displayed in Figure 5.4 (d).

The process followed to obtain a final expression for the nuclear kinetic energy operator in terms of (R, r, ρ) can be summarized in the four images depicted in Figure 5.4. This can be seen as the deconstruction process of the SMA molecule, given that each step increases the degree of abstraction; from a concrete molecular structure to the pure mathematical description of the relationships between different coordinate systems. However, even the last step still retains the essentials of the proton transfer process, which is the most important property of any dynamical model.

The mathematical relationships between dynamical and Cartesian coordinates (see Appendix for the complete development), allow us to obtain an analytic expression of $\hat{T}_N(R, r, \rho)$ (after the convenient algebraic manipulation):

$$
\begin{aligned}
\widehat{T}_N = \ & -\frac{1}{2}\left(\frac{1}{m_{N-CH_3}} + \frac{1}{m_{O-ring}}\right)\frac{\partial^2}{\partial R^2} \\
& -\frac{1}{2}\left[\left(\frac{1}{m_{N-CH_3}} + \frac{1}{m_{O-ring}}\right)\left(\frac{1}{4} + \frac{\rho^2}{R^2}\right) + \frac{1}{m_H}\right]\frac{\partial^2}{\partial r^2} \\
& -\frac{1}{2}\left[\left(\frac{1}{m_{N-CH_3}} + \frac{1}{m_{O-ring}}\right)\left(\frac{1}{4} + \frac{r^2}{R^2}\right) + \frac{r}{R}\left(\frac{1}{m_{N-CH_3}} - \frac{1}{m_{O-ring}}\right) + \frac{1}{m_H}\right]\frac{\partial^2}{\partial \rho^2}
\end{aligned}
$$

(Continues on next page.)

$$
\begin{aligned}
+ \ & \frac{1}{2} \left(\frac{1}{m_{N-CH_3}} - \frac{1}{m_{O-ring}} \right) \frac{\partial}{\partial R} \frac{\partial}{\partial r} \\
+ \ & \left[\frac{r\rho}{R^2} \left(\frac{1}{m_{N-CH_3}} + \frac{1}{m_{O-ring}} \right) + \frac{\rho}{2R} \left(\frac{1}{m_{N-CH_3}} - \frac{1}{m_{O-ring}} \right) \right] \frac{\partial}{\partial r} \frac{\partial}{\partial \rho} \\
- \ & \frac{1}{2R} \left(\frac{1}{m_{N-CH_3}} + \frac{1}{m_{O-ring}} \right) \frac{\partial}{\partial R} \\
+ \ & \frac{1}{2} \left[\frac{1}{R} \left(\frac{1}{m_{N-CH_3}} - \frac{1}{m_{O-ring}} \right) + \frac{r}{R^2} \left(\frac{1}{m_{N-CH_3}} + \frac{1}{m_{O-ring}} \right) \right] \frac{\partial}{\partial r} \\
+ \ & \frac{\rho}{2R^2} \left(\frac{1}{m_{N-CH_3}} + \frac{1}{m_{O-ring}} \right) \frac{\partial}{\partial \rho} & (5.1)
\end{aligned}
$$

At this point we should highlight that the oxygen atom and the aromatic ring have been considered as a whole entity of mass m_{O-ring}. Considering the relative motion of the oxygen atom with respect to the aromatic ring would lead to a more exact expression of $\widehat{T}_N$. However, additional degrees of freedom concerning the relaxation of the ring should be included, raising the complexity of the dynamical model beyond a three-dimensional representation. Hence, the expression obtained in Eq. 5.1 is approximate. Given that in the present general discussion of results we do not focus on the validity of the model, the reader is adressed to Paper II for more details on the subject.

Our quantum dynamical simulations performed with the kinetic energy operator in (5.1) provided a proton transfer time of 11 fs. Even though there is no experimental evidence on the excited state proton transfer time for SMA, it has been observed for a wide variety of aromatic Schiff bases that their characteristic transfer times lie below the detection limit of the most usual spectrometers at the time $i.e.$ below 50 fs.[74, 115] Our theoretical results agree with these experimental findings.

Let us now compare the quantum dynamical model of SMA with the one designed for HAN, in terms of accuracy and mathematical complexity. By the time of our study in HAN, there were more experimental data available about the photophysics of HAN[64, 121, 122] in comparison with SMA. The ES-IPT process in HAN has been described also as an ultrafast process, for which the rest of the molecular skeleton remains unmodified for times substantially

longer than that of the proton transfer itself.

With these considerations, we employed a monodimensional approach for the dynamics of HAN. Concretely, the system was modelized by simply taking the O–H distance and minimizing the energy of the molecule for different bond distance values. After that, every geometry obtained were referenced to each other within an isoinertial coordinate system s. By assigning $s = 0$ to the geometries where the O–H distance matched that of the reactant's potential energy minimum in S_0 (see Paper I for details), the s value for a given structure represents the arc-length distance in configurational space in mass-weighted units of such structure to that which is closest to the minimum in S_0. This approach has been shown to be successful in simplified dynamical studies.[123,124] Proceeding in this fashion, the 1-dimensional nuclear kinetic energy operator simply remains as:

$$\widehat{T}_N = -\frac{\hbar^2}{2}\frac{\partial^2}{\partial s^2} \tag{5.2}$$

Notice that mass is included in the definition of s. Our dynamical simulations in HAN showed that ESIPT was completed within 25.5 fs, in remarkable good agreement with the experimental result of 30 fs.[64]

The difference in mathematical complexity between equations (5.1) and (5.2) is obvious, but other aspects as mathematical derivation or coding implementation must be taken into account. The expression of $\widehat{T}_N$ for HAN is simpler, easier and faster to obtain and implement than the one for SMA. In addition, both expressions provide a comparable level of accuracy in the proton transfer time prediction. Even though many proton transfer processes exist for which a multidimensional treatment of the dynamics becomes compulsory, for ultrafast intramolecular proton transfer processes a reduced monodimensional model is good enough to provide an accurate description of the chemical reaction.

As a final note, we should never forget that any result or conclusion obtained within a given dynamical model directly derives from the physics included in the model, and not from the "real" physiscs of the system. Thus,

we always must be aware of the properties and approximations introduced in the model.

5.1.3 On the reliability of the dynamical simulations

In our studies on HAN and SMA, we have employed two different methods in order to propagate the wave packet's system: the spectral expansion and the MCTDH method, respectively. While the former is well suited for one-dimensional models, the latter is a more robust method that allows the simultaneous treatment of several dynamical coordinates. An important difference between a one-dimensional and a multi-dimensional design of the dynamical model is that the latter allows the analysis along every dynamical coordinate. This can be very useful when trying to determine if a concrete coordinate is relevant for the chemical reaction, as we do in Paper I. In any case, both methods perform the temporal propagation of a wave packet which has been modeled after a reduced dynamical representation of the real system. This feature must be taken into account when analyzing the reliability of the results.

When the time-dependent nuclear Schrödinger equation (Eq. 3.32) has been solved, and hence the wave packet has been propagated in time, the estimation of the proton transfer time can be carried out in several different ways. Concretely, we have defined the proton transfer time from the reactants' disappearance rate *i.e.* the probability to find the system in the reactants region of the PES at a given time. Hence, we have computed the fraction of the probability density function that remains still in the reactant's region, which is also known as survival probability:

$$P(t) = \int_R \mid \Psi(\tau) \mid^2 d\tau \qquad (5.3)$$

where $d\tau$ is the volume element and R denotes the reactant's configurational space.
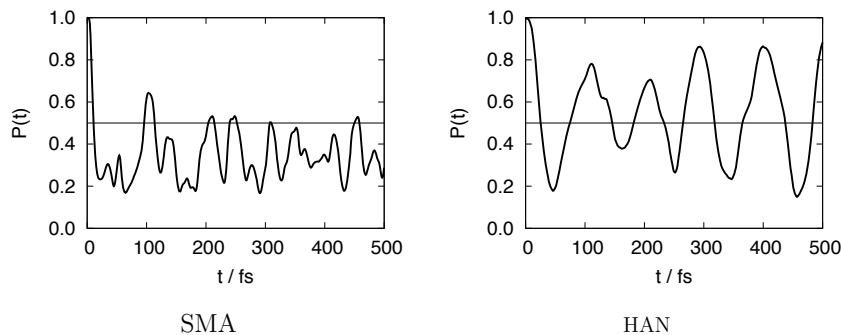
Figure 5.5: *Survival probability function of the reactant especies of SMA (left) and HAN (right) in S_1 after photoexcitation*

In order to obtain a quantitative value for the proton transfer rate, we assume that the time needed to bring $P(t)$ to a value of 0.5 (half of the systems evolved to products) is representative of the time measured experimentally. Figure 5.5 depicts the survival probability function obtained for SMA and HAN. The obtained values for the proton transfer rates are already discussed in Paper I and II. Here we would like to focus on the periodic behaviour observed in the survival probability function.

Undoubtedly, the resonant features observed in Figure 5.5 are not representative of the real system and are unlikely to be found in experimental measures. At large values of time, the real system would have activated other molecular motions that would allow the excess of kinetic energy to "spill" over the different degrees of freedom of the molecule, in this way reducing the kinetic energy of the proton. However, as our reduced dynamical models do not include such degrees of freedom, the systems are forced to bounce between the reactants and products regions. Indeed, the periodic behavior in the survival probability function of SMA is less pronounced, as more degrees of freedom have been included in comparison with HAN. We must take into account that the behavior of the modelled and the real systems will eventually diverge with time. The simulation can be considered as "meaningful" if these recurrences set on after the ESIPT process has been completed.
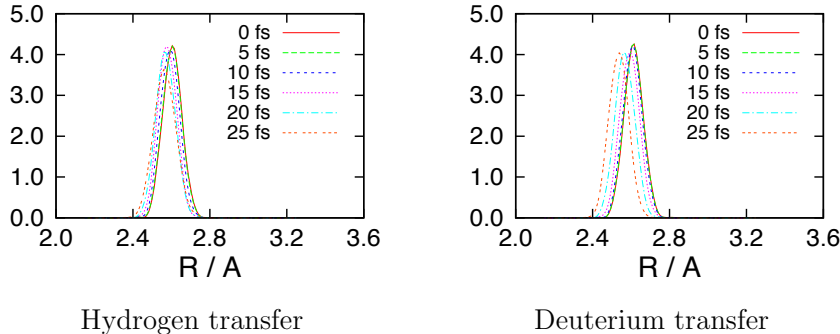
Hydrogen transfer   Deuterium transfer

Figure 5.6: *One-dimensional probability densities of the R coordinate at different times for the hydrogen (left) and deuterium (right) transfer. The coordinates are described in Figure 5.4 (c).*

5.1.4 Mechanistic insights into the proton transfer process

Proton transfer rates are not the only information we can obtain from the theoretical study of ESIPT processes. It is also possible to give some mechanistic information about how the proton transfer proceeds. ESIPT processes have been generally described as ballistic motions *i.e.* the proton transfer motion takes place before any other internal mode can be significantly coupled to it. Through electronic and (more directly) dynamical calculations, we can discern whether the proton transfer is assisted by other motions or not.

If we recall the definition of our reduced dynamical model for SMA (see Figure 5.4), the approach motion between the donor and acceptor atom is included within the coordinate R. As previously mentioned, the multi-dimensional character of a dynamical model allows the analysis of the system's time evolution along a concrete coordinate. Hence, we can observe the evolution of the R coordinate along the dynamical simulation, in order to estimate the degree of coupling with the proton transfer coordinate r.

Figure 5.6 depicts the time evolution of the wave packet's propability density along the R coordinate (the approach between the donor and acceptor atoms) for the first 25 fs of propagation. As we can see, within the dynami-

cal model designed for SMA, the wave packet does not expand significantly along the R coordinate during the simulation time. Even though this results point towards a ballistic motion for the ESIPT process in SMA, this point deserves a deeper analysis. As we have explained before, the kinetic energy operator (5.1) is approximate as we do not have considered the motion of the oxygen atom relative to the aromatic ring. This approximation may have an important effect in the mechanism of the proton transfer, given that the larger mass of the O–ring fragment in comparision with the N–CH$_3$ fragment may prevent the oxygen atom from approaching the nitrogen atom. In order to overtake the limitation of our own model but without increasing its mathematical complexity, we have considered that the oxygen atom carries out most of the internal motion while the aromatic ring remains static by virtue of its larger mass. In this way, we allow the donor and acceptor atoms to approach during the proton transfer process. This can be easily estimated by setting m_{O-ring} in (5.1) to simply m_O. Doing this, we have checked that the proton transfer process proceeds with negligible changes in R.

We have also studied the deuterium transfer process for SMA in order to compare with the previous results. As expected, the probability density of the deuterated system shows significant evolution along shorter values of the R coordinate, as we can see in Figure 5.6. Due to the heaviness of the deuterium atom, the deuterium transfer is slower than the proton transfer, and hence the R coordinate has enough time to be activated and assists the deuterium transfer.

What can be said about the proton transfer mechanism of HAN? First of all, we have to take into account that the mono-dimensional dynamical simulation performed in HAN does not allow to analyze the evolution of the system along a concrete coordinate, as seen for SMA. The evolution of heavy atoms is built-in and inseparable with those of light atoms in the unidimensional coordinate s. Instead of performing a new (and mathematically more complex) dynamical simulation including more degrees of freedom, we chose to carefully look at the experimental data available on the ESIPT of HAN
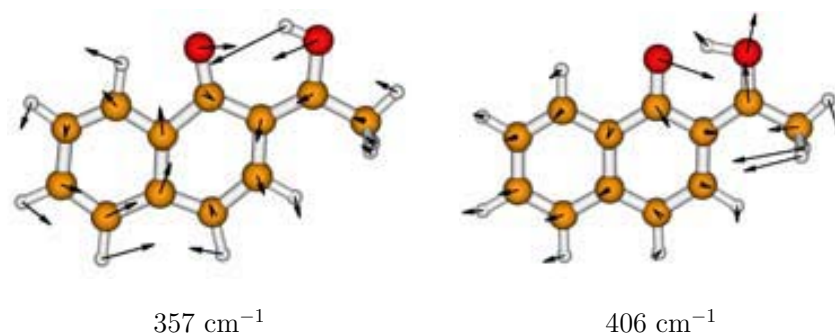
357 cm^{-1} 406 cm^{-1}

Figure 5.7: *Representation of the normal vibrational modes of the products of HAN in S$_1$ most coupled with the proton transfer process. Frequencies have been obtained at the TDDFT/B3-LYP/6-31G(d,p) level of theory.*

(remember that very few experimental data have been reported for SMA), and study it in view of our electronic calculations.

The most recent experimental work on the photophysics of HAN, reported by Lochbrunner *et al.*,[64] established the proton transfer time in about 30 fs, being this the time interval between the photoexcitation of the reactants and the rise of the fluorescence band (attributed to the photoproduct species). In addition, oscillatory contributions in the time-resolved spectrum after electronic excitation of HAN were observed, which were attributed to vibrations that are coupled to the proton-transfer coordinate. These oscillatory contributions were ascribed to motions that facilitate the transfer, like the two oxygen atoms coming closer, so that the proton transfer may proceed with assistance. Even though these oscillatory motions are not likely to contribute on the proton transfer process of HAN, given that internal vibrational modes do not usually activate before 30 fs, Lochbrunner *et al.* compared the vibrations obtained through Fourier transforms of the oscillatory time-resolved transmission signal with the calculated frequencies of the reactant form in S$_0$, in order to identify such modes.[64]

In our electronic study of HAN, we have carried out the full harmonic frequency analysis of the reactant and product species of HAN in S$_0$ and S$_1$ through numerical derivation of the first energy derivatives at the TDDFT level, in order to compare with the experimental results (see Paper I for

details). From the time-resolved experiments,[64] it has been established that only three frequencies are involved in the oscillatory contributions of the time-resolved spectrum. These frequecies amount to 280, 312 and 368 cm^{-1}, and they should be assigned to specific frequencies of the products in the S_1 state. In our theoretical vibrational analysis of the product, the closest values to these are found at 295, 357 and 406 cm^{-1}, so that these frequencies ought to be taken as the ones most directly coupled to the proton-transfer coordinate. In fact, the two higher ones, depicted in Figure 5.7, correspond to modes where motion indicates a clear approximation of the two oxygen atoms and the hydrogen atom. However, in the present case these modes are coupled to the ESIPT process in S_1 in the sense that the proton transfer activates them, not that they facilitate the process.

5.2 Non adiabatic ESIPT processes: Paper III

This second section of general discussions is exclusively devoted to one molecular system, the aromatic Schiff base salicylideneaniline (SA). This system is of special interest and deserves a whole section in itself because it exhibits an ESIPT process for which the presence of competitive non adiabatic processes, more concretely CIs, has been reported,.[125] Hence, SA is a perfect candidate to present the basic features of an ESIPT system competing with non adiabatic processes, and to show how CIs can be accurately described with the electronic methods available. Also, this section serves as a link between the systems that have been presented in the previous section (papers I and II), and those that will be introduced in the next section (articles IV and V), in which the chemical phenomenon reaches the maximum level of complexity with double proton transfer processes coupled with non adiabatic processes. Finally, it is worth noting that all the conclusions obtained in the previous section concerning generalities on ESIPT process can perfectly be applied to SA.

5.2.1 Effects of non adiabatic proccesses on SA

In the Introduction it has been commented that the aromatic Schiff bases are among the most studied compounds in photochemistry, due to their photochromic behavior.[2,126,127] The study on the SMA system depicted in Paper II served us as a first approximation to such a large family of photochromic compounds. Without any doubt, its best known and thoroughly studied member is SA, and the countless studies published on this system[57,58,60,74,111–115,125,128–139] are a proof of it. However, the detailed mechanism about the ESIPT process of SA (depicted in Figure 5.8), and more concretely the time scale for the ESIPT process are still under hot discussion.
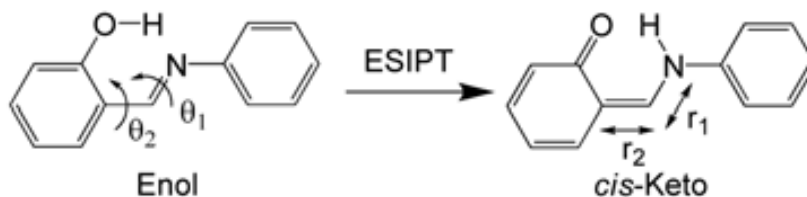
Figure 5.8: *ESIPT process representation in SA. θ_1, θ_2, r_1 and r_2 represent the relevant dihedral angles and bond distances that are discussed in the present section.*

During the long span of time that exists between the different works on SA (from 1964 to 2007), very different time scales for the ESIPT process, from nearly 750 fs[60,125] to less than 50 fs,[74] have been proposed. What is clearly known is that the absorption spectrum of SA presents a band at 344 nm[131] attributed to the photoexcitation of the enol tautomer to a (π,π^*) excited state, and a fluorescence band (largely Stokes-shifted) that is centered at around 570 nm, which is attributed to an excited *cis*-keto form. However, a very low fluorescence QY has been measured (1.2×10^{-4}),[115] and this result strongly suggests the presence of an efficient deactivation path of the electronically excited species. Indeed, such deactivation channels are the main reason behind the discrepancy between the measured time scales for SA.

Several studies have been reported both from the experimental and theoretical point of views, in order to identify these deactivation channels and obtain a clear picture of the photophysics of SA. The studies from Tamai and collaborators[58] have glimpsed these non-radiative processes via spectrocopic measures, which have been assigned to an IC of the excited enol tautomer between S_1 and S_2. However, the fate of the excited enol species in S_2 is not clarified in that work. On the other hand, according to the experimental work of Sekiya and collaborators,[60] not only one but two fast depopulation channels have been detected. They suggest the presence of a first IC from the excited (π,π^*) enol to a (n,π^*) state, and a second IC from the excited (π,π^*) *cis*-keto again to a (n,π^*) state. The photochemical landscape suggested by Sekiya and collaborators for SA is schematically reproduced in Figure 5.9.
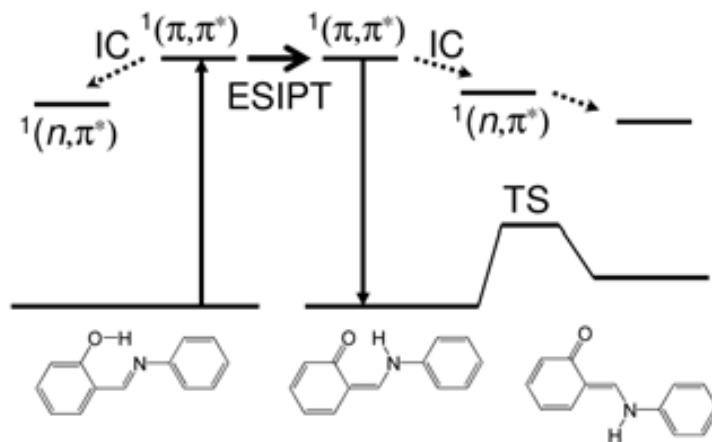
Figure 5.9: *Photoexcitation processes of SA inferred from the studies of Sekiya and collaborators.[60] IC, ESIPT and TS stand for internal conversion, excited state intramolecular proton transfer and transistion state. Figure inspired in Figure 7 of Ref. 60*

Note that the IC processes located in the region of the enol tautomer prevent the ESIPT reaction to take place, and hence directly compete with it. In clear disagreement with these hypothesis, the most recent work of Peón *et al.*[74] suggests a ballistic motion of the transferred proton without interference of any competitive process.

On the theoretical side, only the works of Zgierski and Grabowska[59] have dealt with the dynamics of SA using approximate methods. Their results coincide with the findings of Sekiya and coworkers,[60] and proposing the existence of two IC, one after photoexcitation of the enol tautomer, and the other after the formation of the *cis*-keto tautomer.[59]

Regarding all this information, one could say that the presence of deactivation channels of the excited state that directly compete with the ESIPT process make interpretation of experimental measures difficult, and the results are apparently contradictory. Hence, the ESIPT process of SA might not match a simple ballistic motion of the transferred proton, as predicted for SMA. Given the absolute control that the theoretical chemist can impose on the parameters defining his/her modeled representation of the chemical system, a theoretical study looks desirable to clarify the possible channels

through which the SA might evolve in the excited state. However, in oder
to obtain results of physical relevance, the regions of the PES that present
IC channels must be represented with an appropiate electronic method of
calculation. Previous studies[140–146] reported on different systems undergo-
ing ESIPT processes have revealed that IC proceed mainly through conical
intersections (CIs). For that reason, in what follows we will focus on the
localization and characterization of CIs that may cause the deactivation of
the excited state.

5.2.2 Localization of conical intersections

In the Introduction we have listed several algorithms developed to locate
geometry points belonging to the seam of a CI. However, no matter which
algorithm is used, such a search is not a simple task unless one is lucky
or smart enough to know where the CI is to be found. The availability of
experimental data about the photophysics of the system can be of great help
in order to get a first glimpse of where the CI may lie. The very low QYs
measured for SA clearly indicate that the CI we are looking for might bring
the system from an excited electronic state to S_0.

As we have previously said, the work of Sekiya and collaborators[60] pointed
towards two ICs, the first being located in the region of the enol tautomer
between a (π,π^*) and a (n,π^*) states. The theoretical work of Zgierski and
Grabowska[59] provided more details indicating that this IC take place at a
twisted conformation of the enol tautomer along the θ_1 dihedral angle (see
Figure 5.8 for the definition of θ_1). As a first approximation, we optimized the
ground state energy profile at the DFT level along the rotation of the angle
in the enol tautomer, and then computed the TDDFT vertical transitions for
the four lowest singlet excited states (see Paper III for more computational
details). According to our results depicted in Figure 5.10, at the initial pla-
nar structure (180°) the lowest (n,π^*) state corresponds to the third excited
singlet state (S_3). Such state lies $\sim$15.0 kcal mol^{-1} above the FC excita-
tion point and is thus energetically unreachable. In addition, this state does
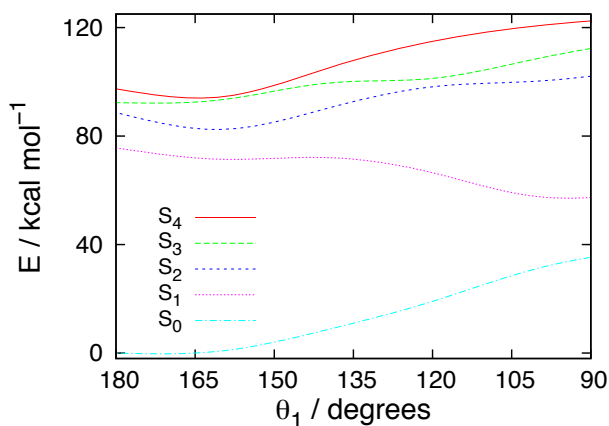
Figure 5.10: *Potential energy profile along the θ_1 dihedral angle of SA. The energy origin is the energy of the minimum enol in the ground state. The S_0 profile has been obtained by relaxed DFT/B3-LYP/6-31G(d,p) optimizations, while the excited-state profiles represent the TDDFT/B3-LYP/6-31G(d,p) vertical transitions from the S_0-relaxed geometries. See Figure 5.8 for the definition of θ_1.*

not intersect with the S_0 when varying the coordinate. However, at largely twisted angles ($\sim 80°$–$90°$) an energetic approach between S_0 and S_1 is observed with an energy difference under 20 kcal mol^{-1}. Given that the energy of the S_1 has been obtained by vertical excitation calculations from S_0, this not too large energy gap between these states opens the possibility of the existence of a CI.

In order to locate a molecular geometry belonging to the seam of the CI between S_0 and S_1, we took a tentative starting geometry of the enol tautomer at 90° of θ_1, and then we performed the energy minimization at the S_1 state and monitored its TDDFT excitation energy (see paper III for computational details). When the excitation energy fell under 3 kcal mol^{-1} (a value low enough for considering the presence of an effective approachement between two electronic states) we stopped the search and took the resulting geometry as an approximate candidate belonging to the seam of the CI. This geometry, depicted in Figure 5.11 (left), presents an energy difference between S_0 and S_1 of 2.67 kcal mol^{-1}, and is characterized by a θ_1 torsional angle of 92°. At this point, one may argue that given the monoreferential

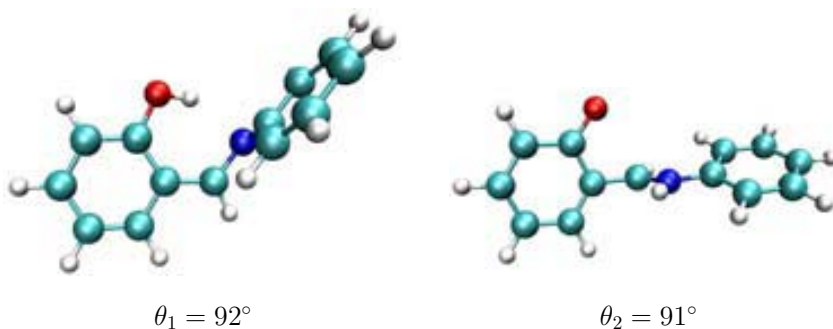$$\theta_1 = 92° \qquad\qquad\qquad \theta_2 = 91°$$

Figure 5.11: *Molecular geometries corresponding to the seam of the conical intersections between S_0 and S_1, located at the enol (left) and cis-keto (right) regions. The geometries have been obtained by TDDFT/B3-LYP/6-31G(d,p) minimizations. See Figure 5.8 for the definition of θ_1 and θ_2.*

nature of TDDFT methodology, it is not adequate to properly locate CIs. However, Tood J. Martínez and collaborators have shown[89] that TDDFT may still provide a decent hint for the location of such structures and for the determination of their energy in comparison with best suited multireferential methods, like CASSCF.

In order to validate our monoreferential TDDFT procedure, we carried out the search of a minimum energy crossing point (MECP), between the S_0 and S_1 states, in the region of the twisted enol tautomer. We employed the Newton-Raphson search algorithm implemented in the MOLCAS package, at a reasonable high multireference level of theory: CASPT2//CASSCF(10,10) cc-pVDZ. From this calculation a structure arised with an energy difference between both states less than 0.2 kcal mol^{-1}. The geometry of this structure is quite similar to the one obtained at the TDDFT level, with a θ_1 torsional angle of 91°; thus validating our TDDFT previous results. Actually, analogous agreements between TDDFT and CASPT2//CASSCF have been previously stated in related photochemical process.[147]

The second IC predicted by Sekiya in SA is supposed to occur in the *cis*-keto tautomer, which is formed just after the ESIPT process.[60] As hinted by the calculations of Zgierski and Grabowska,[59] the excited (π,π^*) *cis*-keto tautomer becomes significantly stabilized by a twist of the phenyl ring, which
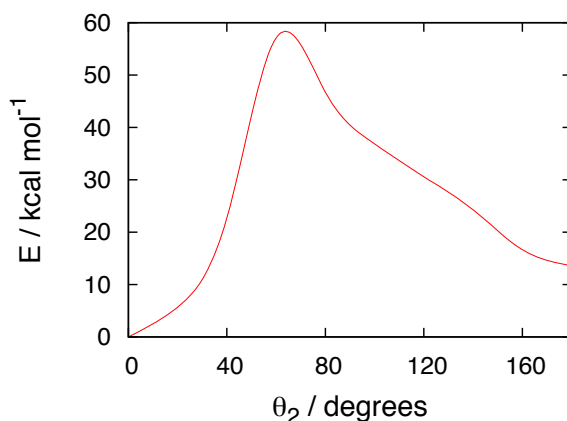
Figure 5.12: *Cis-trans isomerization energy profile along the θ_2 dihedral angle of SA. The energy origin is the energy of the DFT-optimized cis-keto tautomer in S_0. The profile has been obtained by relaxed DFT/B3-LYP/6-31G(d,p) optimizations. See Figure 5.8 for the definition of θ_2.*

is precisely the coordinate leading to the posterior *cis-trans* isomerization process. In fact, if we analyze the DFT reaction coordinate leading from the *cis*-keto tautomer to the *trans*-keto tautomer at the ground state, as depicted in Figure 5.12, it can be seen that the energy evolution presents a very sharp profile and a noticeable peak around 70° for the θ_2 dihedral angle. Such profile contrasts with the more usual smooth evolution of the energy along an isomerization coordinate for the ground electronic state. Such sharpness may indicate the proximity of a second electronic state at the peak region where an intersection may occur.

As for the previous CI in the enol region, we have minimized the energy of a starting highly twisted *cis*-keto geometry (around the θ_2 torsional angle) at the TDDFT level and monitored its excitation energy. The best geometry obtained, showed also in Figure 5.11, presents an energy difference between S_0 and S_1 of 2.88 kcal mol^{-1}, and a θ_2 torsional angle of 91°. Again, we have searched a similar molecular geometry at a multiconfigurational level, using the same methodology previously described. The geometry obtained presents an energy difference between both states less than 0.2 kcal mol^{-1} and a θ_2 torsional angle of 89°, thus validating one more time our DFT-based

methodology.

The main point to stress here is that the localization of CIs has been carried out at the TDDFT level of theory. Even though CIs are regions of the PES that require a multiconfigurational treatment for a proper description, we can see that in this case TDDFT provides accurate results on the localization of CIs. Therefore, the SA system represents a successful example to locate CIs without recourse to a multiconfigurational level of theory.

5.2.3   Characterization of conical intersections

CIs are only relevant for the photochemistry of a given molecular system if they lie under the FC excitation point. Otherwise, they will not be energetically accessible. Besides, once the CI region has been reached by the excited especies, the deactivation channel towards the ground state can only take place along the two degrees of freedom that break the degeneracy (the branching space) at the intersecting region. Hence, in order to obtain a full picture of the deactivation process, not only the location but also the characterization of the branching space has to be achieved.

The identification of the $\vec{g}$ and $\vec{h}$ vectors of the branching space is not a trivial task. The breaking of degeneracy between states may occur through a single molecular coordinate (bond stretching, angle rotation...)[146] or by a combination of molecular motions.[148] Nevertheless, $\vec{g}$, the GD vector, is relatively easy to identify. As we have shown in Eq. 3.27, the GD vector is defined as the gradient of the energy difference between the two intersecting states. Hence, any MECP search algorithm based on following the direction of the gradient will reveal in the process the direction of the GD vector. In view of the energy variation observed for the S_0 and S_1 states along the θ_1 and θ_2 angles, the GD vector can be tentatively identified as the twisting motion of the two aromatic rings.

Before proceeding to identify $\vec{h}$, the DC vector, we would like to verify if TDDFT calculations are suitable to characterize CIs as well as to localize them. To do so, we performed TDDFT and CASSCF single point calcula-
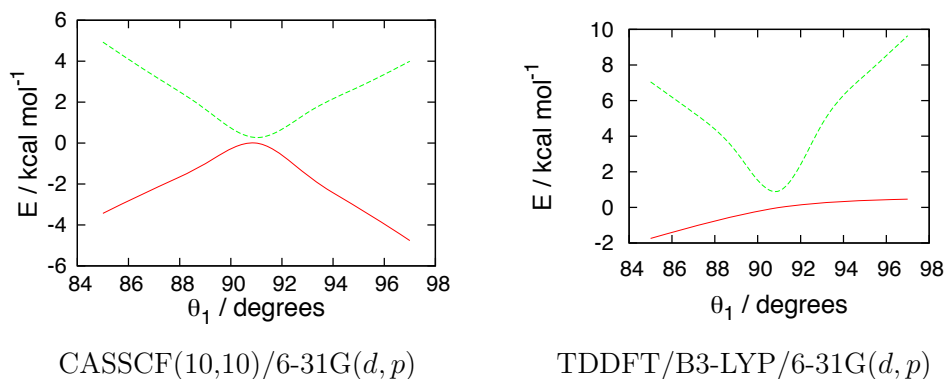
CASSCF(10,10)/6-31G(d,p) TDDFT/B3-LYP/6-31G(d,p)

Figure 5.13: *CASSCF(10,10)/6-31G(d,p) (left) and TDDFT/B3-LYP/6-31G(d,p) (right) comparative representation of the $\vec{g}$ vector's energy variation, corresponding to the conical intersection located at the enol region of SA. See Figure 5.8 for the definition of θ_1.*

tions at several geometries around the θ_1 angle of the obtained MECP enol structure. Results displayed in Figure 5.13 indicate that TDDFT exhibits a change of slope around the CI of the excited electronic state energy, but a monotonous evolution of the ground state energy, in contrast with CASSCF results. Todd Martínez and collaborators already reported[89] on this failure of TDDFT on describing the energy variation around the branching space. In this work, a similar behaviour of the TDDFT energy variation in an intersection region of the $H_2 + H$ system is observed (compare Figure 5.13 with Figure 10 in Ref. 89). No clear explanation has been provided for this event. However, this can be related to deficiencies in the exchange correlation functional. We finally explored the variation of energy of the CIs located for the enol and *cis*-keto tautomer around the corresponding twisting angles at the CASSCF level, as depicted in Figure 5.14.

The characterization of the DC vector is less evident than the GD vector. Nevertheless, as in many aspects of general research, chemical intuition and bibliography search may help to solve that issue. In our case, we came up with some works on biaromatic systems in which the streching of the bond around which the twisting motion takes place is suggested as the DC mode of the branching space.[149,150] In order to verify this assumption, we performed CASSCF single-point calculations around the r_1 and r_2 bond distances (see
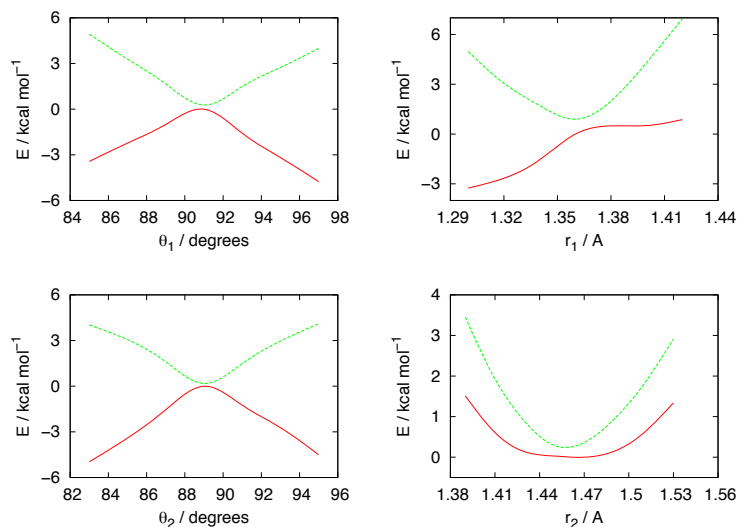
Figure 5.14: *CASSCF(10,10)/6-31G(d,p) energy profiles along the modes that break the degeneracy of the S_0 and S_1 electronic states for the CIs located in the enol (top) and cis-keto (bottom) regions of SA. The gradient difference vector (left) and the derivative coupling vector (right) are ascribed to the θ_1 and θ_2 angles and to the r_1 and r_2 bond distances, respectively. See Figure 5.8 for the definition of θ_1, θ_2, r_1 and r_2.*

Figure 5.8) on the obtained MECP geometries of the enol and *cis*-keto tautomers, respectively. Results displayed in Figure 5.14 corroborate that the r_1 and r_2 bond distances correspond to the $\vec{h}$ vector in the two CIs located in the SA system.

5.2.4   Comparison between mono and multireferential electronic methods

Up to this point, we have seen that TDDFT provides accurate results on the localization (if not characterization) of the CIs between S_0 and S_1 present in the ESIPT process of SA. The next important step in the study would be the calculation of the time scale for the proton transfer and the deactivation process through the CI. As we have previously said, it is necessary to compute the region of the PES relevant for the photochromic process in which the quantum dynamical simulations will be performed. Hence, it is necessary to check if TDDFT can provide good results not only for the CIs but for the
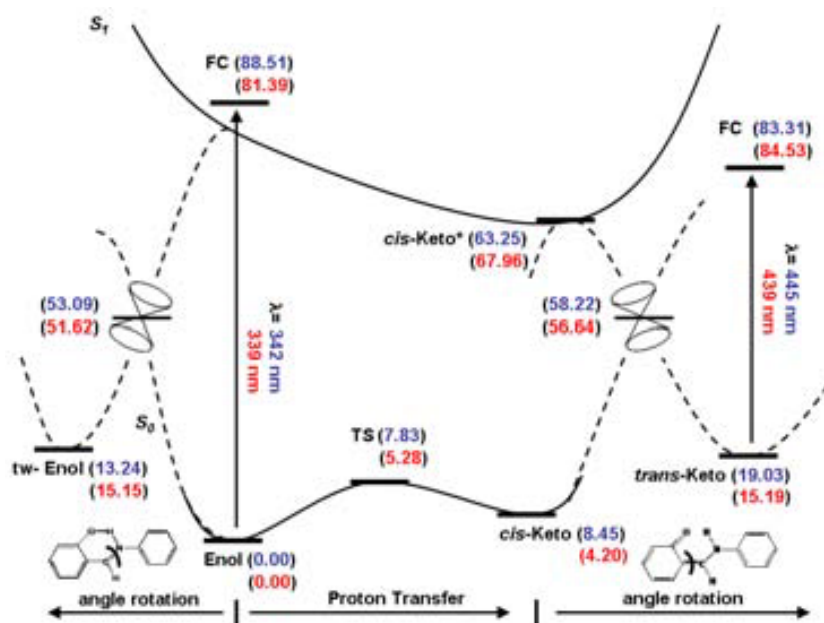
Figure 5.15: *Model of the photochemistry of SA as inferred from our electronic results. Relative energies (in kcal mol^{-1}) are referred to the enol minimum in S_0. Energies displayed in red correspond to DFT (S_0) and TDDFT (S_1) B3-LYP/6-31G(d, p) level of theory, while energies displayed in blue correspond to CASPT2//CASSCF(10,10) cc-pVDZ level of theory.*

whole PES of the ESIPT process.

To do so, we have computed all the stationary points relevant to the ESIPT process (minima, transition state structures, FC excitation points and CIs) at the TDDFT and at the CASPT2//CASSCF(10,10) levels of theory (see Paper III for computational details), being the latter used to validate the results obtained by the former. Figure 5.15 depicts the full picture of the energy variations along the different molecular motions that play a role in the ESIPT process of SA. It has to be noted that the photochemistry of SA involves at least five geometric coordinates (the proton transfer and the two coordinates for each CI). For the shake of clarity, we have designed Figure 5.15 as a one-dimensional profile representation in which solid lines are used for the reaction paths that maintain the planarity *i.e.* the ESIPT process, whereas dashed lines are used for out-of-plane reaction paths, as indicated at the bottom of the figure. The whole energy profile and the different critical

points are widely discussed in Paper III.

As it can be seen in Figure 5.15, both methods reproduce the same relative stability of all the stationary points (being 7 kcal mol^{-1} the largest difference between both methods), but also the FC excitation wavelengths of the enol and *trans*-keto tautomers, which are in turn in good agreement with the experimental values (344 nm[131] and 474 nm,[115] respectively.) We can also see that both methods predict an endoergic proton transfer process at the S_0 state and a barrierless ESIPT process at the S_1. These are general features of a ESIPT reaction that have been previously seen for SMA and HAN in the preceding section.

5.2.5 Estimation of transient time towards conical intersection

In any general dynamical study on ESIPT, the proton transfer process should be considered multidimensional in nature in first instance. However, as we have seen in the dynamics of HAN, the process can be effectively modelled with a one-dimensional approach. In the case of SA, its photochemistry becomes more complex, as there are two different processes leading to the disappearance of the reactants: the ESIPT process and the deactivation of the excited state through CI. Is it then possible to model the dynamics of SA also with highly reduced dynamical models?

The experimental studies of Inokuchi and collaborators[60] performed in SA set the disappearance rate of the excited enol species from the FC excitation point in 500 fs. This rate includes the ESIPT process and the evolution towards the CI in the enol region, as these are the only observed open paths after photoexcitation of SA. On one hand, the ESIPT process in SA takes place along a mainly downhill potential energy profile (see Figure 5.15), and it seems then quite reasonable to assume that this process will involve essentially motion of the proton. On the other hand, our results suggest that transit towards the CI involves purely the torsion of the θ_1 dihedral angle of the enol tautomer. Hence, the two coordinates just described should be

enough to perform the dynamics of the photoactive state. However, could these two coordinates be treated separately?

It is obvious that both ESIPT and deactivation processes occur at the same time after photoexcitation of the reactant species. For a correct dynamical simulation, both ought to be considered simultaneously. Nevertheless, we think it is reasonable to treat the two processes separately, because (*i*) both are energetically strictly downhill processes and (*ii*) both have been described as ultrafast. Proceeding in that way, the complexity on the dynamical treatment is considerably reduced. The original problem has been then reduced to a pair of simple monodimenisional dynamical simulations, for which a resolution procedure has been showed in the previous section. Given that the features of the ESIPT process described for SA are very similar to that previously exposed for the HAN and SMA systems, in what follows we will focus on the dynamics of SA on the CI region.

At this point, a note of caution should be mentioned. Rigorously speaking, a quantum dynamical treatment of the excited enol species through the CI would be unfeasible at present. As we mentioned in Section 3.3, at CI regions the BO approximation fails, and one has to move to a diabatic transformation of the Schrödinger equation. To do so, the coupling terms of the potential energy operator have to be obtained. Even if these coupling terms were worked out, and a quantum dynamical simulation were performed, there would be no direct experimental result to compare to the theoretical prediction yet. As previously mentioned, the experimental works on SA have determined the decay rate of the photoexcited enol tautomer, which includes both ESIPT and deactivation processes. Hence, in our dynamical study on the CIs of SA, we have just determined the time it takes to the wave packet to evolve from the FC excitation point to the CI, but not the passage through it.
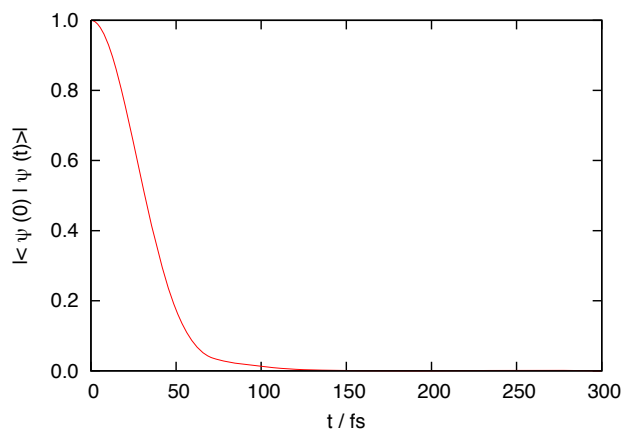
Figure 5.16: *Modulus of the autocorrelation function represented as a function of time for the dynamical simulation of the torsion of the θ_1 dihedral angle in S_1. See Figure 5.8 for the definition of θ_1.*

As in the HAN study, the monodimensional dynamical model of SA was constructed with an isoinertial coordinate system (s_{CI}) asigned to different geometries generated for several values of the rotational angle θ_1. Doing so, the nuclear kinetic energy operator could be written as seen in Eq. 5.2. The potential energy profiles for S_0 and S_1 were built by constrained energy minimization calculations at different values of the θ_1 dihedral angle. After that, the ground vibrational state of S_0 was determined in terms of the isoinertial coordinate and then promoted to the S_1 state. Finally, the time-dependent Schrödinger equation was solved, in that case, by means of a split-operator scheme (See Section 3.4.1).

In this dynamical study, we did not employ the survival function to estimate the rate of the process, as for SMA or HAN. The dynamics of the ESIPT process of HAN and SMA involved basically a proton transfer coordinate. With such a simple motion, is it easy to define univocal structures corresponding to reactans and products, in terms of the donor–proton–acceptor interatomic distances. Hence, the survival function can be easily represented in terms of these coordinates. The integration of the survival function for the values of the coordinate that correspond to the reactants region provides rate

of the process, as seen in the previous study of SMA and HAN. In contrast, the dynamics of SA towards the CI involves motions of larger amplitude than the ESIPT process of SMA or HAN. The evolution towards the CI has been determined as the twisting motion of the aromatic rings. This motion does not allow to clearly define a series of structures that could be identified as "reactants" or "products". Hence, the use of the survival function is not suitable in this case. Instead, we have employed the representation of the modulus of the autocorrelation function $\langle \Psi(0) \mid \Psi(t) \rangle$ in order to analyze the dynamics in S_1. The autocorrelation function provides a quantitative measure of the resemblance between the state $kets$ at different times,[100] as its modulus varies between 1 (when the wave packet at time t completely matches that at time $= 0$) and zero. Thus, we can obtain an estimation of how different is the state of the system at any time in comparison with the initial state. It is natural to assume that when the autocorrelation function drops to zero, the system will have vanished from the FC excitation point.

As we can see in Figure 5.16, the autocorrelation function goes quickly to zero, even though there is heavy atom motion in the process. This may be a consequence of a marked downhill character of the S_1 potential energy profile around the CI region. The time the modulus of the autocorrelation function takes to drop to half of its value at $t = 0$ can be taken as an estimation of how long it takes for the wavepacket to leave the FC area in S_1 to the CI region. Doing so, yields a theoretical estimate of 37.7 fs. Note that this value is well below the experimental findings (500 fs).[60] However, we should remember that this simulation has been carried out in the absence of the interference coming from the evolution of the wavepacket towards the ESIPT channel. In addition, a more strict dynamical treatment of a non-adiabatic system should be done through diabatization of the S_0 and S_1 adiabats and quantification of the couplings between the diabats. Hence, we can consider our estimation as a lower limit for the deactivation channel through this CI.

5.3   Non adiabatic ESIDPT processes: Papers IV, V and Manuscript I

The last section of general discussions represents the final step in the degree of complexity of the proton transfer processes studied in this thesis. Up to now, we have only dealt with single ESIPT processes, which are of great importance in many chemical and biological processes. From now on, we will consider those molecular systems that undergo ESIDPT processes after photoexcitation. It has to be taken into account that this reaction is expected to be more complicated than its single homologue, since two possible limiting mechanisms can be envisaged. In the first limiting mechanism, the two protons transfer in a single step (concerted mechanism), whereas in the second, one proton transfer precedes the other so that the mechanism involves a zwitterionic intermediate (stepwise mechanism). More concretely, we will focus on some members belonging to the family of bipyridyl derivatives, for which the presence of CIs competing with the ESIDPT process has been suggested.[68] Hence, these systems are perfect examples to show the theoretical treatment of double proton transfer processes when coupled with CIs. In addition, we will also see how these special photochemical features can make these compounds potential candidates in the design of optical devices.

5.3.1   ESIDPT processes in bipyridyl derivatives

In the precedent studies on single proton transfer processes on HAN, SMA and SA, we have seen that the electronic-structure characterization of the PES and the ulterior dynamical simulation is a strategy good enough to obtain very accurate results when compared with experimental findings. At least, it sets a limit for the proton transfer rates. The agreement is so good because the proton transfer can only proceed along one single coordinate. This can be easily reproduced by the dynamical simulation, specially when the PES is characterized by a downhill profile from the FC excitation point to the products region.
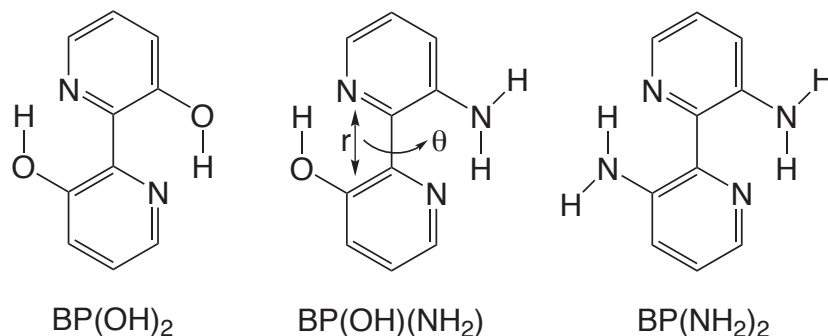
Figure 5.17: *Molecular structures of [2,2'-bipyridyl]-3,3'-diol (left), [2,2'-bipyridyl]-3-amino-3'-ol (center) and [2,2'-bipyridyl]-3,3'-diamine (right). The molecular coordinates θ and r, which will be discussed in the present Section, are also displayed.*

However, in the study of ESIDPT processes, the dynamical simulations attain much more importance than the electronic-structure calculations, given that from the location of stationary points, it is not always possible to discern through which mechanism (concerted and/or stepwise) the proton transfers will proceed.

Let us exemplify this with the best known bipyridyl derivative, [2,2'-bipyridyl]-3,3'-diol ($BP(OH)_2$). As depicted in Figure 5.17, $BP(OH)_2$ presents two proton transfer centers within its molecular structure. Several years ago, Glasbeek and co-workers,[66–70] carried out a series of time-resolved experiments in the sub-picosecond time range, from which it was concluded that the dynamics of ESIDPT featured a branched mechanism consisting in a concerted and a stepwise reaction channels. On the theoretical side, the advisors of the present thesis reported a study on $BP(OH)_2$,,[65] in which it was revealed that the stepwise mechanism was energetically favored over a concerted process (from the electronic point of view). However, quantum dynamical simulations showed branching of the wavepacket between the two routes, thus confirming the experimental results. Besides, ESIDPT processes can become even more complicated (and thus more difficult to theoretically model) if competitive processes intersect with the main chemical reaction.

After their initial studies on $BP(OH)_2$, Glasbeek and co-workers reported
on a very similar system, [2,2'-bipyridyl]-3,3'-diamine $(BP(NH_2)_2)$,[151] in which
the two hydroxyl groups are replaced by amine groups (see Figure 5.17). A
femtosecond fluorescence upconversion study of $BP(NH_2)_2$ revealed very no-
ticeable differences when compared to the photochemistry of $BP(OH)_2$, being
the most notable the very dissimilar QYs: 10^{-5} for $BP(NH_2)_2$ and 0.32 for
$BP(OH)_2$. This points to very efficient mechanisms of deactivation of the
$BP(NH_2)_2$ excited species. As we have seen in the previous section concern-
ing the SA system, such deactivation channels can proceed via CI. Indeed,
Glasbeek and co-workers have proposed the presence of a crossing between
electronic states at twisted geometries of the two pyridylic rings to explain
the very low QY of $BP(NH_2)_2$.[151]

The exploration of the topological features concerning the double pro-
ton transfer process in these two compounds and the localization of possible
CIs is of great importance, given that a dynamical simulation of a double
proton transfer process through CIs will necessarily involve a complex dy-
namical model that must be held up by an accurate electronic study. In
addition to this, the discrepancy between the behaviour between $BP(OH)_2$
and $BP(NH_2)_2$ leaves some interesting questions: why two isoelectronic sys-
tems with a very similar molecular structure exhibit such a different photo-
chemical behavior? Taking into consideration the symmetric nature of both
compounds and their opposite properties, how would a similar compound
but with an assymetrical structure behave? In order to try and cast some
light into these questions, we brought our studies on bipyridyl derivatives
one step beyond and we also analyzed the chemical species which is a hybrid
of the former two: the [2,2'-bipyridyl]-3-amine-3'-ol $(BP(OH)(NH_2))$ deriva-
tive. $BP(OH)(NH_2)$ (also depicted in Figure 5.17) is not a mere hypothetical
compound, as its synthesis has been reported.[152, 153] However, no other ex-
perimental data about this molecule has been reported to date, which leaves
all our results on this compound in the field of predictions, awaiting for
experimental constrast.

5.3.2 A note of caution: TDDFT for certain excited electronic states

As we have seen in our previous study on SA, TDDFT provides comparable results in the energetic description of excited electronic states when compared with multireferential methods. This accurate description does not only include minima, maxima and transition-state structures, but also MECPs. Were this always the case, TDDFT would become an important alternative in the study of the excited states of many-electron systems, given its substantial lower computational cost. However, in our studies of bipyridyl derivatives we have come across a characteristic of TDDFT which makes the method inappropriate to compute certain electronic excited states.

Our study on the $BP(NH_2)_2$ system began with the localization of all the relevant stationary points for the ESIDPT process, as depicted in Figure 5.18. Given the aforementioned dissimilar QY between $BP(OH)_2$) and $BP(NH_2)_2$, we focused on wether or not the final photoproduct was energetically accessible from the FC structure. During the localization of stationary points in S_1, we observed that the energy minima corresponding to reactants and products presented a planar conformation of both pyridylic rings. In contrast, any attempt to obtain an energy minimum in the intermediate (zwitterionic) region led to a highly twisted conformation of the two pyridyl rings. The most remarkable feature of this structure is that it presented a relative energy of 50 kcal mol^{-1} below the reactants' energy minimum in S_1.

In essence, this result should have been interpreted as the accidental location of a MECP between S_0 and S_1, given that the energy of this conformation almost matched the electronic ground-state energy. However, a close inspection of the electronic nature of this structure, as depicted in Figure 5.19, revealed that its electronic excitation was described by a single-electron excitation from the HOMO (π) located on one pyridyl ring to the LUMO (π) located on the other ring. In other words, S_1 was described by a localized intramolecular charge-transfer state. By the time these calculations were in the work, we had come across the excellent review of Dreuw and Head-Gordon on
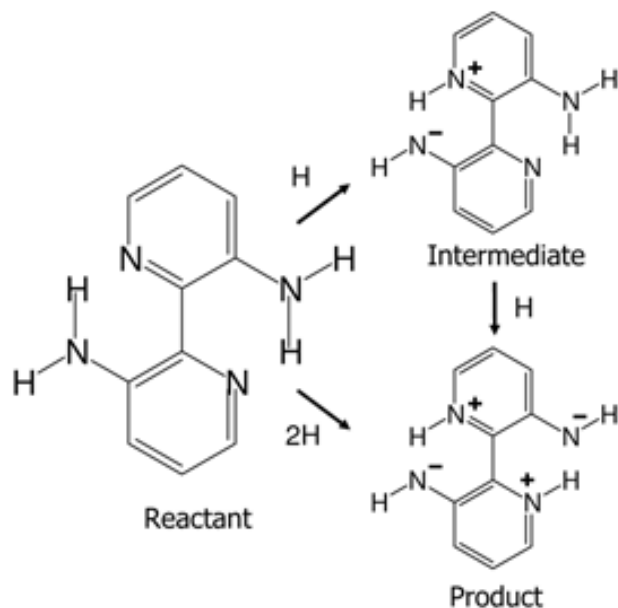
Figure 5.18: *Molecular species involved in the concerted and stepwise mechanisms for double proton transfer in BP(NH$_2$)$_2$. The charges shown are formal charges in the context of a Lewis structure and do not necessarily correspond to the actual charge distribution*

single-reference *ab initio* methods for excited electronic states,[154] in which it was proved that TDDFT tends to overstabilize localized intramolecular charge-transfer states. Besides, the advisors of the present thesis had recently published a study on the 7-azaindole dimer,[42] in which the TDDFT method also failed to describe charge-transfer states. For these reasons we thought, then, that the TDDFT methodology would not be suitable to provide a correct description for this molecular system at such twisted conformations.

However, we observed that forcing absolute planarity (C_S symmetry) during the geometry optimization calculations, the molecular orbitals involved in the description of the charge-transfer state became delocalized over the two pyridyl rings, as we can see in Figure 5.19. Given that the ESIDPT process has been described as ultrafast for these bipyridyl derivatives, $\sim$100 fs for BP(OH)$_2$[66] and BP(NH$_2$)$_2$,[68] it is a reasonable approximation to consider that protons will transfer before any molecular relaxation takes place. Indeed, as we have previously seen in HAN, SMA and SA, ESIPT basically
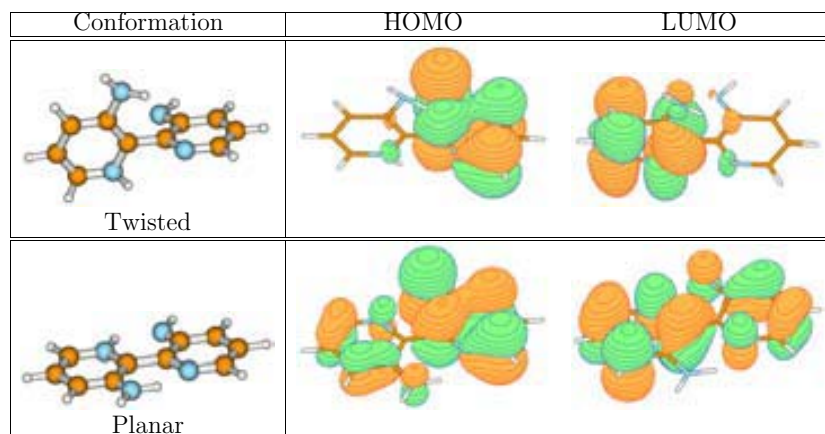
Conformation	HOMO	LUMO
Twisted		
Planar		

Figure 5.19: *Probability isodensity surfaces corresponding to the molecular orbitals involved in the $S_0 \rightarrow S_1$ excitation of the twisted (top) and planar (bottom) conformations of the intermediate species of BP(NH$_2$)$_2$.*

proceeds along the proton transfer coordinate. Hence, we restricted the system to planar geometry in our study because it represented a reasonable approximation to simplify the study of the ESIPT process, and because it avoided the presence of "charge-transfer states" in our TDDFT description of the reaction. While this would not provide good energetic values at the zwitterionic structures, it would allow to have a coherent picture, as for as methodology is concerned, of the full ESIDPT process.

Before proceeding to the next section, an explanatory note should be introduced here. In what follows, we will see that the twisted conformation of the intermediate species actually correspond to a point located on the seam of a CI. However, from all the above, our first attempt to locate CIs (see Papers IV and V) in the bipyridyl systems was performed at the multiconfigurational CASSCF level. Later on, we found the work of Todd J. Martínez and collaborators[89] (which has been already mentioned in our study on SA) on CIs and TDDFT. According to this study, the TDDFT description of a CI (even involving a charge-transfer state) may still be accurate if there is not a total separation of the molecular orbitals describing the electronic excitation of the corresponding CI.

Indeed, our previous study on the CIs in SA was succesfully carried out at the TDDFT level because the molecular orbitals involved in the twisted conformations of SA were delocalized over the molecular structure. The previously mentioned study on the 7-azaindole dimer[42] presented a dramatic failure of the TDDFT description of the system because the molecular orbitals of the charge-transfer state were totally localized on each monomer. Looking again at Figure 5.19, we could say that $BP(NH_2)_2$ may present an intermediate situation between these two. It can be observed that there are certain orbital contribution on the other ring that may overlap with the main molecular orbital at the twisted conformations of $BP(NH_2)_2$. In view of this, we finally adopted a TDDFT methodology in our studies on CIs in the bipyridyl derivatives, as can be seen in Manuscript I.

5.3.3 Relationship between conical intersections and molecular structures

As we have just said, the most important feature in the photophysics of $BP(OH_2)$ and $BP(NH_2)_2$ is their extremely different fluorescence QYs, despite their molecular resemblance. According to Glasbeek and co-workers,[151] this is indicative of very efficient non radiative deactivation paths of the excited state in $BP(NH_2)_2$. They propose in this case the existence of a CI between S_0 and S_1, leading from highly twisted conformation of the intermediate species in S_1, to the original reactant species in S_0. As SA (as seen in the previous section) and as many other molecular systems, the search for MECPs in the $BP(NH_2)_2$ molecule is far from obvious, not to speak of the characterization of the branching space. If no clues of the existence of CIs can be inferred from experimental findings, any attempt to locate a crossing point will be a shot in the dark. In our case, the authors of the study on $BP(NH_2)_2$[151] postulate a CI between S_0 and S_1 when the intermediate species of the ESIDPT adopts a twisted conformations of the two pyridyl rings.

Given that at the time of this study, as previously said, we thought that TDDFT level failed to describe the localized charge-transfer state cor-

responding to the twisted conformation of the intermediate tautomer, we employed the multiconfigurational CASSCF method (see paper IV for more computational details) to perform single point calculations around the twisting angle coordinate of the intermediate species of $BP(NH_2)_2$. From our results observed an energy approach between S_0 and S_1 at a twisted angle of approximately $85°$ is observed, close enough (less than 10 kcal mol^{-1}) to seriously consider the presence of a CI. At this point, it is reasonable to wonder if a similar CI would be present in $BP(OH)_2$ (given the structural resemblances of both compounds) even though the measured QY of 0.32 seems to indicate that this possible CI would not play a role in the global photophysics of $BP(OH)_2$. Proceeding in a similar fashion as in $BP(NH_2)_2$, we found a small energy gap between S_0 and S_1 of $\sim$20 kcal mol^{-1} in the twisted (also $85°$) intermediate region. An energy difference of 20 kcal mol^{-1}, 10 kcal mol^{-1} larger than that found in $BP(NH_2)_2$, casts some doubts about the existence of a CI in this case, and a more accurate electronic study would be necessary to get a better description of the S_0 and S_1 states at this twisted region of $BP(OH)_2$.

By the time of this first study on $BP(NH_2)_2$ and $BP(OH)_2$, corresponding to Paper IV, we were not able to assure the existence of CIs at twisted conformations of the intermediate species, as no MECPs search calculations were performed[†]. However, our single point calculations along the θ coordinate were good enough to theorize about the dissimilar QY between $BP(NH_2)_2$ and $BP(OH)_2$. According to our topological study on the ESIDPT process in both bipyridyl systems (see paper IV), the formation of the final photoproduct in S_1 is endoergic for $BP(OH)_2$ and exoergic for $BP(NH_2)_2$. After photoexcitation, $BP(NH_2)_2$ has not enough energy to reach the region of the final photoproduct. Hence, after the first proton transfer process, the excited intermediate species of $BP(NH_2)_2$ can eventually evolve towards the CI to S_0, thus explaining the very low QY. In contrast, the photoexcited $BP(OH)_2$

[†]These findings have been confirmed by direct MECPs search calculations with the algorithm included in MOLCAS 6.2 package. These still unpublished results are collected in Manuscript I.
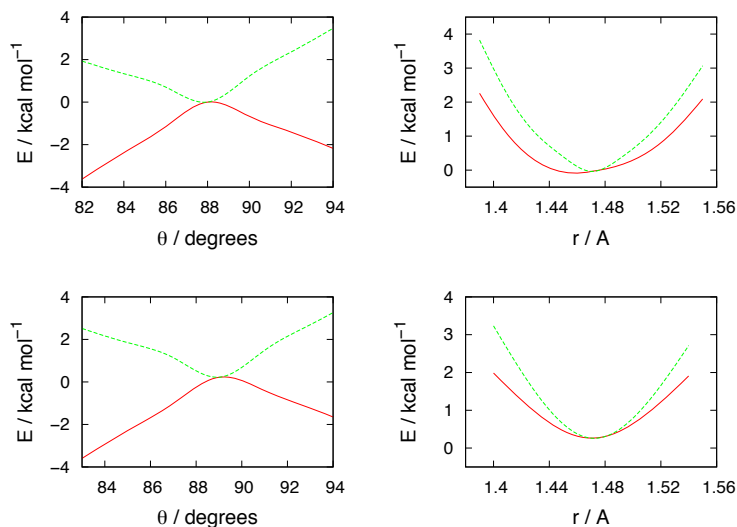
Figure 5.20: *CASSCF(10,10)/6-31G(d,p) energy profiles along the modes that break the degeneracy of the S_0 and S_1 electronic states for the CIs located in the hydroxyl-initiated (top) and the imino-initiated (bottom) intermediates of BP(OH)(NH$_2$). The gradient difference (left) and the derivative coupling (right) vectors are ascribed to the twisting of the dihedral angle θ and the stretching of the r interring distance, respectively. See Figure 5.17 for the definition of θ and r.*

molecules have enough energy to reach the double proton-transferred product. Even if there is a true CI in the region of the twisted intermediate species, this CI will not be as accessible as the one in the BP(NH$_2$)$_2$ system, and hence BP(OH)$_2$ will present a significant QY value.

As for the BP(OH)(NH$_2$) system, this being a hybrid compound between BP(NH$_2$)$_2$ and BP(OH)$_2$, an intermediate behavior would be expected. Being that the ESIDPT process in BP(OH)(NH$_2$) can start from two different proton transfer centers (OH or NH$_2$ groups), two different mono-transferred intermediate especies exist. In fact, both intermediates also present a CI between S_0 and S_1 when twisted around 90°.

These results give further evidences that there may exist a relationship between the geometry of the located MECP and the molecular structure of different, but related, compounds. To settle this question, we analyzed the branching space of the CIs in these bipyridyl derivatives (see Paper V for a more in-depth discussion). From one side, the GD mode can be trivially
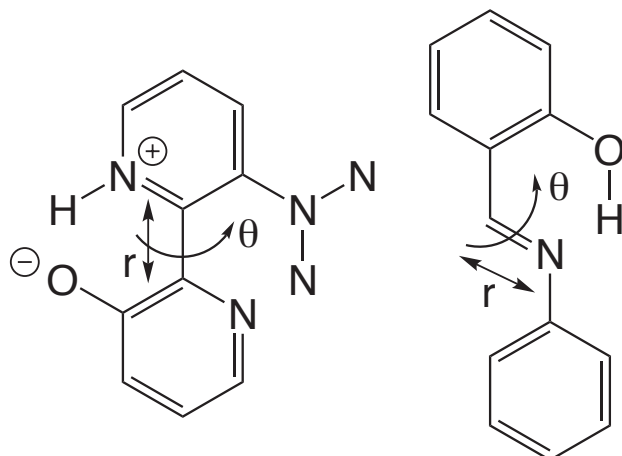
Figure 5.21: *Comparison of the alike biaromatic molecular structure of BP(NH$_2$)$_2$ (left) and SA (right). The vectors corresponding to the branching space of the conical intersections are also indicated. The usual representation of the SA structure has been rotated by 90° in order to better appreciate the molecular similarities between both compounds.*

identified as the twisting of the two pyridyl rings, as it is the coordinate which directly leds to the energy approaching between states. Figure 5.20 depicts the GD mode for the two intermediate hybrids of BP(OH)(NH$_2$) as an example. Less evident is the characterization of the DC mode. However, we can use as a first guess the results obtained for SA in the previous section. Please note in first place the great resemblance of the GD mode depicted in Figure 5.20 and that for SA depicted in Figure 5.14. Second, we can envisage both SA and the bipyridyl derivatives as biaromatic systems, in which the two rings are separated by one or two bond distances, as schematicaly depicted in Figure 5.21. Given that the DC mode in SA was ascribed to the stretching of the bond supporting the twisting coordinate, it is thus reasonable to consider the stretching of the C–C interring bond as the DC mode for the three bipyridyl derivatives. Indeed, the energy variation of the S$_0$ and S$_1$ states along the stretch of the C–C bond for the BP(OH)(NH$_2$) system matches with the expected behaviour of a branching space, as depicted for the two intermediates of the hybrid in Figure 5.20. Similar results have been obtained for the other two bipyridyl derivatives.

These results indicate that the branching space that defines the region of the PES in which two states intersect, is similar for those molecular compounds that share structural similarities in their geometries.

5.3.4   A possible technical application of bipyridyl systems

As we have previously said, the CI proposed in the experimental study of Glasbeek and co-workers[151] consists of the twisting motion of the intermediate species in S_1. This study also suggests that the fate of the molecules crossing the CI is the original reactant species in S_0. According to this, transit through the CI would involve the reversion of the twisting motion and a back-proton transfer process. However, passage through a CI implies the loss of degeneracy towards two different directions. Hence, what is the fate of the excited intermediate species that complete the twisting motion and achieve planarity again? To explain this, we will use only the $BP(NH_2)_2$ system as an illustrative example, due to similar results have been obtained for the other two studied bipyridyl systems (see Manuscript I for a more detailed discussion).

Figure 5.22 represents the likely photochemistry of $BP(NH_2)_2$ as inferred from our electronic-structure results. The left side of the figure contains the relative energy of the stationary points relevant to the ESIDPT and non adiabatic processes in $BP(NH_2)_2$, whereas the right side depicts the molecular labeling and atomic numbering employed.

As we can see, from the orignal reactant especies (DA), which are the only existing minima in S_0, excitation of the appropiate wavelength brings the system to S_1 by a permitted (oscillator strength = 0.322) HOMO (π) $\rightarrow$ LUMO (π^*) exciation. From the FC arrival point, the excited DA molecules (DA*) have enough energy to evolve towards the first proton transfer coordinate to the intermediate species (MI*), but the product of the second proton transfer (DI*) is energetically unreachable. From this point, the DA* molecules can either revert to the DA* region and fluoresce to S_0, or accu-
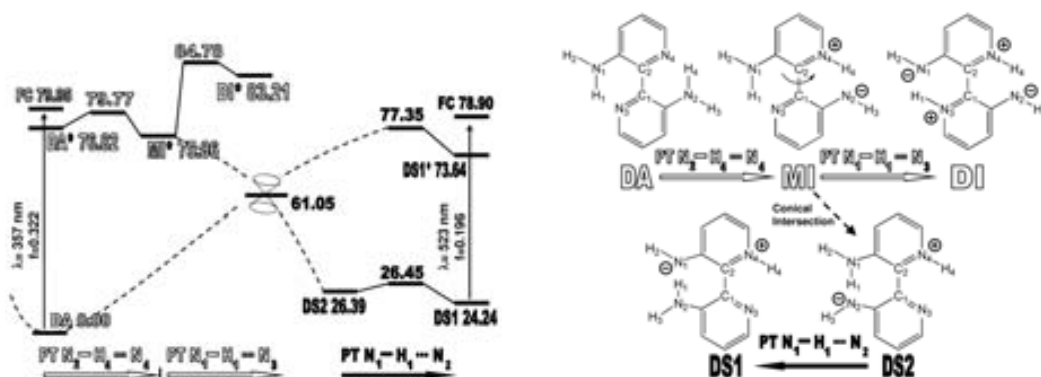
Figure 5.22: *Relative electronic energies (in kcal mol^{-1}) (left) and schematic representation of the molecular geometries (right) corresponding to the most relevant stationary points of the conical intersection region in BP(NH$_2$)$_2$. Energies in S$_0$ and S$_1$ have been obtained at the DFT/B3-LYP/6-31G(d,p) and TDDFT/B3-LYP/6-31G(d,p). The molecular labeling corresponds to the three works collected in the present section (Paper IV, V and Manuscript I), whereas the atom numbering corresponds to the same used in Manuscript I.*

mulate in the intermediate MI* region. The formed MI* species would also fluoresce to S$_0$ if the corresponding energy minimum existed. Instead of that, the only clear open path to S$_0$ is the existing CI through the ring twisting coordinate. According to Figure 5.22, the reversion of the twisting motion would lead to the original DA species (due to the lack of a MI minimum in S$_0$), closing thus the photocycle. The molecular species involved in this photocycle are depicted with white-filled letters in Figure 5.22.

On the other hand, if the MI* species that reach the CI complete the rotational motion of both pyridyl rings, a new family of stable molecular species arise. These new compounds have been labelled as DS by "dark states", given that these states cannot be directly accessed from the ground state of the original bipyridyl tautomer DA. These new molecular species, which are represented with black-filled letters in Figure 5.22, complete the photochemical landscape of BP(NH$_2$)$_2$ (similar diagrams for BP(OH)$_2$ and BP(OH)(NH$_2$) can be seen in Manuscript I). The two stable structures DS1 and DS2 can evolve from one to the other by a proton transfer coordinate in S$_0$. However, only DS1 presents a stable energy minimum in S$_1$. Photoexcitation of DS1 (oscillator strength = 0.196), with a wavelength considerably
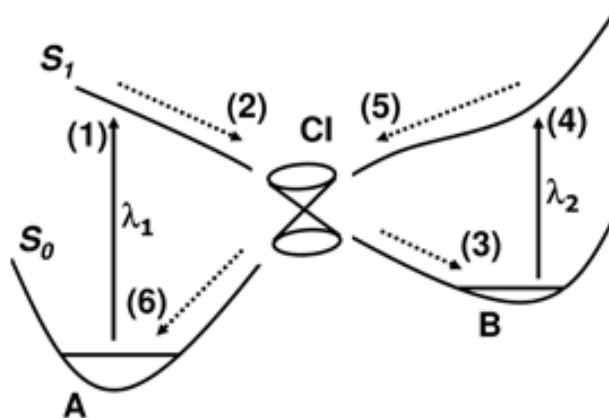
Figure 5.23: *Schematic representation of the process involved in the photocycle of an ideal optical photoswitch. The double cone refers to a conical intersection (CI) region of low energy. λ_1 and λ_2 refer to the wavelengths that photoexcite the A and B species, respectively. The numbering of events follows the sequence of the photocycle steps.*

different than that of DA, would bring the excited DS1* molecule to a FC point from which the system could evolve again to the CI by proton transfer and twisting coordinates, to reach again the original DA minimum, and closing the photocycle.

As we emphasized in the Introduction, the cyclic nature of this photochromic process is interesting to the basic but especially the applied research, as they could represent good candidates in the design of photomemory devices. Very recently, Sobolewski[155] reported a theoretical analysis on the basic features that an organic compound should present in order to act as a reversible molecular switch. According to this study, a molecule showing the simple scheme of Figure 5.23 could be a good candidate for a molecular photomemory, if the photochromic species are stable enough. After the initial excitation of the initial species (writing process), the system can evolve to a different stable tautomer through CI transit. In order to read the photomemory, there should exist a physical property, easy to measure, that could be used to clearly discriminate between the two isomers.

If we now compare the scheme in Figure 5.23 and the energetic diagram in Figure 5.22, we can see that the $BP(NH_2)_2$ has many resemblances with

an ideal optical photoswitch, being the A and B species in Figure 5.23 the DA and DS1 tautomers in Figure 5.22. In addition, as DS1 presents an assymetric molecular structure, a detectable dipolar moment should be present, in contrast to DA that has an inversion center and hence is apolar. Indeed, $BP(NH_2)_2$ fulfills with the requisites of a good candidate to photomemory for several reasons: (i) following the initial excitation, the path to the CIs seems the most likely one given that fluorescence is experimentally known to proceed with a quite low QY (10^{-5}),[151] (ii) the photochromic species DS1 is stable enough, and there is a physical property (the dipolar moment) able to easily discriminate the two forms, and (iii) light of a different wavelength can reverse the whole process.

5.3.5 Perspective: electronic and dynamical treatment of the non adiabatic processes

Previously, we have stated that there may exist a relationship between the molecular structure of different chemical compounds and the characterization of possible CIs present in these molecules. Hence, similar CIs exist for $BP(NH_2)_2$ and $BP(OH)_2$. Even though it is clear that the excited systems in $BP(NH_2)_2$ eventually undergo radiationless transitions to S_0 through the CI due to its very low mesured QY (10^{-5}),[151] it is not so clear why the same does not apply to $BP(OH)_2$ if a similar CI channel exists for that system. This might be explained by dynamical effects. The fact that the CI is not in the main route from reactants to products, and that there are other degrees of freedom that can exchange energy with the reactant ones, might make passage over the CI impossible in the $BP(OH)_2$ case after the first products of the double proton transfer have been formed. In order to ascertain the truthfulness of this hypothesis, dynamical calculations are required.

In contrast to our precedent dynamical studies, the dynamics in these bipyridyl derivatives involve double proton transfer and passage through a CI. Hence, for a realistic treatment of the overall processes, it is necessary to allow the independent motion of both protons and the correct representation
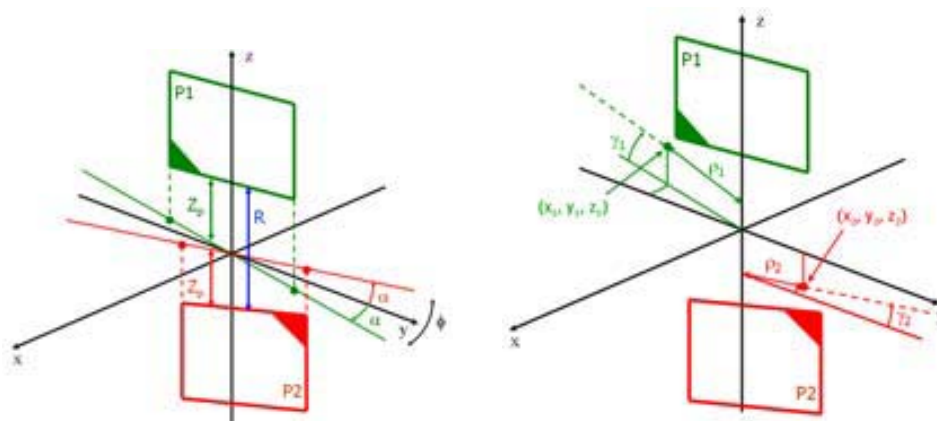
Figure 5.24: *Scheme describing the dynamical coordinates used, for the bipyridyl rings (left) and the two protons (right). The two pydidyl rings are depicted by rectangular foils (P1 and P2) with a mark, which indicates the position of the donor atom. The motion of the two pyridyl rings is constrained in three ways: (i) they can only rotate along the C–C axis, which is completely contained in the z axis, (ii) the relative orientation of P1 and P2 with respect to the z axis is determined by a single angle α, and (iii) their distance to the origin is also described by a single coordinate Z_p. In contrast, the motion of H_1 and H_2 is free in the three Euclidean dimensions.*

of the branching space. These constraints demand many degrees of freedom, at least the branching space and the position of each proton.

Given that the reactive process, with or without inclusion of transit through the CI, is expected to occur in the sub-picosecond timescale, it is reasonable to assume that the internal structure of the pyridyl rings is going to remain essentially unaltered during the process. In such a case, it would be acceptable to consider the molecule formed by two movable fragments (excluding the protons), each one completely rigid and representing a pyridyl ring *i.e.* two rigid planar bodies. Accepting this, the basic system would consist of two rigid bodies and two protons. Each proton can move freely, but each pyridyl ring is restricted to rotate around and displace along one defined axis.

The dynamical model which is derived from all the exposed assumptions, and we propose for the dynamical study of the bipyridyl systems, is depicted in Figure 5.24. All the explicit dynamical coordinates included in our model are as follows:

- Z_p indicates the position of each pyridyl ring.

- α indicates the angle formed by each pyridyl ring with respect to the y axis.

- (x_1, y_1, z_1) and (x_2, y_2, z_2) indicate the positions of H_1 and H_2, respectively.

- R depicts the distance between the two pyridyl rings.

- ϕ depicts the opening angle between the two pyridyl rings

- ρ_1 and ρ_2 indicate the distance of H_1 and H_2 to the rotational axis, respectively.

- γ_1 and γ_2 indicate the angle created by the line linking H_1 and H_2, respectively, to the rotational axis with the zy-plane (which bissects the angle that the two pyridyl rings make).

Note that the ρ_i and γ_i coordinates can alternatively indicate the position of the two protons as the set of coordinates (x_i, y_i, z_i). Because of the properties of the conical intersection it is clear that the degrees of freedom ϕ and R coincide with the $\vec{g}$ and $\vec{h}$ vectors, respectively.

The explicit inclusion of a conical intersection makes the BO approximation meaningless in its vicinity, as we saw in the Introduction chapter. Nevertheless, it is possible to eliminate the kinetic energy couplings between electronic states by switching to the diabatic representation.[78] In the diabatic picture, the kinetic energy operator is diagonal (thus eliminating the singular kinetic energy couplings) but the potential energy operator is instead a full matrix, and hence an *ansatz* to obtain the potential energy off-diagonal elements is necessary.

At the time of writing the present thesis, the deduction of the kinetic energy operator is completed, and work is in progress addressed to the development of mathematical functions describing the elements of the diabatic potential energy operator. Detailed calculations have been done at CASSCF

to pinpoint precisely the locations of the CIs, and quantify the non adiabatic couplings in collaboration with Prof. Josep M. Anglada and Josep M. Bofill. The parametrization of all potential energy elements is carried out with a large number of single-point TDDFT and CASSCF calculations.

We expect to carry out full MCTDH calculations, and to determine the branching ratio between formation of the product of the double proton transfer and transit through the CI for $BP(OH)_2$ and $BP(NH_2)_2$, in this way providing a quantitative explanation to the extreme differences in QY.

6
Conclusions

"It is a capital mistake to theorize before you have all the evidence. It biases the judgment."

Sir Arthur Conan Doyle, *A Study in Scarlet* (1888)

During the course of these four years of research, that mostly culminate with the present thesis, we have pursued a dual goal: the study of the chemical features of standalone and more complex ESIPT process from a theoretical point of view, and the search and comparison of different theoretical methodologies in order to obtain the most accurate results in our studies. Hence, the conclusions here collected, are presented from these two perpectives.

On one hand, concerning the chemical features observed in our studies:

1. We have verified that the electronic energy profiles, corresponding to the S_1 state, of all the studied systems present a barrierless or nearly barrierless situation, which explains the very short proton transfer times experimentally measured.

2. The ultrafast nature of the ESIPT process observed in SMA and HAN has been verified to be the result of the enhancement of the acid and basic characters of the donor and acceptor atoms, respectively, and the loss of aromaticity of the reactant especies following photoexcitation. These two factors eventually lead to the absence of energy barriers and the inversion of the energetic profile between S_0 and S_1.

3. The electronic energy gain that follows the photoexcitation of the reactant especies activates many other internal modes apart from the proton transfer coordinate. Some of these modes, such as the approach of the donor and acceptor atoms, can facilitate the ESIPT process. We have observed in every molecular system studied in this thesis, that ESIPT proceeds before any other mode can assist the proton transfer, as discussed for the SMA and HAN systems. Nevertheless, these modes can become relevant if the transfer process is not so fast, as observed in the deuterated case of SMA.

4. For those experimental works on which a very low quantum yield have been reported, namely SA and $BP(NH_2)_2$, our theoretical studies predict the presence of very efficient deactivation paths, in the form of

conical intersections. Such competitive paths are energetically accessible from the Franck-Condon excitation point.

5. The exploration of the topology around the conical intersections located in SA, allows us to tentatively ascribe the corresponding branching spaces to the the stretching of the interring unsaturated bond, and the twisting angle around that bond. These branching spaces are more clearly depicted in Figure 5.8 (page 82).

6. Similar to the results obtained for SA, the branching spaces concerning the conical intersections located in the bipyridyl systems seem to correspond to the stretching of the interring bond distance, and the interring twisting angle.

7. The two last conclusions concerning the branching spaces of SA and the bipyridyl systems, allow to speculate on the possible relationship between molecular electronic structures and conical intersections. According to our results, molecules exhibiting reasonably similar molecular geometries at conical intersections, may describe their corresponding branching spaces with very similar molecular coordinates.

8. Our calculations predict that the three studied bipyridyl derivatives undergo very different ESIPT processes after photoexcitation, even though these compounds are isoelectronic and exhibit very similar potential energy surgaces on the S_1 state. Hence, not necessarily a relationship between the molecular structure of similar compounds and their photochemistry exists.

9. According to our results, the very dissimilar measured quantum yields of $BP(NH_2)_2$ in comparison with $BP(OH)_2$, is mainly attributed to the endoergic nature of the ESIDPT process in the former, and the presence of a conical intersection for both in the excited intermediate region.

10. In base to electronic calculations, bipyridyl derivatives can be considered as potential candidates for the design of optical devices as photomemories, given that the presence of a new series of stable compounds beyond the CI region permits the exchange between two different molecular geometries with different excitation wavelengths. Among the three bipyridyl derivatives considered, $BP(NH_2)_2$ presents the optimal features to become a photomemory device.

On the other hand, the use and comparison of different methods of calculation, both for the electronic and dynamical points of view, lead us to the following conclusions:

1. The quantum dynamical simulations perfomed on the SMA system, based on a 3-D reduced dynamical model including the approach of the donor and acceptor atoms, have showed a slightly activation of this internal mode that has a minor contribution in the formation time of the product. Thus, the use of 1-D reduced dynamical models (based on collective coordinates) on barrierless or nearly barrierless ESIPT processes, such as HAN, are simple and accurate enough to provide a good description of the proton transfer process.

2. Proton transfer rates can be successfully obtained by monitorization of the integral of the probability function at the reactants region over time. In this fashion, proton transfer times of 11.0 fs and 25.5 fs have been obtained for SMA and HAN, respectively, in good agreement with the available experimental data.

3. Reduced dimensionality models do not include the full dynamical effects due to degrees of freedom coupled to the proton transfer. For ultrafast processes, only the initial stages of the propagation, those in which coupled degrees of freedom have not yet been activated, are meaningful. As observed in SMA and HAN, propagation of the dynamics to longer times brings about unphysical recurrences as the model prevents energy transfer to coupled modes.

4. The electronic-structure study performed on the topology of the ES-IPT process in SA, has shown that TDDFT and CASSCF/CASPT2 methods provide a high degree of agreement in the relative stability of all the stationary points located in S_1, even though the former presents slightly different energies than the latter.

5. The study of the SA system has also revealed that the monoreferential TDDFT method is in reasonable good agreement with the multireferential method CASSCF when computing the energy of minimum energy crossing points. However, TDDFT clearly fails when attempting to describe the energy variation along the branching space of the conical intersections in SA.

6. The dynamical study of the ESIPT process in the SA system has been performed by isolating the proton transfer from the competitive non adiabatic path via conical intersection. Such separation is acceptable as long as both processes are of ultrafast nature, and involve clearly different degrees of freedom. However, this strategy does not provide the branching ratio, only the times of each process.

7. The exploration of the ESIDPT process in the three bipyridyl systems revealed that the TDDFT method fails in the description of localized charge-transfer states. The adoption of a planar approximation on the study of the double proton transfer reaction, which is validated by its ultrafast nature, avoids the appearance of those charge-transfer states. However, if a non planar arrangement of the system is required, such as in the conical intersections located at the intermediates regions, TDDFT still provides accurate results if there is not a complete separation of the molecular orbitals involved in the charge-transfer state.

Bibliography

[1] K. B. Lipkowitz and D. B. Boyd. *Reviews in computational chemistry, Vol. 1.* John Wiley & Sons, New York, 1989.

[2] H. Dürr and H. Bouas-Laurent. *Photochromism: Molecules and systems.* Elsevier, Amsterdam, Revised Edition, 2003.

[3] E. Hadjoudis and M. Mavridis. Photochromism and thermochromism of Schiff bases in the solid state: structural aspects. *Chem. Soc. Rev.*, 33(9):579 − 588, 2004.

[4] Y. Hirshberg and E. Fischer. Low-temperature photochromism and its relation to thermochromism. *J. Chem. Soc.*, 629 − 636, 1953.

[5] Y. Hirshberg and E. Fischer. Multiple reversible color changes initiated by irradiation at low temperature. *J. Chem. Phys.*, 21:1619 − 1620, 1953.

[6] Y. Hirshberg and E. Fischer. Photochromism and reversible multiple internal transitions in some spiropyrans at low temperatures. Part I. *J. Chem. Soc.*, 297 − 303, 1954.

[7] Y. Hirshberg and E. Fischer. Photochromism and reversible multiple internal transitions in some spiropyrans at low temperatures. Part II. *J. Chem. Soc.*, 3129 − 3137, 1954.

[8] Y. Hirshberg. Reversible formation and eradication of colors by irradiation at low temperatures. A photochemical memory model. *J. Am. Chem. Soc.*, 78(10):2304 − 2312, 1956.

[9] R. Heiligman-Rim, Y. Hirshberg and E. Fischer. Photochromism in some spiropyrans. Part III. The extent of phototransformation. *J. Chem. Soc.*, 156 − 163, 1961.

[10] R. S. Murphy, Y. Chen, T. R. Ward, R. H. Mitchell and C. Bohne. Photophysical studies on the photochromism of *trans*-10b,10c-dimethyldihydropyrene. *Chem. Commun.*, (20):2097 − 2098, 1999.

[11] M. T. Indelli, S. Carli, M. Ghirotti, C. Chiorboli, M. Ravaglia, M. Garavelli and F. Scandola. Triplet pathways in diarylethene photochromism: photophysical and computational study of dyads containing ruthenium(II) polypyridine and 1,2-bis(2-methylbenzothiophene-3-yl)maleimide units. *J. Am. Chem. Soc.*, 130(23):7286 − 7299, 2008.

[12] M. Uchida and M. Irie. Two-photon photochromism of a naphthopyran derivative. *J. Am. Chem. Soc.*, 115(14):6442 − 6443, 1993.

[13] M. O'Donnell. Photo-dimerization of solid anthracene. *Nature*, 218:460 − 461, 1968.

[14] V. Malatesta. *Photodegradation of organic photochromes*, pages 370 − 382. Organic photochromic and thermochromic compounds, J. C. Crano and R. J. Guglielmetti (Eds.) Vol. 2, Ch. 2. Plenum, New York, 1999.

[15] L. V. Schäfer, G. Groenhof, A. R. Klingen, G. M. Ullmann, M. Boggio-Pasqua, M. A. Robb and H. Grubmüller. Photoswitching of the fluorescent protein asFP595: Mechanism, proton pathways, and absorption spectra. *Agew. Chem.*, 119(4):530 − 536, 2007.

[16] M. Irie. Special issue: Photochromism. Memories and switches. *Chem. Rev.*, 100(5):6 − 1890, 2000.

[17] T. Fukaminato, T. Umemoto, Y. Iwata, S. Yokojima, M. Yoneyama, S. Nakamura and M. Irie. Photochromism of diarylethene single molecules in polymer matrices. *J. Am. Chem. Soc.*, 129(18):5932 − 5938, 2007.

[18] S. Kobatake, S. Takami, H. Muto, T. Ishikawa and M. Irie. Rapid and reversible shape changes of molecular crystals on photoirradiation. *Nature*, 446:778 − 781, 2007.

[19] T. Yamaguchi, S. Takami and M. Irie. Photochromic properties of 1,2-bis(6-substitute-2-methyl-1-benzofuran-3-yl)ethene derivatives. *J. Photochem. Photobiol. A*, 193(2 − 3):146 − 152, 2008.

[20] M. Rumi, J. E. Ehrlich, A. A. Heikal, J. W. Perry, S. Barlow, Z. Hu, D. McCord-Maughon, H. Röckel, S. Thayumanavan, S. R. Marder, D. Beljonne and J.-L. Brédas. Structure property relationships for two-Photon absorbing chromophores bis-donor diphenylpolyene and bis(styryl)benzene derivatives. *J. Am. Chem. Soc.*, 122(39):9500 − 9510, 2000.

[21] A. Galvan-González, K. D. Belfield, G. I. Stegeman, M. Canva, S. R. Marder, K. Staub, G. Levina and R. J. Twieg. Photodegradation of selected π-conjugated electro-optic chromophores. *J. Appl. Phys.*, 94(1):756 − 763, 2003.

[22] Z.-Y. Hu, A. Fort, M. Barzoukas, A. K. Y. Jen, S. Barlow and S. R. Marder. Trends in optical nonlinearity and thermal stability in electrooptic chromophores based upon the 3-(dicyanomethylene)-2,3-dihydrobenzothiophene-1,1-dioxide acceptor. *J. Phys. Chem. B*, 108(25):8626 − 8630, 2004.

[23] M. Gu, J. O. Amistoso, A. Toriumi, M. Irie and S. Katawa. Effect of saturable response to two-photon absorption on the readout signal level of three-dimensional bit optical data storage in a photochromic polymer. *Appl. Phys. Lett*, 79(2):148 − 150, 2001.

[24] J. O. Amistoso, M. Gu and S. Kawata. Characterization of a confocal microscope readout system in a photochromic polymer under two-photon excitation. *Jap. J. Appl. Phys.*, 41(8):5160 − 5165, 2002.

[25] Colossal Storage Corp. − The "Atomic Switch" A Worlds First! See http://colossalstorage.net/.

[26] TUB − Optisches Institut − Prof. Orlic. See http://www.opttech.tu-berlin.de/microholas/.

[27] P. Zijlstra, J. W. M. Chon and M. Gu. Five-dimensional optical recording mediated by surface plasmons in gold nanorods. *Nature*, 459(21):410 − 413, 2009.

[28] D. Oesterhelt and W. Stoeckenius. Functions of a new photoreceptor membrane. *Proc. Natl. Acad. Sci.*, 70(10):2853 − 2857, 1973.

[29] J. L. Spudich and R. A. Bogomolni. Mechanism of colour discrimination by a bacterial sensory rhodopsin. *Nature*, 312(5994):509 − 513, 1984.

[30] J. C. Lagarias and H. Rapoport. Chromopeptides from phytochrome. The structure and linkage of the PR form of the phytochrome chromophore. *J. Am. Chem. Soc.*, 102(14):4821 − 4828, 1980.

[31] J. M. Kelly and J. C. Lagarias. Photochemistry of 124-kilodalton avena phytochrome under constant illumination in vitro. *Biochemistry*, 24(21):6003 − 6010, 1985.

[32] H.-H. Limbach and J. Manz. Hydrogen transfer: Experiment and theory. Special Issue. *Ber. Bunsenges. Phys. Chem.*, 102:289 − 291, 1998.

[33] K. Giese, M. Petković, H. Naundorf and O. Kühn. Multidimensional quantum dynamics and infrared spectroscopy of hydrogen bonds. *Phys. Rep.*, 430(4):211 − 276, 2006.

[34] S. Habuchi, R. Ando, P. Dedecker, W. Verheijen, H. Mizuno, A. Miyawaki and J. Hofkens. From the cover: Reversible single-molecule photoswitching in the GFP-like fluorescent protein Dronpa. *Proc. Natl. Acad. Sci.*, 102(27):9511 − 9516, 2005.

[35] P.-T. Chou, C.-Y. Wei, C.-P. Chang and C.-H. Chiu. 7-Azaindole-assisted lactam-lactim tautomerization via excited-state double proton transfer. *J. Am. Chem. Soc.*, 117(27):7259 − 7260, 1995.

[36] M. Fischer and P. Wan. *m*-Quinone methides from *m*-hydroxy-1,1-diaryl alkenes via excited-state (formal) intramolecular proton transfer mediated by a water trimer. *J. Am. Chem. Soc.*, 120(11):2680 − 2681, 1998.

[37] O. Vendrell, R. Gelabert, M. Moreno and J. M. Lluch. The operation of the proton-wire in green fluorescent protein. A quantum dynamics simulation. *J. Phys. Chem. B*, 112(17):5500 − 5511, 2008.

[38] S. Kawamura, T. Tsutsui, S. Saito, Y. Murao and K. Kina. Photochromism of salicylideneanilines incorporated in a Langmuir-Blodgett multilayer. *J. Am. Chem. Soc.*, 110(2):509 − 511, 1988.

[39] R. S. Givens, M. B. Kotala and J.-I. Lee. *Mechanistic overview of phototriggers and cage release*, pages 95 − 125. Dynamic studies in biology: Phototriggers, photoswitches and caged biomolecules, M. Goeldner and R. S. Givens (Eds.) Ch. 2. Wiley-Vch, Weinheim, 2005.

[40] K. Zhang, J. E. T. Corrie, V. R. N. Munasinghe and P. Wan. Mechanism of photosolvolytic rearrangement of *p*-hydroxyphenacyl esters: evidence for excited-state intramolecular proton transfer as the primary photochemical step. *J. Am. Chem. Soc.*, 121(24):5625 − 5632, 1999.

[41] C. A. Taylor, M. A. El-Bayoumi and M. Kasha. Excited-state two-proton tautomerism in hydrogen-bonded *N*-heterocyclic base pairs. *Proc. Natl. Acad. Sci.*, 63(2):253 − 260, 1969.

[42] R. Gelabert, M. Moreno and J. M. Lluch. The charge-transfer $\pi\pi^*$ excited state in the 7-Azaindole dimer. A hybrid configuration interactions singles/time-dependent density functional theory description. *J. Phys. Chem. A*, 110(3):1145 − 1151, 2006.

[43] D. Zhong, A. Douhal and A. H. Zewail. Femtosecond studies of protein-ligand hydrophobic binding and dynamics: Human serum albumin. *Proc. Natl. Acad. Sci.*, 97(26):14056 − 14061, 2000.

[44] O. Shimomura and F. H. Johnson. Properties of the bioluminescent protein aequorin. *Biochemistry*, 8(10):3991 − 3997, 1969.

[45] M. Chalfie, Y. Tu, G. Euskirchen, W. W. Ward and D. C. Prasher. Green fluorescent protein as a marker for gene expression. *Science*, 263(5148):802 − 805, 1994.

[46] R. Y. Tsien. The green fluorescent protein. *Annu. Rev. Biochem.*, 67:509 − 544, 1998.

[47] L. Serrano-Andrés and M. Merchán. Quantum chemistry of the excited state: 2005 review. *J. Mol. Struct.*, 729(1 − 2):99 − 108, 2005.

[48] W. Domcke, D. R. Yarkony and H. Köppel. *Conical intersections: Electronic structure, dynamics & spectroscopy*. World Scientific Publishing, Singapore, Advanced Series in Physical Chemistry Vol. 15 edition, 2004.

[49] M. A. Robb, M. Olivucci and F. Bernardi. *Photochemistry*, pages 2056 − 2064. Encyclopedia of Computational Chemistry. Wiley, Chichester, P. v. R. Schleyer edition, 1998.

[50] J. M. Ortiz-Sánchez, R. Gelabert, M. Moreno and J. M. Lluch. Theoretical study on the excited-state intramolecular proton transfer in the aromatic Schiff base salicylidene methylamine: an electronic structure and quantum dynamical approach. *J. Phys. Chem. A*, 110(14):4649 − 4656, 2006.

[51] J. M. Ortiz-Sánchez, R. Gelabert, M. Moreno, J. M. Lluch. A comparative study on the photochemistry of two bipyridyl derivatives: [2,2'-bipyridyl]-3,3'-diamine and [2,2'-bipyridyl]-3,3'-diol. *ChemPhysChem*, 8(8):1199 − 1206, 2007.

[52] J. M. Ortiz-Sánchez, R. Gelabert, M. Moreno and J. M. Lluch. Electronic and quantum dynamical insight into the ultrafast proton transfer of 1-hydroxy-2-acetonaphthone. *J. Chem. Phys.*, 127(8):084318−1 − 084318−8, 2007.

[53] J. M. Ortiz-Sánchez, R. Gelabert, M. Moreno and J. M. Lluch. Study of the photochemical properties and conical intersections of [2,2'-bipyridyl]-3-amine-3'-ol. *ChemPhysChem*, 9(14):2068 − 2076, 2008.

[54] J. M. Ortiz-Sánchez, R. Gelabert, M. Moreno and J. M. Lluch. Electronic-structure and quantum dynamical study of the photochromism of the aromatic Schiff base salicylideneaniline. *J. Chem. Phys.*, 129(21):214308−1 − 214308−11, 2008.

[55] J. M. Ortiz-Sánchez, R. Gelabert, M. Moreno, J. M. Lluch, J. M. Anglada and J. M. Bofill. The bipyridyl derivatives as photomemory devices. A comparative electronic-structure study. *Submitted*.

[56] T. Kawato, H. Kanatomi, H. Koyama and T. Igarashi. Photoisomerization and thermoisomerization II: steric requirements for photochromism and thermochromism of *N,N'*-bis (salicylidene)diamines. *J. Photochem.*, 33(2):199 − 208, 1984.

[57] K. Kownacki, A. Mordzinski, R. Wilbrandt and A. Grabowska. Laser-induced absorption and fluorescence studies of photochromic Schiff bases. *Chem. Phys. Lett.*, 227(3):270 − 276, 1994.

[58] S. Mitra and N. Tamai. A combined experimental and theoretical study on the photochromism of aromatic anils. *Chem. Phys.*, 246(3):463 − 475, 1999.

[59] M. Z. Zgierski and A. Grabowska. Photochromism of salicylideneaniline (SA). How the photochromic transient is created: A theoretical approach. *J. Chem. Phys.*, 112(14):6329 − 6337, 2000.

[60] C. Okabe, T. Nakabayashi, Y. Inokuchi, N. Nishi and H. Sekiya. Ultrafast excited-state dynamics in photochromic *N*-salicylideneaniline studied by femtosecond time-resolved REMPI spectroscopy. *J. Chem. Phys.*, 121(19):9436 − 9442, 2004.

[61] S. Lochbrunner, A. J. Wurzer and E. Riedle. Microscopic mechanism of ultrafast excited-state intramolecular proton transfer: A 30-fs study of 2-(2'-Hydroxyphenyl)benzothiazole. *J. Phys. Chem. A*, 107(49):10580 − 10590, 2003.

[62] K. Stock, T. Bizjak and S. Lochbrunner. Proton transfer and internal conversion of *o*-hydroxybenzaldehyde: Coherent versus statistical excited-state dynamics. *Chem. Phys. Lett.*, 354(5 − 6):409 − 416, 2002.

[63] S. Lochbrunner, K. Stock and E. Riedle. Direct observation of the nuclear motion during ultrafast intramolecular proton transfer. *J. Mol. Struct.*, 700(1 − 3):13 − 18, 2004.

[64] S. Lochbrunner, A. Szeghalmi and K. Stock. Ultrafast proton transfer of 1-hydroxy-2-acetonaphthone: Reaction path from resonance Raman and transient absorption studies. *J. Chem. Phys.*, 122(24):244315−1 − 244315−9, 2005.

[65] R. Gelabert, M. Moreno and J. M. Lluch. Quantum dynamics study of the excited state double-proton transfer in [2,2'-bipyridyl]-3,3'-diol. *Chem. Phys. Chem.*, 5(9):1372 − 1378, 2004.

[66] H. Zhang, P. van der Meulen and M. Glasbeek. Ultrafast single and double proton transfer in photo-excited [2,2'-bipyridyl]-3,3'-diol. *Chem. Phys. Lett.*, 253(1 − 2):97 − 102, 1996.

[67] D. Marks, H. Zhang, M. Glasbeek, P. Borowicz and A. Grabowska. Solvent dependence of (sub)picosecond proton transfer in photo-excited [2,2'-bipyridyl]-3,3'-diol. *Chem. Phys. Lett.*, 275(3 − 4):370 − 376, 1997.

[68] P. Toele, H. Zhang and M. Glasbeek. Femtosecond fluorescence anisotropy studies of excited-state intramolecular double-proton transfer in [2,2'-bipyridyl]-3,3'-diol in solution. *J. Phys. Chem. A*, 106(15):3651 − 3658, 2002.

[69] D. Marks, P. Prosposito, H. Zhang and M. Glasbeek. Femtosecond laser selective intramolecular double-proton transfer in [2,2'-bipyridyl]-3,3'-diol. *Chem. Phys. Lett.*, 289(5 − 6):535 − 540, 1998.

[70] P. Prosposito, D. Marks, H. Zhang and M. Glasbeek. Femtosecond double proton-transfer dynamics in [2,2'-bipyridyl]-3,3'-diol in sol-gel glasses. *J. Phys. Chem. A*, 102(45):8894 − 8902, 1998.

[71] S. R. Logan. *Fundamentos de cinética química*. Addison Wesley Iberoamericana, 2000.

[72] R. G. W. Norrish and G. Porter. Chemical reactions produced by very high light intensities. *Nature*, 164(4172):658, 1949.

[73] A. H. Zewail. *Femtochemistry: Atomic-scale dynamics of the chemical bond using ultrafast lasers*, page 103. Les Prix Nobel, The Nobel Prizes 1999: Nobel Prizes, Presentations, Biographies, and Lectures. Almquist & Wiksell, Stockholm, T. Frängsmyr, 2000.

[74] W. Rodríguez-Córdoba, J. S. Zugazagoitia, E. Collado-Fregoso and J. Peon. Excited state intramolecular proton transfer in Schiff bases. Decay of the locally excited enol state observed by femtosecond resolved fluorescence. *J. Phys. Chem. A*, 111(27):6241 − 6247, 2007.

[75] R. G. Parr and W. Yang. *Density-functional theory of atoms and molecules*. Oxford University Press, New York, 1989.

[76] A. Szabo and N. S. Ostlund. *Modern quantum chemistry: Introduction*. Dover, New York, 1983.

[77] I. N. Levine. *Quantum chemistry*. Prentice Hall, 5th Edition, 2000.

[78] G. A. Worth and L. S. Cederbaum. Beyond Born-Oppenheimer: molecular dynamics through a conical intersection. *Annu. Rev. Phys. Chem.*, 55(1):127 − 158, 2004.

[79] D. R. Yarkony. Diabolical conical intersections. *Rev. Mod. Phys.*, 68(4):985 − 1013, 1996.

[80] D. R. Yarkony. Systematic determination of intersections of potential energy surfaces using a Lagrange multiplier constrained procedure. *J. Phys. Chem.*, 97(17):4407 − 4412, 1993.

[81] J. M. Anglada and J. M. Bofill. A reduced-restricted-quasi-Newton-Raphson method for locating and optimizing energy crossing points between two potential energy surfaces. *J. Comput. Chem.*, 18(8):992 − 1003, 1997.

[82] L. De Vico, M. Olivucci and R. Lindh. New general tools for constrained geometry optimizations. *J. Chem. Theory and Comput.*, 1(5):1029 − 1037, 2005.

[83] M. J. Bearpark, M. A. Robb and H. B. Schlegel. A direct method for the location of the lowest energy point on a potential surface crossing. *Chem. Phys. Lett.*, 223(3):269 − 274, 1994.

[84] A. Toniolo, M. Ben-Nun and T. J. Martínez. Optimization of conical intersections with floating occupation semiempirical configuration interaction wave functions. *J. Phys. Chem. A*, 106(18):4679 − 4689, 2002.

[85] S. Yamazaki and S. Kato. Locating the lowest free-energy point on conical intersection in polar solvent: Reference interaction site model self-consistent field study of ethylene and CH_2NH^+. *J. Chem. Phys.*, 123(11):114510−1 − 114510−13, 2005.

[86] C. Ciminelli, G. Granucci and M. Persico. The photoisomerization mechanism of azobenzene: A semiclassical simulation of nonadiabatic dynamics. *Chem. Eur. J.*, 10(9):2327 − 2341, 2004.

[87] T. W. Keal, A. Koslowski and W. Thiel. Comparison of algorithms for conical intersection optimisation using semiempirical methods. *Theor. Chem. Acc.*, 118(5 − 6):837 − 844, 2007.

[88] F. Sicilia, L. Blancafort, M. J. Bearpark and M. A. Robb. New algorithms for optimizing and linking conical intersection points. *J. Chem. Theory Comput.*, 4(2):257 − 266, 2008.

[89] B. G. Levine, C. Ko, J. Quenneville and T. J. Martínez. Conical intersections and double excitations in time-dependent density functional theory. *Mol. Phys.*, 104(5 − 7):1039 − 1051, 2006.

[90] F. Furche and R. Ahlrichs. Adiabatic time-dependent density functional methods for excited state properties. *J. Chem. Phys.*, 117(16):7433 − 7447, 2002.

[91] R. Ahlrichs, M. Bär, M. Häser, H. Horn and C. Kölmel. Electronic structure calculations on workstation computers: The program system turbomole. *Chem. Phys. Lett.*, 162(2):165 − 169, 1989.

[92] K. Andersson, M. Barysz, A. Bernhardsson, M. R .A. Blomberg, Y. Carissan, D. L. Cooper, M. P. Fülscher, L. Gagliardi, C. de Graaf, B. A. Hess, D. Hagberg, G. Karlström, R. Lindh, P.-Å. Malmqvist, T. Nakajima, P. Neogrády, J. Olsen, J. Raab, B. O. Roos, U. Ryde, B. Schimmelpfennig, M. Schütz, L. Seijo, L. Serrano-Andrés, P. E. M. Siegbahn, J. Stålring, T. Thorsteinsson, V. Veryazov and P.-O. Widmark. Molcas Version 6.2. Dept. of Theor. Chem., Chem. Center, Univ. of Lund, P. O. Box 124, S-221 00 Lund, Sweden, Lund 2002.

[93] A. R. Leach. *Molecular modelling. Principles and applications*. Prentice Hall, Essex, 2001.

[94] J. Z. H. Zhang. *Theory and application of quantum molecular dynamics*. World Scientific, New York, 1999.

[95] H. Tal-Ezer and R. Kosloff. An accurate and efficient scheme for propagating the time dependent Schrödinger equation. *J. Chem. Phys.*, 81(9):3967 − 3971, 1984.

[96] T. J. Park and J. C. Light. Unitary quantum time evolution by iterative Lanczos reduction. *J. Chem. Phys.*, 85(10):8570 − 8576, 1986.

[97]   M. D. Feit, J. A. Fleck Jr. and A. Steiger. Solution of the Schrödinger equation by a spectral method. *J. Comput. Phys.*, 47(3):412 − 433, 1982.

[98]   R. Kosloff. Time-dependent quantum-mechanical methods for molecular dynamics. *J. Phys. Chem.*, 92(8):2087 − 2100, 1988.

[99]   W. H. Press, S. A. Teukolsky, W. T. Vetterling and B. P. Flannery. *Fast fourier transform*, pages 600 − 640. Numerical Recipes 2nd Ed. Ch. 12. Cambridge University Press, New York, 1992.

[100] J. J. Sakurai. *Modern quantum mechanics*. Addition-Wesley, New York, 1994.

[101] N. Makri and W. H. Miller. Time-dependent self-consistent field (TDSCF) approximation for a reaction coordinate coupled to a harmonic bath: Single and multiple configuration treatments. *J. Chem. Phys.*, 87(10):5781 − 5787, 1987.

[102] H.-D. Meyer, U. Manthe and L. S. Cederbaum. The multi-configurational time-dependent Hartree approach. *Chem. Phys. Lett*, 165(1):73 − 78, 1990.

[103] M. H. Beck, A. Jäckle, G. A. Worth and H.-D. Meyer. The multiconfiguration time-dependent Hartree (MCTDH) method: A highly efficient algorithm for propagating wavepackets. *Phys. Rep.*, 324(1):1 − 105, 2000.

[104] G. A. Worth, M. H. Beck, A. Jäckle and H.-D. Meyer. The MCTDH package, version 8.3. Ruprecht-Karls.Universität Heidelberg, Heidelberg, Germany, 2000. See http://www.pci.uni-heidelberg.de/tc/usr/mctdh/.

[105] H. Naundorf, G. Worth, H.-D. Meyer and O. Kühn. Multiconfiguration time-dependent Hartree dynamics on an ab initio reaction surface: ultrafast laser-driven proton motion in phthalic acid monomethylester. *J. Phys. Chem. A*, 106(5):719 − 724, 2002.

[106] M. Petković and O. Kühn. Ultrafast wave packet dynamics of an intramolecular hydrogen transfer system: From vibrational motion to reaction control. *Chem. Phys.*, 304(1 − 2):91 − 102, 2004.

[107] G. A. Worth, H.-D. Meyer and L. S. Cederbaum. State filtering by a bath: up to 24 mode numerically exact wavepacket propagations. *Chem. Phys. Lett.*, 299(5):451 − 456, 1999.

[108] M. D. Coutinho-Neto, A. Viel and U. Manthe. The ground state tunneling splitting of malonaldehyde: Accurate full dimensional quantum dynamics calculations. *J. Chem. Phys*, 121(19):9207 − 9210, 2004.

[109] O. Vendrell, F. Gatti, D. Lauvergnat and H.-D. Meyer. Full dimensional (15D) quantum-dynamical simulation of the protonated water dimer I: Hamiltonian setup and analysis of the ground vibrational state. *J. Chem. Phys.*, 127(18):184302−1 − 184302−17, 2007.

[110] M. H. Beck and H.-D. Meyer. An efficient and robust integration scheme for the equations of motion of the multiconfiguration time-dependent Hartree (MCTDH) method. *Z. Phys. D*, 42(2):113 − 129, 1997.

[111] A. Grabowska and K. Kownacki. Structural aspects of photochromism of the internally H-bonded Schiff bases. "A minimal chromophore". *Acta Phys. Pol. A*, 88(6):1081 − 1088, 1995.

[112] K. Kownacki, L. Kaczmarek and A. Grabowska. Single versus double proton transfer in the photochromic Schiff bases. Electronic spectroscopy and synthesis of model compounds. *Chem. Phys. Lett.*, 210(4 − 6):373 − 379, 1993.

[113] M. Z. Zgierski and A. Grabowska. Theoretical approach to photochromism of aromatic Schiff bases: A minimal chromophore salicylidene methylamine. *J. Chem. Phys.*, 113(19):7845 − 7852, 2000.

[114] M. Ziółek, J. Kubicki, A. Maciejewski, R. Naskręcki and A. Grabowska. Excited state proton transfer and photochromism of an aromatic Schiff base. Pico- and femtosecond kinetics of the *N,N*'-bis(salicylidene)-*p*-phenylenediamine (BSP). *Chem. Phys. Lett.*, 369(1 − 2):80 − 89, 2003.

[115] M. Ziółek, J. Kubicki, A. Maciejewski, R. Naskręcki and A. Grabowska. An ultrafast excited state intramolecular proton transfer (ESPIT) and photochromism of salicylideneaniline (SA) and its double analogue salicylaldehyde azine (SAA). A controversial case. *Phys. Chem. Chem. Phys.*, 6(19):4682 − 4689, 2004.

[116] T. Carrington and W. H. Miller. Reaction surface description of intramolecular hydrogen-atom transfer in malonaldehyde. *J. Chem. Phys.*, 84(8):4364 − 4370, 1986.

[117] N. Shida, P. F. Barbara and J. E. Almlof. A theoretical study of multidimensional nuclear tunneling in malonaldehyde. *J. Chem. Phys.*, 91(7):4061 − 4072, 1989.

[118] S. Scheiner. Theoretical studies of excited state proton transfer in small model systems. *J. Phys. Chem. A*, 104(25):5898 − 5909, 2000.

[119] E. Bosch, M. Moreno, J. M. Lluch and J. Bertrán. Bidimensional tunneling dynamics of malonaldehyde and hydrogenoxalate anion. A comparative study. *J. Chem. Phys.*, 93(8):5685 − 5692, 1990.

[120] J. J. Paz, M. Moreno and J. M. Lluch. Bidimensional tunneling splitting in the $\tilde{A}$ $^1B_2$ and $\tilde{X}$ $^1A_1$ states of tropolone. *J. Chem. Phys.*, 103(1):353 − 359, 1995.

[121] J. A. Organero, I. García-Ochoa, M. Moreno, J. M. Lluch, L. Santos and A. Douhal. A theoretical insight into the internal H-bond and related rotational motion and proton transfer processes of 1-hydroxy-2-acetonaphthone in the S_0 state. *Chem. Phys. Lett.*, 328(1 − 2):83 − 89, 2000.

[122] J. A. Organero, M. Moreno, L. Santos, J. M. Lluch and A. Douhal. Photoinduced proton transfer and rotational motion of 1-hydroxy-2-acetonaphthone in the S_1 state: A theoretical insight into its photophysics. *J. Phys. Chem. A*, 104(36):8424 − 8431, 2000.

[123] R. Gelabert, M. Moreno, J. M. Lluch and A. Lledós. Structure and dynamics of LRh"H$_4$" (L = Cp, Tp) systems. A theoretical study. *Organomet.*, 16(17):3805 − 3814, 1997.

[124] R. Gelabert, M. Moreno, J. M. Lluch, A. Lledós, V. Pons and D. M. Heinekey. Synthesis and properties of compressed dihydride complexes of iridium: Theoretical and spectroscopic investigations. *J. Am. Chem. Soc.*, 126(28):8813 − 8822, 2004.

[125] N. Otsubo, C. Okabe, H. Mori, K. Sakota, K. Amimoto, T. Kawato and H. Sekiya. Excited-state intramolecular proton transfer in photochromic jet-cooled *N*-salicylideneaniline. *J. Photochem. Photobiol. A*, 154(1):33 − 39, 2002.

[126] R. Exelby and R. Grinter. Phototropy (or photochromism). *Chem. Rev.*, 65(2):247 − 260, 1965.

[127] A. Senier and F. G. Shepheard. Salicylidene-*m*-toluidine, a new phototropic compound; salicylideneamines: Salicylamides. *J. Chem. Soc.*, 95:441 − 445, 1909.

[128] M. D. Cohen, G. M. J. Schmidt and (Mrs.) S. Flavian. Topochemistry. Part VI. Experiments on photochromy and thermochromy of crystalline anils of salicylaldehydes. *J. Chem. Soc.*, 2041 − 2051, 1964.

[129] T. Sekikawa, T. Kobayashi and T. Inabe. Femtosecond fluorescence study of the substitution effect on the proton transfer in thermochromic salicylideneaniline crystals. *J. Phys. Chem. A*, 101(4):644 − 649, 1997.

[130] T. Rosenfeld, M. Ottolenghi and A. Y. Meyer. Photochromic arils. Structure of photoisomers and thermal relaxation ptocesses. *Mol. Photochem.*, 5(1):39 − 60, 1973.

[131] P. F. Barbara, P. M. Rentzepis and L. E. Brus. Photochemical kinetics of salicylideneaniline. *J. Am. Chem. Soc.*, 102(8):2786 − 2791, 1980.

[132] M. I. Knyazhansky, A. V. Metelitsa, A. J. Bushkov and S. M. Aldoshin. Role of structural flexibility in fluorescence and photochromism of the salicylideneaniline: the "aldehyde" ring rotation. *J. Photochem. Photobiol. A*, 97(3):121 − 126, 1996.

[133] S. Mitra and N. Tamai. Femtosecond spectroscopic study on photochromic salicylideneaniline. *Chem. Phys. Lett.*, 282(5 − 6):391 − 397, 1998.

[134] S. Mitra and N. Tamai. Dynamics of photochromism in salicylideneaniline: A femtosecond spectroscopic study. *Phys. Chem. Chem. Phys.*, 5(20):4647 − 4652, 2003.

[135] K. Ogawa, J. Harada, T. Fujiwara and S. Yoshida. Thermochromism of salicylideneanilines in solution: Aggregation-controlled proton tautomerization. *J. Phys. Chem. A*, 105(13):3425 − 3427, 2001.

[136] V. Vargas and L. Amigo. A study of the tautomers of *N*-salicylidene-*p*-X-aniline compounds in methanol. *J. Chem. Soc., Perkin Trans. 2*, (7):1124 − 1129, 2001.

[137] M. I. Knyazhansky, A. V. Metelitsa, M. E. Kletskii, A. A. Millov and S. O. Besugliy. The structural transformations and photo-induced processes in salicylidene alkylimines. *J. Mol. Struct.*, 526(1 − 3):65 − 79, 2000.

[138] V. Vargas. Time-resolved fluorescence of salicylideneaniline compounds in solution. *J. Phys. Chem. A*, 108(2):281 − 288, 2004.

[139] M. E. Kletskii, A. A. Millov, A. V. Metelitsa, M. I. Knyazhansky. Role of structural flexibility in the fluorescence and photochromism of salicylideneaniline: The general scheme of the phototransformations. *J. Photochem. Photobiol. A*, 110(3):267 − 270, 1997.

[140] M. J. Paterson, M. A. Robb and L. Blancafort and A. D. DeBellis. Theoretical study of benzotriazole UV photostability: Ultrafast deactivation through coupled proton and electron transfer triggered by a charge-transfer state. *J. Am. Chem. Soc.*, 126(9):2912 − 2922, 2004.

[141] A. L. Sobolewski, W. Domcke and C. Hättig. Photophysics of organic photostabilizers. Ab initio study of the excited-state deactivation mechanisms of 2-(2'-hydroxyphenyl)benzotriazole. *J. Phys. Chem. A*, 110(19):6301 − 6306, 2006.

[142] A. L. Sobolewski and W. Domcke. Photophysics of intramolecularly hydrogen-bonded aromatic systems: Ab initio exploration of the excited-state deactivation mechanisms of salicylic acid. *Phys. Chem. Chem. Phys.*, 8(29):3410 − 3417, 2006.

[143] J. D. Coe, B. G. Levine and T. J. Martínez. Ab initio molecular dynamics of excited-state intramolecular proton transfer using multireference perturbation theory. *J. Phys. Chem. A*, 111(44):11302 − 11310, 2007.

[144] A. L. Sobolewski and W. Domcke. Computational studies of the photophysics of hydrogen-bonded molecular systems. *J. Phys. Chem. A*, 111(46):11725 − 11735, 2007.

[145] Y. Nosenko, G. Wiosna-Sałyga, M. Kunitski, I. Petkova, A. Singh, W. J. Buma, R. P. Thummel, B. Brutschy and J. Waluk. Proton transfer with a twist? Femtosecond dynamics of 7-(2-pyridyl)indole in condensed phase and in supersonic jets. *Angew. Chem., Int. Ed.*, 47(32):6037 − 6040, 2008.

[146] A. Migani, L. Blancafort, M. A. Robb and A. D. DeBellis. An extended conical intersection seam associated with a manifold of decay paths: Excited-state intramolecular proton transfer in o(it)-hydroxybenzaldehyde. *J. Am. Chem. Soc.*, 130(22):6932 − 6933, 2008.

[147] S. Fantacci, A. Migani and Massimo Olivucci. CASPT2//CASSCF and TDDFT//CASSCF mapping of the excited state isomerization path of a minimal model of the retinal chromophore. *J. Phys. Chem. A*, 108(7):1208 − 1213, 2004.

[148] A. M. Tokmachev, M. Boggio-Pasqua, M. J. Bearpark and M. A. Robb. Photostability via sloped conical intersections: A computational study of the pyrene radical cation. *Phys. Chem. A*, 112(43):10881 − 10886, 2008.

[149] K. Tokumura, O. Oyama, H. Mukaihata and M. Itoh. Rotational isomerization of phototautomer produced in the excited-state proton transfer of 2,2'-bipyridin-3-ol. *J. Phys. Chem. A*, 101(8):1419 − 1421, 1997.

[150] W. Rettig, V. Kharlanov and M. Maus. Excited-state relaxation properties of ionic and nonionic donor-acceptor biphenyl derivatives. *Chem. Phys. Lett.*, 318(1 − 3):173 − 180, 2000.

[151] P. Toele and M. Glasbeek. Ultrafast excited-state intramolecular double proton transfer dynamics of [2,2'-bipyridyl]-3,3'-diamine. *Chem. Phys. Lett.*, 407(4 − 6):487 − 492, 2005.

[152] L. Kaczmarek. Bipyridines. Part XVI. Synthesis of novel 1,2,3,7-oxatriazepine and 1,2,3-triazine fused systems by the diazotization of [2,2'-bipyridine]-3,3'-diamine. *Pol. J. Chem.*, 59(1):9 − 15, 1985.

[153] L. Kaczmarek. Bipyridines. Part XVII. A convenient synthesis of some bipyridinediols and furodipyridines. *Pol. J. Chem.*, 59(10 − 12):1141 − 1148, 1985.

[154] A. Dreuw and M. Head-Gordon. Single-refence ab initio methods for the calculation of excited states of large molecules. *Chem. Rev.*, 105(11):4009 − 4037, 2005.

[155] A. L. Sobolewski. Reversible molecular switch driven by excited-state hydrogen transfer. *Phys. Chem. Chem. Phys.*, 10(9):1243 − 1247, 2008.

7
Publications

"We have a habit in writing articles published in scientific journals to make the work as finished as possible, to cover up all the tracks, to not worry about the blind alleys or describe how you had the wrong idea first, and so on. So there isn't any place to publish, in a dignified manner, what you actually did in order to get to do the work."

Richard P. Feynman, Nobel Lecture 1966

Paper I

J. M. Ortiz-Sánchez, R. Gelabert, M. Moreno and J. M. Lluch. Electronic and quantum dynamical insight into the ultrafast proton transfer of 1-hydroxy-2-acetonaphthone. *J. Chem. Phys.* 127(8): 084318-1 – 084318-8, 2007.

Electronic and quantum dynamical insight into the ultrafast proton transfer of 1-hydroxy-2-acetonaphthone

Juan Manuel Ortiz-Sánchez, Ricard Gelabert, Miquel Moreno,[a] and José M. Lluch

Departament de Química, Universitat Autónoma de Barcelona, 08193 Bellaterra, Barcelona, Spain

The ultrafast proton-transfer dynamics of 1-hydroxy-2-acetonaphthone has been theoretically analyzed in the ground and first singlet excited electronic states by density functional theory calculations and quantum dynamics. The potential energies obtained in the ground electronic state reveal that the proton-transfer process does not lead to a stable keto tautomer unless the transfer of the hydrogen from the enol form is accompanied by an internal rotation of the newly formed O–H bond. Calculations in the first singlet excited electronic state point to a very low barrier for the formation of the keto tautomer. The analysis of the calculated frequencies of the two tautomers in the excited state unveils a coupling of the skeletal motions (low frequency modes) with the proton-transfer process, as it has been stated from time-resolved experiments. The electronic energies obtained by the time-dependent density functional theory formalism have been fitted to a monodimensional potential energy surface in order to perform an exact quantum dynamics study of the process. Our results show that the proton-transfer process is completed within 25.5 fs, in remarkable good agreement with experiments. © *2007 American Institute of Physics.*
[DOI: 10.1063/1.2756530]

I. INTRODUCTION

The study of photoinduced proton-transfer processes has received considerable attention in the last few years. This is so because the proton-transfer reactions play a fundamental role in many chemical and biological processes such as acid-base equilibria and energy transport in cells.[1,2] Given the usually very fast nature of these processes, they can only be followed by using femtochemistry techniques. From a theoretical point of view, proton-transfer processes are also specially suited for consideration as the relative low number of atoms implied in the process allows for quite sophisticated and accurate quantum-electronic calculations. Also the dynamics of the whole process can be followed using molecular dynamics techniques that would be too time consuming were it not for the ultrafast nature of the process. The synergy between experimental and theoretical results has allowed for quite important advancements in both sides, a progress that has not reached the end yet.

Among the different proton-transfer processes, the study of excited state intramolecular proton transfer (ESIPT) is particulary attractive as these systems have a well defined starting geometry and the time the transfer starts can be measured precisely so that in this case the comparison between experimental and theoretical data is more direct. ESIPT usually occurs in molecules with intramolecular hydrogen bonds and proceeds by excitation of the normal tautomer followed by ultrafast hydrogen (or proton) transfer in an excited singlet state (usually of $\pi\pi^*$ type). In many of the best known molecular systems that follow this picture, the hydrogen belonging to a hydroxyl group (enol tautomer)

transfersto a neighboring nitrogen atom (keto tautomer). 2-(2′-hydroxyphenyl) benzoxazole (HBO) and several of its derivatives are the more extensively studied systems that belong to this category. For these systems it has been recently shown that ESIPT proceeds in a ballistic way within 50 fs and leads subsequently to a ringing of the molecule in several normal modes of low frequency.[3–6] More recently the same authors have reported a similar work on 1-hydroxy-2-acetonaphtone (HAN).[7] In this case the hydrogen-donor and acceptor atoms are both oxygens so that the reaction is almost symmetric, as seen in Scheme 1.

This recent femtochemistry study of HAN by Lochbrunner *et al.*[7] is by no means the only work on this well studied system nowadays.[8–14] In any case, the work by Lochbrunner *et al.*[7] is the more precise one from the dynamic point of view, as the results are obtained by transient absorption spectroscopy with a time resolution of 30 fs. From the previous studies it was well known that the so-called enol structure is the most stable tautomer in the ground electronic state (S_0). Even if there were some controversy about the feasibility of the ESIPT in HAN,[15,16] it seems clear now that upon photo-excitation to the first singlet excited state (S_1), the system
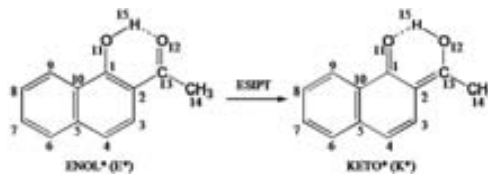
SCHEME 1. Molecular structures of enol (E^*) and keto (K^*) tautomers of 1-hydroxy-2-acetonaphthone (HAN) at the S_1 state. The atom numbering used in this work is also depicted.

[a]Electronic mail: mmf@qf.uab.es

127, 084318-1

undergoes a proton-transfer process to the (more stable) keto tautomer (K^* in Scheme 1, note that an asterisk is used to denote the excited electronic state). K^* is responsible for the fluorescence spectra of HAN, which exhibit a moderate Stokes shift of only $\sim$4000 cm^{-1} (this value is usually larger when ESIPT is present, this being the reason behind the doubts on the actual photochemistry of HAN). The recent work by Lochbrunner *et al.*[7] adds to this picture the dynamics of the process. The delay of 30 fs measured for the fluorescence band to appear (attributed to K^*) indicates that this is the time needed to transfer the proton. The rise is well modeled by a step function so that the ESIPT can be considered a ballistic motion. The subsequent exponential transmission increase on a time scale of 150 fs is interpreted in terms of intramolecular vibrational redistribution. The oscillatory contributions to the coherent excitation of vibrational normal modes in the keto form of the S_1 state, adopted by the molecule after ESIPT, make it possible to measure the modes that are more directly coupled to the proton-transfer coordinate. They are ascribed to motions that facilitate the transfer, that is, modes where the two oxygen atoms come closer so that the proton transfer may proceed without tunneling.

In this paper we undertake an affordable but complete theoretical study of the proton-transfer reaction in S_1, the first excited singlet electronic state of HAN. We will investigate the features of the potential energy surface in S_1 using just first-principles methods. These data will be used later on to follow the dynamics of the photochemical process again, using a purely theoretical method that will permit to solve the nuclear Schrödinger equation and thus follow the time evolution of the system. In the end we will have a complete set of results that will shed light on the actual dynamics of the tautomerization reaction in HAN from a molecular point of view. These results may also serve as a basis for similar studies on a plethora of related systems that are known to undergo ESIPT processes.

II. METHOD OF CALCULATION

A. Electronic-structure calculations

We have used electronic density functional methods to explore the topology of the ground (S_0) and first $\pi\pi^*$ singlet excited (S_1) electronic states. Density functional theory (DFT) and time-dependent DFT (Ref. 17) (TDDFT) optimizations have been performed for the S_0 and S_1 states, respectively, with the three-parameter hybrid functional of Becke with the correlation functional of Lee, Yang, and Parr (B3LYP).[18,19] The TURBOMOLE program (version 5.4),[20,21] which implements analytical gradients at the TDDFT level, has been used to perform the TDDFT calculations. For minima in S_0, analytical vibrational frequencies have been computed, whereas expensive numerical vibrational frequencies have been calculated for energy minima in S_1. Also, an intrinsic reaction coordinate (IRC) calculation has been perfomed at the DFT level with the GAUSSIAN03 package.[22] As we stated in a previous work,[23] the B3LYP functionals used in the GAUSSIAN03 and TURBOMOLE packages differ very little in the relative stability of the calculated points, which implies a very little effect on our results. This small differ-

ence comes from the use of a different form of the local correlation functional: The GAUSSIAN03 package uses the VWN(III) local correlation functional, whereas TURBOMOLE uses VWN(V).[24] For all optimizations, the 6-31G(d,p) (Ref. 25 and 26) basis set has been used throughout.

B. Molecular dynamics calculations

To determine the time scale of the photoinduced proton transfer in the excited state a wave packet propagation has been used. In order to simulate the experimental setup of this experiment, an appropriate initial quantum state for the system ($|\Psi_0\rangle$) is prepared through diagonalization of the matrix representation of the Hamiltonian for the electronic ground state, and selection of the lowest energy eigenvector. This vibrational state of the electronic ground state is the initial state of the dynamics. Next, this wave packet is placed in the Franck-Condon region of S_1 to simulate the photoexcitation. $|\Psi_0\rangle$ does not represent a stationary state in S_1, and to determine the time evolution of this state the time-dependent Schrödinger equation has to be solved,

$$i\hbar\frac{d}{dt}|\Psi(t)\rangle = \hat{H}|\Psi(t)\rangle, \tag{1}$$

or equivalently, given that the Hamiltonian operator is not time dependent,

$$|\Psi(t)\rangle = e^{-i\hat{H}t/\hbar}|\Psi_0\rangle, \tag{2}$$

where

$$\hat{H} = \hat{T} + V_{S_1}(\mathbf{q}). \tag{3}$$

Here, $\mathbf{q}$ is a given set of coordinates to represent the system and upon which the potential energy surface is defined.

Time evolution has been then carried out in a numerically exact manner. The matrix representation of the Hamiltonian operator in S_1 has been diagonalized to obtain the energies ($\{E_i^{S_1}\}_{i=1-N}$) and eigenvectors ($\{|\varphi_i^{S_1}\rangle\}_{i=1-N}$). If completeness is assumed for the set of states (in practice, $N \rightarrow \infty$), the following spectral representation of the time evolution operator in S_1 can be accepted as exact:[27]

$$e^{-i\hat{H}t/\hbar} = \sum_{i=1}^{N} |\varphi_i^{S_1}\rangle e^{-iE_i^{S_1}t/\hbar}\langle\varphi_i^{S_1}|. \tag{4}$$

Time evolution is obtained then in a straightforward manner by computing the wave packet at different t values with the following equation, which gives directly the amplitude of the wave function at time t:

$$\Psi(\mathbf{q},t) = \langle\mathbf{q}|\Psi(t)\rangle = \sum_{i}^{N} \langle\mathbf{q}|\varphi_i^{S_1}\rangle e^{-iE_i^{S_1}t/\hbar}\langle\varphi_i^{S_1}|\Psi_0\rangle$$

$$= \sum_{i}^{N} \varphi_i^{S_1}(\mathbf{q})e^{-iE_i^{S_1}t/\hbar}\langle\varphi_i^{S_1}|\Psi_0\rangle. \tag{5}$$

As will be described in the Results section, an isoinertial monodimensional coordinate has been used for $\mathbf{q}$ to describe the system. This choice renders the potential energy surfaces and also all wave functions monodimensional.

In the preceeding paragraphs, whenever a matrix representation of an operator is needed the *sync* discrete variable representation of Colbert and Miller has been used.[28] The grid used to construct such matrix representations was of 50 points. This means that the value of N in the preceeding equations is also 50. Convergence of the dynamical calculation was ascertained by changing the value of N and checking that the results remained stable. As will be described, the dynamics has been computed for 500 fs. All along this time special attention has been devoted to the unitarity of the time evolution operator in use. The norm of $|\Psi(t)\rangle$ has been mostly constant and equal to $1.000\,00\pm0.000\,05$ throughout. It is worth mentioning that the propagation is exact, and this small deviation from unity is due to the fact that the spectral expansion in Eq. (5) has been truncated to some finite value of i (actually $N=50$).

III. RESULTS AND DISCUSSION

As in the previous section we will divide the main results section into two parts, the first devoted to analyze the purely electronic-structure calculations and a second one where the previous electronic results are used to perform nuclear dynamics simulations of the ESIPT process.

A. Electronic-structure calculation

The energy profile of the proton-transfer reaction in HAN has been previously reported at different levels of calculation.[10,13,14] In the most recent of such works, Organero *et al.*[14] located the stationary points (reactants, products, and transition states) using the Hartree-Fock method in the ground electronic state (S_0) and the configuration interaction singles method (CIS) in the first singlet excited electronic state (S_1). Energies in S_0 were recalculated at the Møller-Plesset perturbation theory up to second order. Our first task in this paper has been the recalculation of the relevant geometries using DFT formalism in S_0 and the corresponding TD-DFT method in S_1. The stationary points in the S_0 state have been localized by full minimization and characterized at the DFT level of calculation, while only the zeroth-order stationary points in the S_1 state have been directly located at the TDDFT level. At present, to characterize stationary points in the TDDFT scheme1, numerical second derivatives must be computed (due to the unavailability of analytic second derivatives), which is a fairly expensive calculation. Instead, relaxed potential energy profiles for both proton transfer and acetyl rotation have been computed, using as a reaction coordinate the distance between the O_{11}–H_{15} bond and the C_1–C_2–C_{13}–O_{12} dihedral angle, (which is equivalent to the rotation around the C_2–C_{13} bond) respectively. Results are graphically depicted in Fig. 1

The energy profile in S_0 is quite similar to the one previously obtained:[14] there is a considerable energy barrier for the tautomerization (57.01 kcal mol^{-1}) and the whole tautomerization process is clearly endoergic by 20.92 kcal mol^{-1}. It is to be noted that the direct keto tautomer is not a true minimum in the potential energy surface of S_0 and that the located minimum corresponds, in fact, to a rotamer (KR), where the carbonyl group has been rotated by
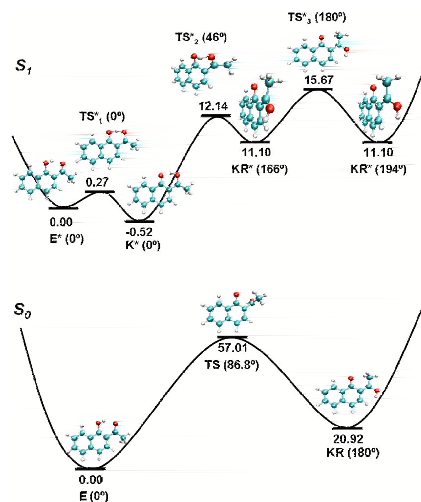

FIG. 1. (Color online) Schematic energy profile including the involved structures for proton transfer and twisting motion of HAN in both the S_0 (lower half) and S_1 (upper half). Energies relative to E or E* are given in kcal mol^{-1}. We indicate in parentheses the angle of the acetyl rotation around the C_2–C_{13} bond. Note that both KR* structures are displayed in a different orientation to appreciate the twist of the C_2–C_{13} bond.

180°. Then both initial (enol, E) and final KR structures are planar (except for the methyl group), but the transition state has the carbonyl group almost perpendicular (86.8°) so that the transition state corresponds, in fact, to a rotation of the C_2–C_{13} bond (atom numeration is indicated in Scheme 1) once the proton has been transferred. In other words, the reaction coordinate from E to KR includes both the proton transfer and the internal rotation around the C_2–C_{13} bond. Given that the new O–H bond is already formed in the transition state (O–H distance=0.98 Å) it is clear that the proton transfer takes place before the rotation has been completed. To confirm this assumption, the IRC path has been evaluated from the transition state structure to the reactants in S_0 at the DFT level. Results show a completely formed H_{15}–O_{12} bond even for small rotation values of the C_2–C_{13} bond ($\sim15°$).

Things are different in the first excited electronic state S_1. This state is of $\pi\pi^*$ type, as already observed in the previous CIS calculations.[14] Also, as it is usually seen for aromatic systems that undergo ESIPT, the energy profile of the tautomerization process is now slightly exoergic, as depicted in Fig. 1, and the energy barrier for the process is quite small. At the level of calculation used here, the keto tautomer K* lies just 0.52 kcal mol^{-1} below the enol minimum E*. The transition state linking both structures is also quite low in energy as it rises only 0.27 kcal mol^{-1} above E* so that the tautomerization is now a quite feasible process, specially taking into account that the excited state is accessed upon irradiation so that the starting structure is not the enol minimum E* but, according to the Franck-Condon principle, the result of the vertical excitation from the ground-state minima. This point lies 4.64 kcal mol^{-1} above E* so that it

lies well above the transition state and tautomerization may occur as an over-the-barrier process in a very short (maybe a few femtoseconds) time, as observed experimentally. This point will be considered in more detail in the next subsection. The small potential energy barrier between the E* and the K* structures and their similar energies also suggest that an equilibrium between both species could be reached likely in a short time. Evidences of such an equilibrium have been found in several experimental works.[7,8,14]

This equilibrium may also affect the fluorescence spectrum of HAN. The very broad absorption bands observed in the spectra of HAN in gas phase and apolar media (350–400 nm)[7,8] are well described within our theoretical setup as the TDDFT calculation of the vertical excitation (i.e., the excited state energy at the geometry of the minimum in S_0, according to the Franck-Condon principle) gave a value of 349 nm. As for the fluorescence band, it is also very broad and experimentally found between 400 and 500 nm.[7,8] It is usually fully ascribed to emission from the keto tautomer formed after ESIPT, but if our theoretical calculations are accurate it could well come from relaxations of both E* and K*, tautomers assuming that these structures are at equilibrium. Our calculated vertical transitions for the reverse $S_1 \rightarrow S_0$ transitions are 397 and 432 nm (for E* and K*, respectively), slightly too low values but within the broad experimental range. A point in favor of this interpretation is the observation of two close maxima in the fluorescence spectra (see Fig. 1 in Ref. 7) that could well appear as the consequence of the overlap of two fluorescence bands.

The rest of the energy profile in S_1 depicted in the top of Fig. 1 corresponds to the internal rotation around the C_2-C_{13} bond and presents two additional minima labeled KR* in Fig. 1 as they are rotamers of the keto form. The planar (C_S) rotamer that appears after a rotation of 180° (the rotational angle along the C_2-C_{13} bond in degrees is indicated in parentheses for all the labeled structures in Fig. 1) is not a minimum but a transition state structure linking two equivalent nonplanar minima found at 166° and 194° (that is, 14° away from the planar transition state in both directions). In the previous CIS calculations,[14] these KR* structures were the lowest lying ones in S_1, but now they are found at quite high energy (11.10 kcal mol^{-1} above E*) so that at our improved level of calculation it is concluded that these structures cannot be accessed upon photoexcitation to S_1. However, even if TDDFT calculations are usually giving quite reliable energies for excited states, clearly more accurate than the CIS ones, higher level (and thus more expensive) calculations would be necessary to actually ascertain the relative position of these rotamers with respect to the original E* and K* tautomers and the role they might play in the whole photochemistry of HAN.[14,29] In any case, as already pointed out by Lochbrunner *et al.*,[7] the time scale of these internal rotations will be too long to interfere with the dynamics of the ESIPT, the process we are going to analyze using purely theoretical procedures in the next subsection.

As a final point of this static study of the different tautomers of HAN, let us analyze the vibrational frequencies in S_1. This study is of relevance for the dynamics of the process, as time-resolved transmission changes after electronic

TABLE I. Calculated frequencies (in cm^{-1}) for the different tautomers. Obtained frequencies have been multiplied by a factor of 0.96. Numbers in parentheses indicate the position of each frequency when ordered from lower to higher values.

S_0		S_1	
Enol	Keto rotamer	Enol	Keto
192 (5)	189 (5)	192 (5)	192 (5)
302 (8)	317 (8)	293 (8)	295 (8)
339 (9)	323 (9)	350 (9)	357 (9)
406 (10)	381 (10)	405 (11)	406 (11)
476 (13)	468 (14)	452 (13)	464 (13)
517 (14)	491 (15)	513 (16)	505 (16)
553 (15)	535 (16)	549 (17)	530 (17)
589 (18)	599 (18)	582 (18)	592 (18)
660 (19)	660 (20)	641 (20)	641 (20)
869 (27)	844 (26)	860 (27)	865 (27)

excitation of HAN show oscillatory contributions that are attributed to normal modes that are coupled to the proton-transfer coordinate. These modes are ascribed to motions that affect the O–O distance (so that they facilitate the proton-transfer). Lochbrunner *et al.*[7] compare the vibrations obtained through Fourier transformations of the oscillatory time-resolved transmission with the calculated frequencies of the enol form in S_0 (assuming that frequencies in the excited S_1 state are about 10% lower than in the electronic ground state). The TURBOMOLE program, used to perform the TD-DFT calculations in S_1, can be used to compute (through numerical derivation of the first energy derivatives as explained before) the harmonic frequencies in an excited electronic state. Table I presents the results of some selected modes. We do not give here the whole set of frequencies (there are 66 normal modes in HAN), as in the previous work by Lochbrunner *et al.*,[7] the full list of frequencies (with the vibrational assignement for each mode) is already provided for the ground-state enol tautomer. Instead, in Table I just the frequencies that affect the atoms involved in the proton transfer are posted (that is, frequencies that involve the motion of the O–H···O fragment). These frequencies are likely candidates to be coupled with the proton-transfer reaction coordinate so that their values and changes along the proton-transfer reaction are relevant.

Results in Table I are not restricted to the excited S_1 state but the ground-state frequencies are also shown. These are quite similar to the ones reported by Lochbrunner *et al.*[7] but not identical, as the functionals used in the DFT calculations are not identical. We have also included the frequencies of the two tautomers (of course for the gound state the keto results actually correspond to the rotameric KR structure). As previously suggested,[30] the harmonic B3LYP[6-31G(d,p)] frequencies are multiplied by a factor of 0.96 to obtain more accurate values when comparing to spectroscopical data.

It is noteworthy that the list of frequencies in Table I is larger than the number of frequencies originally considered by Lochbrunner *et al.*[7] as the ones most directly coupled to the proton-transfer coordinate: only four frequencies are analyzed in that work, whereas we have considered ten in Table
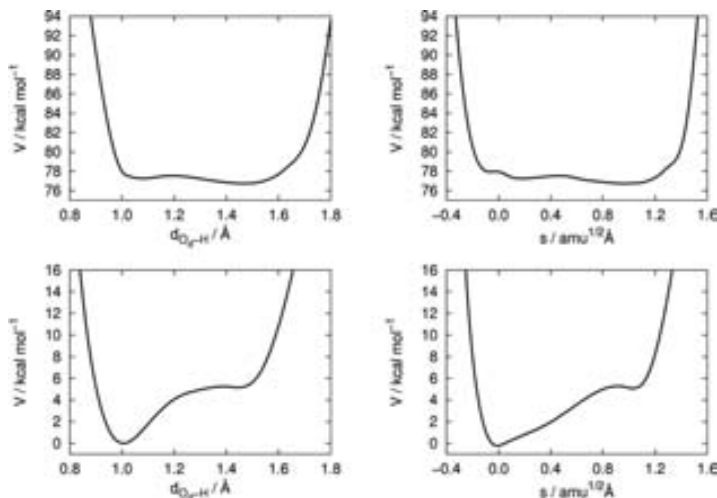
FIG. 2. Potential energy profiles (in kcal mol^{-1}) as a function of the donor O–H distance (in Å, left) and the collective isoinertial coordinate s (in amu$^{1/2}$ Å, right) for the ground electronic state (bottom) and first excited singlet state (top). Energy origin is the potential energy minimum in S_0. Origin of the isoinertial coordinate s is the relaxed structure within each state for which the donor O–H distance is 1.0 Å.

I. In fact, from the time-resolved experiments, just three frequencies are revealed to be involved in the oscillatory transmission change. These frequencies amount to 280, 312, and 368 cm^{-1}, and they should be assigned to specific frequencies of the keto form in the S_1 state. The closest values to these in Table I are found at 295, 357, and 406 cm^{-1} so that these frequencies ought to be taken as the ones most directly coupled to the proton-transfer coordinate. In fact, the two higher ones correspond to modes, where motion indicates a clear approximation of the two oxygen atoms. In the other mode, at 295 cm^{-1}, this motion is much more tenuous (though present). In fact, there are other modes with a more relevant motion along the O–O coordinate, mainly the ones with frequencies of 192, 530, and 592 cm^{-1}.

Comparison of S_0 and S_1 frequencies does not disclose any important difference within the values posted in Table I, though some changes in the total ordering are seen. A comparison of the enol and keto frequencies shows also minor numerical differences, in no case larger than 30 cm^{-1}. Of course, this fact applies basically to the purely skeletal modes such as the ones reported in Table I. Larger differences affect vibrations that involve the motion of the transferring hydrogen and the surrounding atoms.

B. Molecular dynamics calculations

In the preceeding section it has been discussed that the ESIPT in S_1 corresponds to a process with small barrier and slightly exoergic. Because of excess energy after photoexcitation, this probably means that the proton will indeed move very fast. Experimentally a value of 30 fs has been measured as the delay in the appearance of the fluorescence band that is attributed to the K species and in turn identified with the time taken by the proton to transfer. In the current section we will develop a simple yet sufficient model based on quantum dynamics that will allow us to derive a value for the proton-transfer time, purely on theoretical grounds.

To do quantum dynamics, it is necessary to have some kind of estimate of the potential energy surface of the electronic state involved. While the real chemical process—proton transfer—is acknowledged to be multidimensional (i.e., to involve many degrees of freedom of the molecular system), it is also true that the proton transfer at hand has been described as *ultrafast* and hence will consist mostly of proton motion and maybe a certain degree of donor-acceptor atom motion, while the rest of the molecular skeleton remains unmodified for times substantially longer than that of the proton transfer itself.

With these considerations in mind, a monodimensional (1D) approach has been used that represents appropriately the main characteristics of the process. First, relaxed potential energy profiles for both S_0 and S_1 have been constructed by means of constrained energy minimization at different values of the donor O–H distances, spanning the complete range from reactants to products of the proton transfer. Later on, the potential energy values thus obtained are referenced to each other within an isoinertial coordinate system s. In this system, the value $s=0$ has been assigned to the geometries where the donor O–H distance matches that of the potential energy minimum in S_0 (1.0 Å). The rest of the geometries are assigned s values that represent the distance in isoinertial units to the point preceeding each of them in terms of the donor O–H distance. Operating in this way, the s value of a structure represents the arc-length distance in configurational space and mass-weighted units of such structure to that which is closest to the minimum in S_0. It is natural to assume that changes in the value of s between any two different structures are due to motion of the transferring proton, but because the potential energy profile has been obtained through constrained minimization of all geometrical parameters except the donor O–H distance, all atoms have moved and thus their motion is at least partially present in s. Equivalent approaches have been previously used with success in simplified dynamical studies.[31,32] Figure 2 shows the poten-
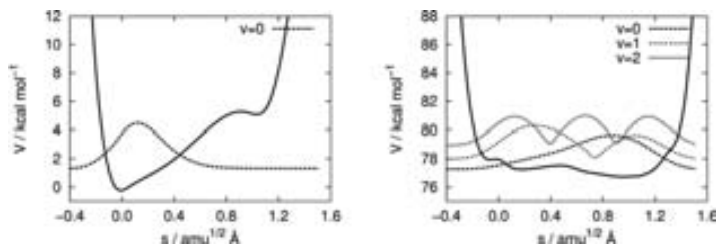
FIG. 3. Probability density functions of the ground vibrational state of S_0 (left) and of the first few vibrational states in S_1 (right). The y-axis scale refers to the energy values only. Probability density functions are represented in arbitrary units but at the same scale.

tial energy profiles as a function of the donor O–H distance and of the s isoinertial coordinate. As defined, values of s close to zero are indicative of structures very similar to the reactant (that is, enol), whereas large and positive values of s represent structures similar to the proton-transfer product (keto structures).

Now a quantum dynamics study is possible since the potential energy field acting on the nuclei is known. As explained in the Computational Details section Eq. (5), an analytic spectral expansion of the time evolution operator in terms of the vibrational eigenstates of S_1 has been used. The dynamical study proceeds by simulating the experimental process as follows. The ground vibrational state of S_0 in terms of s is taken as the initial state of the system after photoexcitation, which simply is represented by placing this state in the S_1 state. This ground vibrational state is determined by selecting the eigenvector associated with the smallest eigenvalue of the matrix representation of the S_0 Hamiltonian

$$\hat{H}^{S_0} = -\frac{\hbar^2}{2}\frac{\partial^2}{\partial s^2} + V^{S_0}(s), \tag{6}$$

where V^{S_0} corresponds to the potential energy surface of the ground electronic state. Note that the usual m^{-1} dependence in the kinetic term is actually included in the s definition. Figure 3 displays the probability density function derived from this initial state. As can be seen, it is markedly localized in the reactants' area as it befits the shape of the potential energy function for S_0.

After $|\Psi_0\rangle$ is determined, the photoexcitation process is simulated by promoting this state to S_1. This is possible and meaningful because the choice of $s=0$ is the same for S_0 and S_1, corresponding to two structures where the donor O–H distance is the same (1.0 Å); even though for values of s far from zero, it is true that both monodimensional paths could visit areas of configurational space that would be increasingly different. While $|\Psi_0\rangle$ is a stationary state of S_0, it is not a stationary state of S_1 and its time evolution can be easily determined by using Eq. (5). To do this, the vibrational eigenstates of S_1 are needed. These can be readily obtained through diagonalization of the matrix representation of the Hamiltonian of S_1, an equation analogous to Eq. (6). The densities for the first three states of the complete series of 50 vibrational states are depicted in Fig. 3. It is worth noting that increasingly more energetic states display more pronounced amplitudes toward shorter values of s, that is, "reactantlike" structures. The highest vibrational state depicted in Fig. 3 ($v=2$) shows an almost regular distribution along

all the accessible values of s. The same behavior is found for the rest of the calculated vibrational states ($v > 2$), which are analogous to the well known results of the particle-in-a-box system. Of course this just indicates that the higher energy levels do not see the small variations of the potential energy in the region between the two minima and just feel the sudden energy raise at the extreme values of the coordinate s.

The excited state dynamics have been followed for up to 500 fs for convenience. The main result of the dynamical study is the time it takes to transfer the proton to the products' side of the potential energy profile. To this end, the survival probability is defined as the fraction of the probability density function that remains still in the reactants' region at a given time,

$$P(t) = \int_{-\infty}^{s^*} ds |\Psi(s,t)|^2, \tag{7}$$

where $s^* = 0.54$ amu$^{1/2}$ Å is the value of s at the saddle point in the potential energy profile for S_1, taken here as the border between reactants and products. Figure 4 displays the time evolution of the survival probability. Thus, a value of $P(t) = 0$ indicates that upon chemical measurement 100% of the systems would be found to be product (keto) structures at time t, whereas a value of $P(t) = 1$ would indicate that upon measurements all systems would be found to be reactants.

Analysis of Fig. 4 reveals a periodic transfer of the system from reactants to products with a period of approximately 100 fs. If one assumes that the time needed to bring $P(t)$ to a value of 0.5 is representative of the time measured experimentally as that of the proton transfer, then in view of our results this is predicted to be $\sim$25.5 fs, remarkably close to the value experimentally reported. In fact, values under
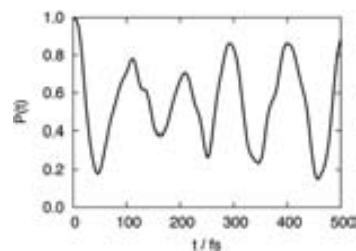

FIG. 4. Survival probability of the reactant species E* in S_1 after photoexcitation.

50 fs have also been found theoretically for other systems, where the proton transferred along purely downhill potential energy profiles.[23]

It is worth remarking that the resonant features in the survival probability depicted in Fig. 4 are unlikely to be found in experimental measures. At large t values, the real system would have activated other vibrational degrees of freedom of the molecule (vibrations), perhaps after a few recurrences of the wave packet. As such, the energy content of the degrees of freedom that corresponds to the proton motion would be certainly lower than at the beginning of the experiment and, as a result, the system is likely to stabilize in product form. In our simple theoretical model this is not possible, simply because these coupled vibrations are not there. Thus, the model system is forced to return to reactants in a periodic manner. Consequently, the information in Fig. 4 will diverge increasingly from experimental measurements at large values of time.

As mentioned before, from the experimental standpoint, it has been suggested that the E^* and K^* forms are in equilibrium during the experimental measurement time. This postulated equilibrium cannot be observed as such from our simulations, that is, a time independent state achieved as $t \rightarrow \infty$. The reason for this is that our model is monodimensional and closed. Our dynamical simulation shows that the smallest value of $P(t)$ is reached in about 46 fs (that being 0.18 approximately, or 82% keto form). From then on the wave packet bounces back and interferences between inbound and outbound waves are observed. This behavior is better described as a resonance between the excited keto and enol forms, with a period $T \sim 110$ fs, similar to what is observed in a Rabi oscillation.[33] However, in absolute terms, our simulation predicts that such an equilibrium, as has been postulated experimentally, would establish itself very fast, at any rate within at most very few hundreds of femtoseconds, given that an almost complete conversion of the E^* into K^* takes place, during the first oscillation, within 50 fs. Thus the experimental suggestion of an equilibrium in S_1 between E^* and K^* can be considered, as validated by dynamical simulations.

IV. CONCLUSIONS

In this paper we have completed a quite comprehensive theoretical study of the proton transfer in the ground (S_0) and first singlet excited (S_1) electronic states of HAN. Our quantum-electronic calculations at the DFT level for S_0 and the equivalent TDDFT level for S_1 have revealed that the proton transfer in S_0 does not lead to a stable tautomer unless the transfer of the hydrogen is accompanied by an internal rotation of the newly formed O–H bond. In any case, the very high energy barrier calculated for this process will prevent the reaction in S_0 from taking place.

Things are different in S_1 as the calculations there point to the keto tautomer as the more stable species. The energy barrier for the ESIPT is also quite low, well below the energy of the vertical transition from the minimum of S_0, so that ESIPT in HAN may be an ultrafast process, as pointed out by Lochbrunner *et al.* in a recent experimental work.[7] Analysis

of the calculated frequencies of the two tautomers in S_1 has also been done in order to characterize the skeletal motions (low frequency modes) that are most likely coupled to the ESIPT process. These modes should have an important component corresponding to the internal motion of the O–H···O fragment, and our analysis reveals the presence of ten frequencies in the range of 200–900 cm^{-1} that may be involved in such a coupling. In fact, from time-resolved experiments, three frequencies within this range are identified as responsible for the oscillatory transmission change after photoexcitation of HAN measured by Lochbrunner *et al.*

The electronic calculations in S_1 have been used to fit a 1D potential energy surface for the ESIPT. This potential energy surface is necessary to perform a quantum dynamics study of the process. This allows for a crude estimation of the time needed for the proton to move from the enol structure at the geometry of the minimum energy in S_0 up to the more stable (in S_1) keto tautomer. Our 1D dynamic method is exact (except for very minor numerical errors that have been minimized) and shows that the ESIPT involves a very fast motion and is completed within 25.5 fs, in remarkable good agreement with the experimental result of 30 fs. After that time, our dynamics shows a periodic behavior of the survival probability so that the proton oscillates between the two, almost degenerated, keto and enol minima. This behavior is not likely to be found in experimental measures, as the vibrational degrees of freedom coupled to the proton motion will progressively take away the initial energy of the proton motion. Instead, the actual process in HAN will probably lead to an equilibrium between both tautomers in S_1.

Our global results are probably to be applied to other systems for which a very fast proton transfer in the $\pi\pi^*$ excited state is found. These include the HBO already cited in the Introduction[3–6] and closely related molecules.[34] Electronic calculations have also disclosed a similar energy profile in the $\pi\pi^*$ excited state of other systems.[35,36] In all these cases the very low (or inexistent) energy barrier and similar energies of both tautomers point to an ESIPT that would probably proceed in a balistic way.

ACKNOWLEDGMENTS

[1] *Proton Transfer in Hydrogen-Bonded Systems*, edited by T. Bountis (Plenum, New York, 1992).
[2] Phys. Chem. Chem. Phys. **102**, 289 (1998), special issue on Hydrogen Transfer: Experiment and Theory.
[3] S. Lochbrunner and E. Riedle, Recent Res. Devel. Chem. Physics **4**, 31 (2003).
[4] S. Lochbrunner, A. J. Wurzer, and E. Riedle, J. Phys. Chem. A **107**, 10580 (2003).
[5] K. Stock, T. Bizjak, and S. Lochbrunner, Chem. Phys. Lett. **354**, 409 (2002).
[6] S. Lochbrunner, K. Stock, and E. Riedle, J. Mol. Struct. **700**, 13 (2004).
[7] S. Lochbrunner, A. Szeghalmi, K. Stock, and M. Schmitt, J. Chem. Phys.

122, 244315 (2005).

[8] A. Douhal, F. Lahmani, and A. Zehnacker-Rentien, Chem. Phys. **178**, 493 (1993).

[9] J. Catalán and J. C. del Valle, J. Am. Chem. Soc. **115**, 4321 (1993).

[10] J. Catalán, J. Palomar, and J. L. G. de Paz, Chem. Phys. Lett. **269**, 151 (1997).

[11] S. Tobita, M. Yamamoto, N. Kurahayashi, R. Tsukagoshi, Y. Nakamura, and H. Shizuka, J. Phys. Chem. A **102**, 5206 (1998).

[12] C. Lu, R. M. R. Hsieh, I. R. Lee, and P. Y. Cheng, Chem. Phys. Lett. **310**, 103 (1999).

[13] J. A. Organero, I. García-Ochoa, M. Moreno, J. M. Lluch, L. Santos, and A. Douhal, Chem. Phys. Lett. **328**, 83 (2000).

[14] J. A. Organero, M. Moreno, J. M. Lluch, L. Santos, and A. Douhal, J. Phys. Chem. A **104**, 8424 (2000).

[15] J. Catalán and J. L. G. de Paz, J. Phys. Chem. A **105**, 7315 (2001).

[16] J. A. Organero, A. Vargas-Díaz, M. Moreno, L. Santos, and A. Douhal, J. Phys. Chem. A **105**, 7317 (2001).

[17] R. Bauernschmitt and R. Ahlrichs, Chem. Phys. Lett. **256**, 454 (1996).

[18] A. D. Becke, J. Chem. Phys. **98**, 5648 (1993).

[19] C. T. Lee, W. T. Yang, and R. G. Parr, Phys. Rev. B **37**, 785 (1988).

[20] F. Furche and R. Ahlrichs, J. Chem. Phys. **117**, 7433 (2002).

[21] R. Ahlrichs, M. Bär, M. Haser, H. Horn, and C. Kolmel, Chem. Phys. Lett. **162**, 165 (1989).

[22] M. J. Frisch, G. W. Trucks, H. B. Schlegel *et al.*, GAUSSIAN 03, Revision C.03, Gaussian, Inc., Wallingford, CT, 2004.

[23] J. M. Ortiz-Sánchez, R. Gelabert, M. Moreno, and J. M. Lluch, J. Phys. Chem. A **110**, 4649 (2006).

[24] S. H. Vosko, L. Wilk, and M. Nusair, Can. J. Phys. **58**, 1200 (1980).

[25] P. C. Hariharan and J. A. Pople, Theor. Chim. Acta **28**, 213 (1973).

[26] M. M. Francl, W. J. Pietro, W. J. Hehre, J. S. Binkley, M. S. Gordon, D. J. Defrees, and J. A. Pople, J. Chem. Phys. **77**, 3654 (1982).

[27] J. J. Sakurai, *Modern Quantum Mechanics* (Addition-Wesley, New York, 1994).

[28] D. T. Colbert and W. H. Miller, J. Chem. Phys. **96**, 1982 (1992).

[29] J. A. Organero, L. Tormo, and A. Douhal, Chem. Phys. Lett. **363**, 409 (2002).

[30] A. P. Scott and L. Radom, J. Phys. Chem. **100**, 16502 (1996).

[31] R. Gelabert, M. Moreno, J. M. Lluch, A. Lledós, V. Pons, and D. M. Heinekey, J. Am. Chem. Soc. **126**, 8813 (2004).

[32] R. Gelabert, M. Moreno, J. M. Lluch, and A. Lledós, Organometallics **16**, 3805 (1997).

[33] C. Cohen-Tannoudji, B. Diu, and F. Laloë, *Quantum Mechanics* (Wiley, New York, 1977).

[34] R. de Vivie-Riedle, V. D. Waele, L. Kurtz, and E. Riedle, J. Phys. Chem. A **107**, 10591 (2003).

[35] A. J. A. Aquino, H. Lischka, and C. Hättig, J. Phys. Chem. A **109**, 3201 (2005).

[36] L. Sobolewski and W. Domcke, Phys. Chem. Chem. Phys. **1**, 3065 (1999).

Paper II

J. M. Ortiz-Sánchez, R. Gelabert, M. Moreno and J. M. Lluch. Theoretical study on the excited-state intramolecular proton transfer in the aromatic schiff base salicylidene methylamine: an electronic structure and quantum dynamical approach. *J. Phys. Chem.* A 110(14): 4649 – 4656, 2006.

Theoretical Study on the Excited-State Intramolecular Proton Transfer in the Aromatic Schiff Base Salicylidene Methylamine: an Electronic Structure and Quantum Dynamical Approach

Juan Manuel Ortiz-Sánchez, Ricard Gelabert,* Miquel Moreno, and José M. Lluch

Departament de Química, Universitat Autònoma de Barcelona, 08193 Bellaterra, Barcelona, Spain

Received: January 23, 2006; In Final Form: February 23, 2006

The proton-transfer dynamics in the aromatic Schiff base salicylidene methylamine has been theoretically analyzed in the ground and first singlet (π,π^*) excited electronic states by density functional theory calculations and quantum wave-packet dynamics. The potential energies obtained through electronic calculations that use the time-dependent density functional theory formalism, which predict a barrierless excited-state intramolecular proton transfer, are fitted to a reduced three-dimensional potential energy surface. The time evolution in this surface is solved by means of the multiconfiguration time-dependent Hartree algorithm applied to solve the time-dependent Schrödinger equation. It is shown that the excited-state proton transfer occurs within 11 fs for hydrogen and 25 fs for deuterium, so that a large kinetic isotope effect is predicted. These results are compared to those of the only previous theoretical work published on this system [Zgierski, M. Z.; Grabowska, A. *J. Chem. Phys.* **2000**, *113*, 7845], reporting a configuration interaction singles barrier of 1.6 kcal mol^{-1} and time reactions of 30 and 115 fs for the hydrogen and deuterium transfers, respectively, evaluated with the semiclassical instanton approach.

1. Introduction

Photochromism in organic molecules[1−3] has been the target of many studies, both from the experimental and theoretical points of view.[4−7] Photochromism is well-known to be among the fastest chemical reactions occurring in nature, and includes processes such as cis−trans isomerization, photochemical ring-closure−ring-opening reactions, or excited-state intramolecular proton transfer (ESIPT).

A very special interest has been placed on aromatic molecules, and more concretely on the family of the aromatic Schiff bases.[8] These compounds comprise a wide range of structures, including one or two proton-transfer centers involving functional groups with opposite pK_a tendencies (e.g., OH and imine), which can lead to single or double ESIPT processes. This large variety of possible structures has attracted much attention over the past years, and examples such as salicylideneaniline (SA) or *N,N'*-bis(salicylidene)-*p*-phenylenediamine (BSP) have been thoroughly studied.[9−14] The structures of these molecules are depicted in Figure 1.

It is agreed that the photoexcitation of these compounds, which has mainly been characterized as a HOMO−LUMO ($\pi \rightarrow \pi^*$) transition, is followed by an ultrafast proton transfer along the intramolecular hydrogen bond of the *o*-hydroxyl group to the imine nitrogen to give the cis-keto tautomer within a few femtoseconds. The (π,π^*) singlet state of the cis-keto form undergoes subsequent isomerization to a trans-keto form as the final photoproduct. In addition, the excited cis-keto form can also return back again to the ground state by either a thermal or a photochemical process, completing the reversible cycle. The reversible nature of this process has great importance in technological applications in devices such as rewritable molecular memories and switches.[15−20] However, facts such as the
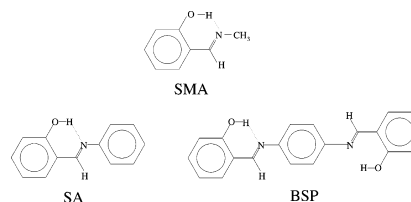

Figure 1. Structures of some relevant photochromic Schiff bases: SMA, SA, and BSP.

existence of many isomeric structures and the possibility of conical intersections before and after the proton transfer make this mechanism still ambiguous and controversial, especially the depopulation processes following the ESIPT.

As a complement to the modern ultrafast experimental techniques such as time-resolved laser spectroscopy, which is very helpful in the study of photochromic processes,[21] theoretical studies are a powerful and valuable tool in the analysis of these processes. The availability of advanced theoretical methods allows one to deal with many-atom systems with good accuracy and reasonable cost. However, the necessity to begin with smaller systems in order to better understand the complexity of larger systems, for example, SA or BSP, is still present. The simplest aromatic Schiff base that presents photochromic properties is the salicylidene methylamine (SMA), also depicted in Figure 1.

Despite its simple molecular structure, very little has been published about the properties and behavior of SMA. The synthesis,[22] a study of the enol-keto equilibrium as a function of temperature in a protic solvent (methanol) performed by electronic absorption and Raman spectroscopy,[23] and complete spectral data on SMA involving the transient absorption spectra[24] have been reported. From the latter work, the absorption

* Corresponding author. E-mail: ricard.gelabert@uab.es.

maximum energy of SMA has been measured to be around 32 000 cm^{-1}, which is, up to now (to our knowledge) one of the few direct experimental measurements we can compare our theoretical results to.

On the other hand, just one theoretical study, by Zgierski and Grabowska,[25] has been reported for SMA. In that work, an exploration of the ground and first singlet excited electronic states was performed at the HF/6-31G(d) and CIS/6-31G(d) levels of theory, respectively, in addition to some complementary calculations carried out with the TDDFT/B3LYP/6-31G(d) and semiempirical CNDO/S+CISD methods. According to their results, five energy minima corresponding to the enol, cis-keto, and three trans-keto tautomers were located. A small energy barrier for the ESIPT was calculated on the first singlet excited electronic state of 1.62 kcal mol^{-1}. Also, dynamical calculations were performed applying the semiclassic instanton approach,[26] with the use of the geometries and force field of the stationary points located in the first singlet excited state. Their results predicted that the proton-transfer reaction would take place within 30 fs for hydrogen and 115 fs for deuterium.

Nevertheless, it should be remembered that the configuration interaction singles (CIS) level tends to exaggerate the excitation and barrier energies for the ESIPT.[27,28] On the other hand, dynamical calculations with the energy origin placed in the energy minima rather than in the vertical excitation energies tend to increase the time scale of the processes. For these reasons, in the present work, we want to focus on the ESIPT reaction of SMA from the theoretical point of view, first applying more accurate quantum electronic methods to study the topology of the ground and first singlet excited electronic states, and then using these results to carry out quantum dynamical calculations, starting from the vertical excitation energies, to determine the time scale of proton transfer in the first singlet excited electronic state.

2. Computational Details

Two different sets of calculations were necessary to study the dynamics of the ESIPT in SMA. First, electronic-structure calculations have been used to explore the topology of the ground (S_0) and first A' (π,π^*) singlet excited (S_1) electronic states. Second, dynamical calculations have been performed on the S_0 and S_1 potential energy surfaces to quantify the time scales of the process. The details of both sets of calculations follow.

2.1. Electronic-Structure Calculations. Two different electronic methodologies were employed in order to perform the exploration of the S_0 and S_1 states. First, optimizations with Hartree−Fock (HF) for S_0 and CIS[29] for S_1 were performed with the Gaussian 03 program,[30] mainly to compare the results to those previously published. Second, density functional theory (DFT) and time-dependent DFT (TD-DFT)[31] optimizations were performed for the S_0 and S_1 states, respectively. The three-parameter hybrid functional of Becke with the correlation functional of Lee, Yang, and Parr (B3LYP)[32,33] was chosen. Since the Gaussian suite of programs does not allow one to perform optimizations in the TD-DFT scheme, we made use of the TURBOMOLE program (version 5.6)[34,35] for such calculations. Complementary calculations with the complete active space self-consistent field (CASSCF) method[36] and the CASSCF at the second-order perturbation theory (CASPT2) energy point calculations, both with an active space of 12 electrons and 10 molecular orbitals of A'' symmetry, including all the π system, were carried out with the MOLCAS program (version 6.2)[37] to evaluate vertical excitation energies. For all cases, the 6-31G(d,p)[38,39] basis set was used.

The calculations necessary for building the potential energy surfaces for the S_0 and S_1 electronic states used in the dynamical simulations were performed with the Gaussian 03 program, as we verified that the results produced by the B3LYP functionals used in the Gaussian and TURBOMOLE packages differ by up to 0.04 kcal mol^{-1} in the relative stability of the stationary points we calculated. This small difference comes from the use of a different form of the local correlation functional. The Gaussian package uses the VWN(III) local correlation functional, whereas TURBOMOLE uses VWN(V).[40]

2.2. Nuclear Quantum Dynamical Calculations. Quantum dynamical calculations were carried out by means of wave-packet propagation on a three-dimensional reduced model of the S_0 and S_1 potential energy hypersurfaces. A time-dependent self-consistent field approximation was adopted.[41] In particular, the Heidelberg multiconfiguration time-dependent Hartree package (MCTDH)[42] was used. Recently, this method has successfully been applied in different aspects of multidimensional intramolecular proton-transfer systems.[43−45] A brief description of the method is presented here.

The MCTDH method is a general algorithm to solve the time-dependent Schrödinger equation. The MCTDH wave function is expanded in a sum of the products of so-called single-particle functions (SPFs). The SPFs $\varphi(\mathbf{q},t)$ may be one- or multidimensional functions, and, in this case, the coordinate $\mathbf{q}$ is a collective function, $\mathbf{q} = (Q_k, ..., Q_j)$. Because the SPFs are time-dependent, they follow the wave packet, and often a rather small number of SPFs suffices for convergence.

The ansatz for the MCTDH wave function reads

$$\Psi(Q_1, ..., Q_f, t) \equiv \Psi(q_1, ..., q_p, t) = \sum_{j_1}^{n_1} \cdots \sum_{j_p}^{n_p} A_{j_1, ..., j_p} \prod_{\kappa=1}^{p} \varphi_{j_\kappa}^{(\kappa)}(q_\kappa, t) \quad (1)$$

where f denotes the number of degrees of freedom, and p is the number of MCTDH particles, also called the combined modes. There are n_κ SPFs for the κth particle. The equations of motion for the coefficient vector $\mathbf{A}$ and for the SPFs are derived from a variational principle. It is important to note that MCTDH uses, in a variational sense, optimal SPFs, as this ensures the fastest convergence. The equations of motion are complicated, but because there are comparatively few equations to be solved, the MCTDH method can be very efficient.

The solution of the equations of motion requires that one builds the mean fields at every time step. The development of the constant mean-field integrator has reduced the number of mean-field evaluations by typically a factor of 10, but a fast evaluation of the mean fields is still essential. Such a fast algorithm exists if the Hamiltonian can be written as a sum of the products of monoparticle operators:

$$\hat{H} = \sum_{r=1}^{s} c_r \prod_{\kappa=1}^{p} \hat{h}_r^{(\kappa)} \quad (2)$$

where $\hat{h}_r^{(\kappa)}$ operates on the κth particle only, and c_r represents numbers. The Hamiltonian for this work will be designed to fit to this product form.

3. Results and Discussion

3.1. Electronic-Structure Calculations. *3.1.1. Ground Electronic State.* The exploration of the electronic ground state led to the optimization of five minima at all levels of calculation. These structures, which were previously characterized at the
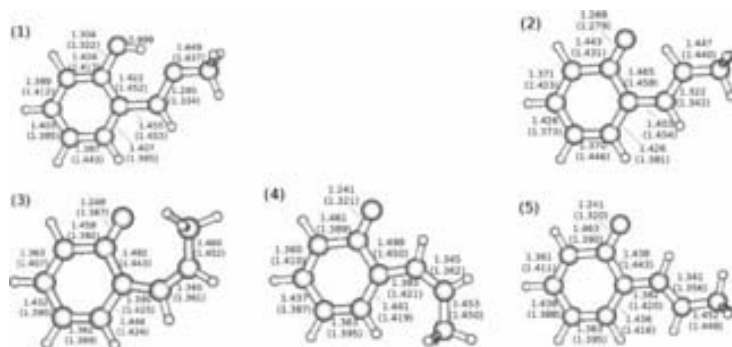
Figure 2. Optimized geometrical structures of the tautomers of the SMA molecule: (1) enol, (2) cis-keto, (3) trans-keto *a*, (4) trans-keto *b*, and (5) trans-keto *c*. Some distances in Å at the $S_0(S_1)$ states are given for the DFT(TD-DFT) levels. The values for the excited enol form were obtained after optimization of the ground electronic state enol geometry fixing the O–H distance at 0.999 Å.

TABLE 1: Ground Electronic State Relative Potential Energies (kcal mol^{-1}) of the Five Different Tautomers of the SMA and of the Transition State for the Proton Transfer (TS)

structure	HF	DFT
enol	0	0
cis-keto	8.40	5.00
trans-keto *a*	21.15	19.12
trans-keto *b*	18.32	18.49
trans-keto *c*	15.67	16.18
TS (enol → cis-keto)	14.81	5.90

HF/6-31G(d) level by Zgierski and Grabowska, are (in the same nomenclature employed in ref 25) the enol, the cis-keto and the three trans-keto (*a*, *b*, and *c*) tautomers (Figure 2).

Table 1 shows the relative potential energies of all optimized structures referred to the enol form (in kcal mol^{-1}). It is observed that the proton transfer in S_0 is an endoergic process at both levels of calculations.

Results obtained at the HF level agree with those previously published by Zgierski and Grabowska[25] with just small differences due to the slightly different basis set used. Of the five minima located, only the trans-keto *a* form does not possess a symmetry plane. The transition-state geometry of the proton transfer between the enol and the cis-keto forms was also located and characterized with an imaginary frequency of 1641*i* cm^{-1}, leading to an energy barrier of 14.81 kcal mol^{-1}.

DFT calculations agree with the HF results in assigning the relative stability of the five isomers of the SMA. A transition-state structure was also found with an imaginary frequency of 951*i* cm^{-1}, leading to a energy barrier of 5.90 kcal mol^{-1}. This value is not as high as the one calculated for the HF level of theory. In any case, the reverse energy barrier lays only 0.90 kcal mol^{-1} above the cis-keto minimum, which could hardly prevent the cis-keto form from reverting to the enol.

According to all these results, the net proton-transfer reaction cannot take place in the S_0 state.

3.1.2. First Singlet Excited Electronic State. As previously stated, one of the few experimental measurements published for the SMA in the S_1 state is the energy of the absorption maximum. We theoretically evaluated this energy at the different methods of calculation with single-point excitation calculations from the optimized enol structure in S_0. The results are displayed and compared to the experimental data in Table 2. As we have previously mentioned, CIS exaggerates the excitation energy. It can be seen that CASSCF and CASPT2 make a better

TABLE 2: Calculated Vertical Excitation Energies (cm^{-1}) of the Optimized Enol Tautomer of SMA from the Ground Electronic State to the First (π,π^*) Singlet Excited Electronic State

CIS	45 278
CASSCF	33 940
CASPT2	35 346
TD-DFT	32 796
experimental value (ref 24)	~32 000

TABLE 3: First Singlet Electronic State Relative Potential Energies (kcal mol^{-1}) of the Five Different Tautomers of the SMA and of the Transition State for the Proton Transfer (TS)

structure	CIS	TD-DFT
enol	16.14	
cis-keto	0	0
trans-keto *a*	9.28	5.09
trans-keto *b*	6.24	2.97
trans-keto *c*	2.92	−0.44
TS (enol → cis-keto)	17.32	

prediction, whereas TD-DFT is closest to the experimental result.

In Table 3, the relative stabilities of all the optimized structures in the S_1 potential surface related to the cis-keto form (in kcal mol^{-1}) is presented. In contrast to what has been observed in the exploration of the S_0 state, the proton transfer becomes exoergic, and the energy barrier decreases substantially in the S_1 state. The cis-keto tautomer becomes more stable than the enol form in both cases. At the TD-DFT level, the enol form could not even be located as a stable minimum, and the trans-keto *c* tautomer becomes the most stable structure at the TD-DFT level.

CIS calculations practically coincide with the data published by Zgierski and Grabowska.[25] We can observe that the proton-transfer reaction becomes largely exoergic, and that there is an important decrease in the energy barrier in comparison with the S_0 state, which is a first indication of the existence of an ESIPT.

TD-DFT results are quite different in the exploration of the S_1 state in comparison with the DFT exploration of S_0. All the attempts failed to locate a TD-DFT minimum in the enol region. This suggests a barrierless ESIPT process, which involves the absence of a transition-state structure. A set of relaxed reaction coordinate calculations was carried out varying the O–H distance and allowing the rest of the geometry to relax and attain minimum energy. The reaction profile obtained, depicted in
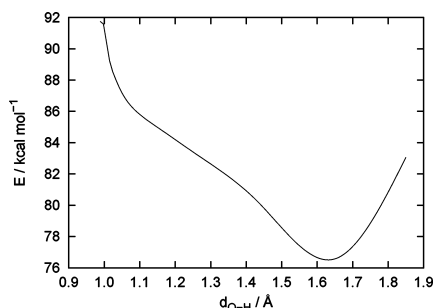
Figure 3. TD-DFT proton-transfer reaction profile relaxed along the O—H distance for the first (π,π^*) singlet excited electronic state. Energy origin is the energy of the DFT-optimized enol form in S_0.

Figure 3, confirms that the ESIPT is indeed barrierless at this level of theory.

Figure 2 also depicts the values for some relevant interatomic distances in all forms of the SMA at the DFT and TD-DFT levels. It is worth noting that the enol—cis-keto proton transfer in S_0 involves a substantial energy barrier because of the loss of aromaticity along the process. This effect is notably weaker in S_1 because the enol form has already lost a certain aromatic character in the excitation process. In effect, in the excited form of the enol tautomer, the C—C distances in the six-member ring present quite disparate values (the difference between the longest and shortest distances is equal to 0.067 Å), in comparison with S_0 (where this difference equals 0.035 Å), indicating a loss of aromaticity, which favors the ESIPT reaction.

As a conclusion of this electronic study of SMA, we believe that the DFT/TD-DFT methods provide, with a not-too-high cost of calculation, reasonably accurate results for the SMA system that are in good agreement with the experimental data published. Furthermore, it is accepted that the DFT/TD-DFT levels provide a good description for the excitation energy of valence excited (π,π^*) states.[46] This encouraged us to use this level of calculation in the building up of the S_0 and S_1 potential energy surfaces needed in our quantum dynamical calculations.

3.2. Nuclear Quantum Dynamical Calculations. To our knowledge, the dynamical study previously published for the ESIPT in SMA[25] was carried out with the approximate semiclassical instanton approach on CIS-quality electronic structure data. Because our results applying the DFT/TD-DFT methodology show us that the proton transfer is actually a barrierless process in S_1, we concluded that a quantum dynamics simulation with the energy origin at the vertical excitation would be more suitable for this system.

However, before studying any molecular system from the dynamical point of view, it is necessary to describe it properly by choosing a set of coordinates adapted to the physical representation of the reaction. This choice is a very important step in the dynamical study of any system because it will define the form of the molecular Hamiltonian operator.

Rigorous quantum dynamical study of a molecular system is a daunting task, even for small systems. In the time-dependent picture, part of the problem lies within the implicit difficulty in propagating a highly dimensional wave packet representing the state of the system. Highly efficient wave-packet propagation algorithms such as MCTDH[42] have eased this task, which, even though still far from being routine work, is now possible for systems of moderate size. A very serious limitation of this kind of study, however, resides in the adequate representation of the
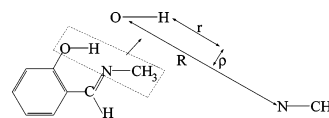

Figure 4. Definition of the three-dimensional set of coordinates model for the proton-transfer reaction in SMA.

potential energy surface, which conditions the time evolution of the system.

Before starting the dynamical study of the intramolecular proton transfer in the excited state for SMA, it is worth remembering that the amount of experimental data about the subject is exiguous, which will hinder proper comparison of theoretical predictions and experimental findings. Previous studies have relied on the existence of a potential energy barrier in S_1, which does not seem to exist. Accordingly, the purpose of the dynamical simulation will be to establish a reasonable value for the rate of the process through the use of a reasonably accurate quantum dynamical simulation carried out on a portion of the potential energy surface relevant to the process computed at an appropriate level of computation. To this end, we will apply several approximations that will render the system in a simple enough form but allow meaningful results to be obtained.

In what follows, we describe the model we used for the dynamical simulation of the ESIPT in SMA. It seems to be a reasonable assumption to restrict the motion of the proton to the molecular plane, which also contains the donor and acceptor atoms. As dynamical coordinates to represent the system, we chose a set of three internal coordinates relevant for the intramolecular proton transfer: (i) the distance between the oxygen and nitrogen atoms (R), (ii) the distance between the position of the hydrogen atom and the mediatrix of the O—N segment (r), and (iii) the distance between the position of the hydrogen atom and the straight line linking the donor and acceptor atoms at any time (ρ). It has been known for a time that, besides the position of the transferring proton, the distance between the donor and acceptor atoms is of great importance and thus should be included in the simulation.[47,48] It must be noted that, within our description, the values of $r \leq 0.0$ Å determine the reactant region, while values of $r > 0$ approximately correspond to the product region. This set of coordinates is centered in the proton transfer region of the molecule, as graphically depicted in Figure 4.

Next, the potential energy surfaces for the S_0 and S_1 states in the form $\hat{V}(R,r,\rho)$ are needed. To obtain these, a simple structure generator program was coded, which generates a structure from a set of values R, r, and ρ as follows: We divide the SMA molecule into four fragments: the aromatic ring and the ancillary C—H atoms (fragment 1), the oxygen atom (fragment 2), the N—CH$_3$ group (fragment 3), and the proton (fragment 4). Taking as a starting point the structure of the potential energy minimum in S_0 of SMA, the program moves fragments 2 and 3 apart to a distance value R. In doing so, the internal structure of all fragments is kept rigid, and both the N—CH$_3$ group and the O atom are moved apart proportionally to the inverse ratio of their masses while the ring remains static. This choice brings about configurations that are chemically more acceptable than, for instance, keeping the oxygen atom statically bound to the ring and placing the changes in R on the displacement of fragment 3 alone. The proton is finally placed according to the values of r and ρ, and a point energy calculation is performed for this structure at the DFT and TD-DFT levels for S_0 and S_1, respectively, with the B3LYP functional and the 6-31G(d,p) basis set, using the Gaussian 03 package. A total of 720 points

ESIPT in SMA

J. Phys. Chem. A, Vol. 110, No. 14, 2006 **4653**

were calculated, with 12 points for R (from $+2.15$ to $+3.25$ Å), 15 points for r (from $+0.70$ to -0.70 Å), and 4 points for ρ ($+1.34$, $+0.84$, $+0.34$, and -0.15 Å), with $+0.34$ Å being the value of ρ at the DFT-optimized enol structure at the S_0 surface. Few points were included in ρ in comparison with those in R and r, since we verified that the ρ coordinate does not vary substantially along the proton-transfer reaction in both the S_0 and the S_1 states. This set of coordinates allows the two-dimensional motion of the proton in the molecular plane, as well as the approach of the donor and acceptor atoms, which has been proved to be relevant in proton-transfer processes.[47,48] We note that, while the coordinate set resulting from this approach is a convenient one, the dynamical treatment is approximate because of the specific procedure followed to compute the potential energy surface, specifically because changing the distance between the donor and acceptor atoms also modifies other coordinates that have been kept outside the dynamical model (e.g., the distance between the oxygen atom and its binding site in the ring, or the distance between the nitrogen atom and the carbon atom bound to the ring).

To obtain the expression of the kinetic energy operator, we adopted the following procedure: First, according to the restriction of motion in a plane, we only need to assign two Cartesian coordinates for each fragment, which leads us to a set of six Cartesian coordinates. Second, we establish the mathematical relationships between these six Cartesian coordinates and our set of three coordinates R, r, and ρ. For this we need to consider three more coordinates, corresponding to the two Cartesian coordinates of the center of mass and the global rotational angle of the three fragments in the plane. Finally, after some algebraic manipulation employing the chain rule, the ∇^2 operator can be expressed in terms of our new set of coordinates. In the final expression, the second derivatives with respect to the center-of-mass Cartesian coordinates can be separated. Furthermore, introducing the additional approximation that the global rotation in the plane does not significantly affect the proton transfer process, we finally reach an expression of the Hamiltonian operator which only depends on R, r, and ρ:

$$\hat{H} = \hat{T} + \hat{V}(R,r,\rho) \qquad (3)$$

where $\hat{T}$ is

$$\hat{T} = -\frac{1}{2}\left(\frac{1}{m_{N-CH_3}} + \frac{1}{m_{O-ring}}\right)\frac{\partial^2}{\partial R^2} -$$
$$\frac{1}{2}\left[\left(\frac{1}{m_{N-CH_3}} + \frac{1}{m_{O-ring}}\right)\left(\frac{1}{4} + \frac{\rho^2}{R^2}\right) + \frac{1}{m_H}\right]\frac{\partial^2}{\partial r^2} -$$
$$\frac{1}{2}\left[\left(\frac{1}{m_{N-CH_3}} + \frac{1}{m_{O-ring}}\right)\left(\frac{1}{4} + \frac{r^2}{R^2}\right) + \frac{r}{R}\left(\frac{1}{m_{N-CH_3}} - \frac{1}{m_{O-ring}}\right) +$$
$$\frac{1}{m_H}\right]\frac{\partial^2}{\partial \rho^2} + \frac{1}{2}\left(\frac{1}{m_{N-CH_3}} - \frac{1}{m_{O-ring}}\right)\frac{\partial}{\partial R}\frac{\partial}{\partial r} +$$
$$\left[\frac{r\rho}{R^2}\left(\frac{1}{m_{N-CH_3}} + \frac{1}{m_{O-ring}}\right) + \frac{\rho}{2R}\left(\frac{1}{m_{N-CH_3}} - \frac{1}{m_{O-ring}}\right)\right]\frac{\partial}{\partial r}\frac{\partial}{\partial \rho} -$$
$$\frac{1}{2R}\left(\frac{1}{m_{N-CH_3}} + \frac{1}{m_{O-ring}}\right)\frac{\partial}{\partial R} + \frac{1}{2}\left[\frac{1}{R}\left(\frac{1}{m_{N-CH_3}} - \frac{1}{m_{O-ring}}\right) +$$
$$\frac{r}{R^2}\left(\frac{1}{m_{N-CH_3}} + \frac{1}{m_{O-ring}}\right)\right]\frac{\partial}{\partial r} + \frac{\rho}{2R^2}\left(\frac{1}{m_{N-CH_3}} + \frac{1}{m_{O-ring}}\right)\frac{\partial}{\partial \rho} \qquad (4)$$
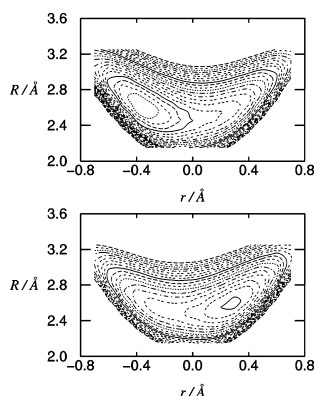
Figure 5. DFT/TD-DFT 6-31G(d,p) two-dimensional potential energy surface cuts (R, r, $\rho = +0.34$ Å) for the ground (top) and first singlet excited (bottom) electronic states of the SMA. The coordinates are explained in Figure 4.

where m_H, m_{N-CH_3}, and m_{O-ring} denote the masses of the transferred proton (fragment 4), the N−CH$_3$ fragment (fragment 3), and the O−ring fragment (fragment 1 + fragment 2) of SMA, respectively. The resulting Hamiltonian is approximate: the kinetic energy term above assumes that the O atom and fragment 1 (the aromatic ring) do not move with respect to each other, while the potential energy surfaces have been constructed allowing such motion to chemically consider more significant structures. Because of this, the dynamical treatment is implicitly approximate, even within the three dimensions considered.

Figure 5 depicts the cuts of the S_0 and S_1 potential energy surfaces obtained (for $\rho = +0.34$ Å). Because each point of the grid was obtained by energy point calculations without allowing the molecule to relax, and the actual value of ρ for the cis-keto minimum in S_0 is slightly different ($+0.41$ Å), the product energy minimum does not appear in this particular cut of S_0. Nevertheless, any dynamical calculation performed on S_0 requires a good description of the reactant region rather than that of the product. According to the values collected in Table 3, there is no reactant minimum in S_1 for the TD-DFT level of theory, which agrees with the absence of the reactant energy minimum in the S_1 cut. We also verified that no exit channels exist neither in S_0 nor in S_1, so no absorbing potentials were necessary.

The steps followed in the dynamical calculations with the MCTDH package were as follows: First, the mesh of points for S_0 and S_1 were fitted by means of the POTFIT program, which is included in the MCTDH package, into direct product form, as required in eq 2. The initial wave packet consisted of a Gaussian function, which was propagated in imaginary time (i.e., relaxed) on the S_0 potential energy surface to locate the ground vibrational state. Finally, the resulting wave function was promoted to the S_1 potential surface according to the Franck−Condon principle. All the dynamical calculations performed were verified to be converged with respect to the basis of both primitive and SPF functions. Figure 6 shows six snapshots of the two-dimensional probability density of the wave packet for the first 25 fs of propagation, in the plane formed by r and R, with $\rho = +0.34$ Å.

As can be seen, the head of the wave packet reaches the product area along the r coordinate within 10 fs. From that point on, because our model is closed and does not include the rest
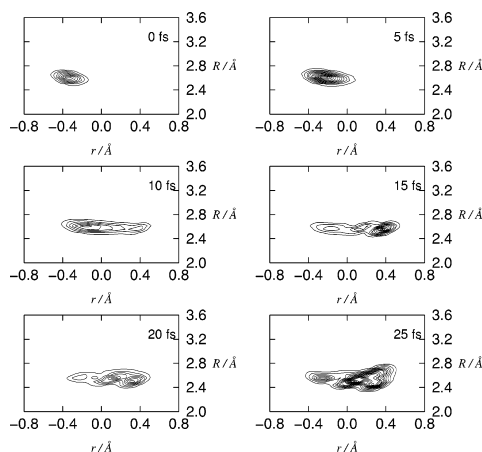
Figure 6. Snapshots of the (r, R, $\rho = +0.34$ Å) probability density for the three-dimensional simulation on the first excited electronic state at different times. The coordinates are explained in Figure 4.
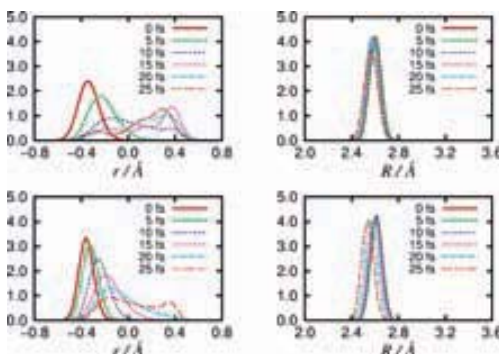

Figure 7. One-dimensional probability densities of the three-dimensional model at different times for r (left) and R (right) coordinates for the hydrogen (top) and deuterium (bottom) transfer. The coordinates are explained in Figure 4.

of vibrational modes, the propagated wave packet collides with the potential energy wall beyond the cis-keto region and consequently reflects. As a result, too many interference effects are observed. In addition to this, very little coupling with the R coordinate can be noticed, as the wave packet does not expand significantly along the R coordinate during the simulation time. If we plot the one-dimensional probability density for the r and R coordinates over time (Figure 7), it can be clearly seen how the wave packet propagates, collides, and comes back along the r coordinate in 25 fs, while the one-dimensional density of probability for the R coordinate does not vary substantially within the same time. The same behavior was observed for the ρ coordinate.

The isotopic substitution of the transferred proton for a deuterium was also studied. We compare in Figure 7 the one-dimensional probability densities for the r and R coordinates for the isotopic substituted system with the previous case. As expected, a slower evolution of the wave packet along the r coordinate is observed for the deuterated case, whereas, along the R coordinate, the wave packet moves further to shorter values than those in the nondeuterated case.
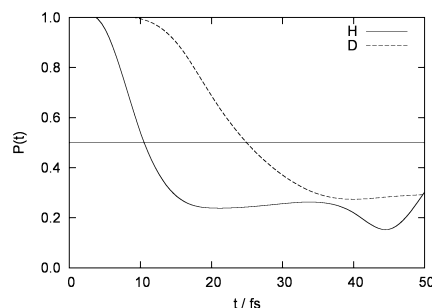

Figure 8. Survival probabilities for the hydrogen and deuterium transfers for the first 50 fs of propagation. The horizontal line sets the point where the 50% of the reactant turns into product.

To quantify the amount of remaining reactant during the proton-transfer reaction, we calculated the survival probability (eq 5) for the first 50 fs of propagation,

$$P(t) = \int d\tau h_r(\tau) |\Psi(\tau)|^2 \qquad (5)$$

where $d\tau$ is the volume element, and $h_r(\tau)$ is equal to 1 in the reactant region ($r \leq 0.0$ Å) and equal to 0 in the product region ($r > 0.0$ Å). Solving eq 5 is equivalent to integrating the one-dimensional probability density curves for $r \leq 0$. The results are depicted in Figure 8. It can be observed how the curve for the hydrogen transfer decreases much faster than that for the deuterium transfer. Within 11 fs, approximately 50% of the nondeuterated reactant has turned into product, whereas the deuterated SMA needs 25 fs to transform the same amount of reactant, so a strong kinetic isotope effect is observed.

As mentioned before, the dynamical model is approximate because it assumes that the oxygen atom does not move relative to the aromatic ring, while the potential energy surface has been constructed allowing this motion. This is necessary to scan relevant parts of the potential energy surface when constructing it. It would make less physical sense if increasing the value of R would only move the N—CH$_3$ fragment away, leaving the O atom at a fixed distance from the aromatic ring, but it represents an approximation beyond the reduction of the system to a three-dimensional model. From a chemical point of view, in such a fast process, keeping the internal structure of the aromatic ring frozen seems to be a reasonable approximation. However, rather than assuming that *both* the oxygen atom and the ring move solidarily, it seems more reasonable that the oxygen atom is the one that carries out most of the internal motion, while the aromatic ring remains static by virtue of its larger mass. A "correct" treatment in which this motion is considered is complex. It would require an increase in the number of dynamical parameters, making the potential energy evaluation much more expensive, and finally requiring a much more intricate kinetic energy term. Because of the large difference in mass between the oxygen atom and the aromatic ring, most of the motion will be experienced by the oxygen atom. A simple way to assess the sensitivity of the conclusions obtained so far would be to redo the dynamical calculations, but this time assuming that *only* the oxygen atom is moving. This can be estimated approximately by setting m_{O-ring} in eq 2 to simply m_O. If one does this, one sees that the hydrogen transfer process shows negligible changes, whereas for deuterium transfer, the transfer time increases slightly to 27 fs.

ESIPT in SMA

4. Conclusions

The proton-transfer dynamics in the aromatic Schiff base SMA has been theoretically analyzed by means of electronic-structure calculations at the HF and DFT levels of theory for the ground electronic state (S_0), and at the CIS and TD-DFT levels of theory for the first singlet excited electronic state (S_1), combined to quantum nuclear dynamics simulation. Complementary calculations at the CASSCF and CASPT2 levels have been carried out to determine vertical excitation energies. The SMA system presents five stable structural conformations in S_0: enol, cis-keto, and three different trans-keto tautomers. All of them are planar or almost planar. Our DFT electronic calculations show that the enol form is the most stable one. The proton-transfer reaction is endoergic, with an energy barrier of 5.9 kcal mol^{-1} and a reverse energy barrier of only 0.9 kcal mol^{-1}, which does not allow the net proton-transfer reaction to take place.

Upon the (π,π^*) excitation of the enol form, a loss of aromaticity in the six-membered ring is observed, which destabilizes the structure and sets the cis-keto as the most stable tautomer in S_1. At the TD-DFT level of theory, the enol form does not correspond to a stable structure minimum, therefore only four minima could be located. In addition to this, the proton-transfer reaction becomes exoergic and barrierless. Finally, we highlight that the DFT/TD-DFT energy calculations and geometry optimizations have performed quite well in describing the photochemistry of SMA.

Two three-dimensional potential energy surfaces were fitted from a large set of electronic structure calculations for S_0 (DFT level of theory) and S_1 (TD-DFT level of theory). The time evolution of the wave packet was calculated with the MCTDH algorithm. Our quantum dynamical calculations predict a time scale of 11 and 25 fs for the hydrogen and deuterium transfers, respectively, in S_1. The process is somewhat faster than predicted by Zgierski and Grabowska (30 and 115 fs for the hydrogen and deuterium transfers, respectively).[25] This speed-up, especially for the deuterium case, can be explained if we take into account the barrierless nature of the process and the fact that the starting point of our dynamics was the Franck−Condon excitation energy of the enol form. However, taking into account that DFT tends to overestimate the strength of hydrogen bonds, and thus underestimate the energy barrier, it could be said that our measured rates are an upper limit for the rate of the studied process. Given that, as previously said, the CIS method overestimates the energy barriers, our results, together with the ones obtained by Zgierski and Grabowska,[25] fix the range of the actual rate of the excited-state proton transfer in SMA.

Finally, it must be remarked that, even when dealing with a barrierless process, a quantum dynamical treatment leads to a strong H/D kinetic isotope effect in S_1 for the enol−cis-keto proton transfer.

References and Notes

(1) Bouas-Laurent, H.; Durr, H. *Pure Appl. Chem.* **2001**, *73*, 639.
(2) Exelby, R.; Grinter, R. *Chem. Rev.* **1965**, *65*, 247.
(3) Senier, A.; Shepheard, F. G. *J. Chem. Soc.* **1909**, *95*, 1943.
(4) Barbara, P. F.; Rentzepis, P. M.; Brus, L. E. *J. Am. Chem. Soc.* **1980**, *102*, 2786.
(5) Vargas, V. *J. Phys. Chem. A* **2004**, *108*, 281.
(6) T. Rosenfeld, M. O.; Meyer, A. Y. *Mol. Photochem.* **1973**, *5*, 39.
(7) Knyazhansky, M. I.; Metelitsa, A. V.; Kletskii, M. E.; Millov, A. A.; Besugliy, S. *J. Mol. Struct.* **2000**, *526*, 65.
(8) Hadjoudis, E.; Mavridis, I. M. *Chem. Soc. Rev.* **2004**, *33*, 579.
(9) Zgierski, M. Z.; Grabowska, A. *J. Chem. Phys.* **2000**, *112*, 6329.
(10) Okabe, C.; Nakabayashi, T.; Inokuchi, Y.; Nishi, N.; Sekiya, H. *J. Chem. Phys.* **2004**, *121*, 9436.
(11) Mitra, S.; Tamai, N. *Chem. Phys.* **1999**, *246*, 463.
(12) Kownacki, K.; Mordzinski, A.; Wilbrandt, R.; Grabowska, A. *Chem. Phys. Lett.* **1994**, *277*, 270.
(13) Rawat, M. S. M.; Norula, J. L. *Indian J. Chem., Sect. B* **1987**, *26*, 232.
(14) Kawato, T.; Kanatomi, H.; Koyama, H.; Igarashi, T. *J. Photochem.* **1986**, *33*, 199.
(15) Sackmann, E. *J. Am. Chem. Soc.* **1971**, *93*, 7088.
(16) Rau, H.; Luddecke, E. *J. Am. Chem. Soc.* **1982**, *104*, 1616.
(17) Irie, M.; Mohri, M. *J. Org. Chem.* **1988**, *53*, 803.
(18) Yokoyama, Y. *Chem. Rev.* **2000**, *100*, 1717.
(19) Irie, M. *Chem. Rev.* **2000**, *100*, 1685.
(20) Benniston, A. C. *Chem. Soc. Rev.* **2004**, *33*, 573.
(21) Ziolek, M.; Kubicki, J.; Maciejewski, A.; Naskrecki, R.; Grabowska, A. *Phys. Chem. Chem. Phys.* **2004**, *6*, 4682.
(22) Goodson, L. H.; Christopher, H. *J. Am. Chem. Soc.* **1949**, *71*, 1117.
(23) Lee, H.; Kitagawa, T. *Bull. Chem. Soc. Jpn.* **1986**, *59*, 2897.
(24) Grabowska, A.; Kownacki, K.; Kaczmarek, L. *Acta Phys. Pol., A* **1995**, *88*, 1081.
(25) Zgierski, M. Z.; Grabowska, A. *J. Chem. Phys.* **2000**, *113*, 7845.
(26) Siebrand, W.; Smedarchina, Z.; Zgierski, M. Z.; Fernández-Ramos, A. *Int. Rev. Phys. Chem.* **1999**, *18*, 5.
(27) Scheiner, S. *J. Phys. Chem. A* **2000**, *104*, 5898.
(28) Vendrell, O.; Moreno, M.; Lluch, J. M. *J. Chem. Phys.* **2002**, *117*, 7525.
(29) Foresman, J. B.; Head-Gordon, M.; Pople, J. A.; Frisch, M. J. *J. Phys. Chem.* **1992**, *96*, 135.
(30) Frisch, M. J.; Trucks, G. W.; Schlegel, H. B.; Scuseria, G. E.; Robb, M. A.; Cheeseman, J. R.; Montgomery, J. A., Jr.; Vreven, T.; Kudin, K. N.; Burant, J. C.; Millam, J. M.; Iyengar, S. S.; Tomasi, J.; Barone, V.; Mennucci, B.; Cossi, M.; Scalmani, G.; Rega, N.; Petersson, G. A.; Nakatsuji, H.; Hada, M.; Ehara, M.; Toyota, K.; Fukuda, R.; Hasegawa, J.; Ishida, M.; Nakajima, T.; Honda, Y.; Kitao, O.; Nakai, H.; Klene, M.; Li, X.; Knox, J. E.; Hratchian, H. P.; Cross, J. B.; Bakken, V.; Adamo, C.; Jaramillo, J.; Gomperts, R.; Stratmann, R. E.; Yazyev, O.; Austin, A. J.; Cammi, R.; Pomelli, C.; Ochterski, J. W.; Ayala, P. Y.; Morokuma, K.; Voth, G. A.; Salvador, P.; Dannenberg, J. J.; Zakrzewski, V. G.; Dapprich, S.; Daniels, A. D.; Strain, M. C.; Farkas, O.; Malick, D. K.; Rabuck, A. D.; Raghavachari, K.; Foresman, J. B.; Ortiz, J. V.; Cui, Q.; Baboul, A. G.; Clifford, S.; Cioslowski, J.; Stefanov, B. B.; Liu, G.; Liashenko, A.; Piskorz, P.; Komaromi, I.; Martin, R. L.; Fox, D. J.; Keith, T.; Al-Laham, M. A.; Peng, C. Y.; Nanayakkara, A.; Challacombe, M.; Gill, P. M. W.; Johnson, B.; Chen, W.; Wong, M. W.; Gonzalez, C.; Pople, J. A. *Gaussian 03*, revision C.03; Gaussian, Inc.: Wallingford, CT, 2004.
(31) Bauernschmitt, R.; Ahlrichs, R. *Chem. Phys. Lett.* **1996**, *256*, 454.
(32) Becke, A. D. *J. Chem. Phys.* **1993**, *98*, 5648.
(33) Lee, C.; Yang, W.; Parr, R. *Phys. Rev. B* **1988**, *37*, 785.
(34) Furche, F.; Ahlrichs, R. *J. Chem. Phys.* **2002**, *117*, 7433.
(35) Ahlrichs, R.; Bär, M.; Häser, M.; Horn, H.; Kölmel, C. *Chem. Phys. Lett.* **1989**, *162*, 165.
(36) Anderson, K.; Malmqvist, P.-A.; Roos, B. O. *J. Chem. Phys.* **1992**, *96*, 1218.
(37) Andersson, K.; Barysz, M.; Bernhardsson, A.; Blomberg, M. R. A.; Carissan, Y.; Cooper, D. L.; Fülscher, M. P.; Gagliardi, L.; de Graaf, C.; Hess, B. A.; Hagberg, D.; Karlström, G.; Lindh, R.; Malmqvist, P.-A.; Nakajima, T.; Neogrády, P.; Olsen, J.; Raab, J.; Roos, B. O.; Ryde, U.; Schimmelpfennig, B.; Schütz, M.; Seijo, L.; Serrano-Andrés, L.; Siegbahn, P. E. M.; Stålring, J.; Thorsteinsson, T.; Veryazov, V.; Widmark, P.-O. *MOLCAS*, version 6.2; Lund University: Lund, Sweden, 2000.
(38) Hariharan, P.; Pople, J. *Theor. Chim. Acta* **1973**, *28*, 213.
(39) Francl, M.; Petro, W.; Hehre, W.; Binkley, J.; Gordon, M.; DeFrees, D.; Pople, J. *J. Chem. Phys.* **1982**, *77*, 3654.
(40) Vosko, S. H.; Wilk, L.; Nusaic, M. *Can. J. Phys.* **1980**, *58*, 1200.
(41) Makri, N.; Miller, W. H. *J. Chem. Phys.* **1987**, *87*, 5781.
(42) Worth, G. A.; Beck, M. H.; Jäckle, A.; Meyer, H.-D. *The MCTDH Package*, version 8.2; Ruprecht-Karls-Universität Heidelberg, Heidelberg,

Germany, 2000. Meyer, H.-D. *The MCTDH Package*, version 8.3; Ruprecht-Karls-Universität Heidelberg, Heidelberg, Germany, 2002. See http://www.pci.uni-heidelberg.de/tc/usr/mctdh/.

(43) Naundorf, H.; Worth, G.; Meyer, H.-D.; Kühn, O. *J. Phys. Chem. A* **2002**, *106*, 719.

(44) Petković, M.; Kühn, O. *J. Phys. Chem. A* **2003**, *107*, 8458.

(45) Petković, M.; Kühn, O. *Chem. Phys.* **2004**, *304*, 91.

(46) Dierksen, M.; Grimme, S. *J. Phys. Chem. A* **2004**, *108*, 10225.

(47) Bosch, E.; Moreno, M.; Lluch, J. M.; Bertrán, J. *J. Chem. Phys.* **1990**, *93*, 5685.

(48) Paz, J. J.; Moreno, M.; Lluch, J. M. *J. Chem. Phys.* **1995**, *103*, 353.

Paper III

Electronic-structure and quantum dynamical study of the photochromism of the aromatic Schiff base salicylideneaniline

Juan Manuel Ortiz-Sánchez, Ricard Gelabert, Miquel Moreno,[a] and José M. Lluch
Departament de Química, Universitat Autònoma de Barcelona, 08193 Bellaterra, Barcelona, Spain

The ultrafast proton transfer dynamics of salicylideneaniline has been theoretically analyzed in the ground and first singlet excited electronic states using density functional theory (DFT) and time-dependent DFT calculations, which predict a (π, π^*) barrierless excited state intramolecular proton transfer (ESIPT). In addition to this, the photochemistry of salicylideneaniline is experimentally known to present fast depopulation processes of the photoexcited species before and after the proton transfer reaction. Such processes are explained by means of conical intersections between the ground and first singlet (π, π^*) excited electronic states. The electronic energies obtained by the time-dependent density functional theory formalism have been fitted to a monodimensional potential energy surface in order to perform quantum dynamics study of the processes. Our results show that the proton transfer and deactivation of the photoexcited species before the ESIPT processes are completed within 49.6 and 37.7 fs, respectively, which is in remarkable good agreement with experiments. © 2008 American Institute of Physics.
[DOI: 10.1063/1.3032215]

I. INTRODUCTION

Aromatic Schiff bases are among the most studied compounds in the photochemistry area because of their photochromic behavior.[1–3] Upon photoexcitation the ground state stable structure of a photochromic compound is switched into some metastable form (the photochromic transient) that eventually reverts to the ground state original structure. The reversible cyclic nature of this process is the key feature of their importance in technical applications in the fields of optical data processing and storage devices.[4–6] In aromatic Schiff bases the photochromism likely arises from an excited state intramolecular proton transfer (ESIPT) reaction that may be followed by a plethora of other photochemical processes such as *cis-trans* isomerizations, thermal deactivation, and internal conversion (IC) through conical intersections (CIs) or intersystem crossing. In fact, ESIPT is a ubiquitous process in chemistry and biology.[7–10]

The best known and most thoroughly studied photochromic Schiff base is salicylideneaniline (SA). The molecular structure of SA in the original enol (E^*) structure and the keto (K^*) form that results after intramolecular proton transfer at the first singlet excited state are depicted in Scheme 1. Numerous experimental studies[11–31] on SA have been devoted to analyze the mechanism and dynamics of the proton transfer reaction from the primary excited enol form to the keto tautomer and the creation of the photochromic tautomer in the ground electronic state. Given the long span of time that exists between the different works (from 1964 to 2007), the methods used and the precision of the measurements have largely changed along time. In spite of the large amount of data acquired and the use of quite sophisticated techniques

in the past works (that fall in the high technological field called femtochemistry because the time resolution data are below the subpicosecond range) the results are not fully consistent and much controversy is still present regarding the full photochemical behavior of SA.

The absorption spectrum of SA shows a quite prominent band at 300–400 nm attributed to the photoexcitation to a (π, π^*) excited state. The fluorescence spectrum presents also a single band, largely Stokes shifted, that is centered at around 570 nm. This band is believed to come from the *cis*-keto tautomer (also a (π, π^*) state). The quantum yield of the fluorescence is quite low (1.2×10^{-4}).[29] From the time-resolved experiments[21,29–31] arises a global picture of the photochromism in SA that starts with photoexcitation to the (π, π^*) excited state from where the hydroxylic proton is quickly transferred to the nitrogen imino atom resulting in the fluorescent *cis*-keto tautomer. This species is the precursor of the photochromic transient, believed to be a ground state keto tautomer. This transient has a long lifetime (on the order of milliseconds) and a maximum absorption band at 474 nm.[29] However, the detailed mechanism about the species involved in the whole process and the time of the different steps is not a settled question. The main discrepancy is found in the time scale for the ESIPT process itself. Otsubo *et al.*[25] and Okabe *et al.*[30] proposed a process occurring under 750 fs. Mitra and Tamai[19–21] brought its characteristic time to 200–300 fs, whereas Ziólek *et al.*[29] envisaged a much faster process (<50 fs). Recent results, using apparatus with better time resolution, have confirmed the value of 50 fs for the ESIPT process.[31] The ultrafast time scale of ESIPT and the lack of hydrogen/deuterium isotope effect lead the authors of this last work to conclude that ESIPT in the first (π, π^*) excited state implies a ballistic motion where the initial wave packet evolves in a purely repulsive potential

[a]Electronic mail: mmf@qf.uab.cat.
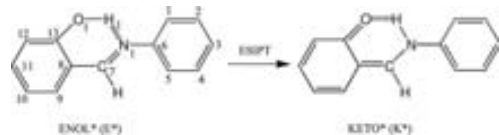
SCHEME 1. Molecular structures of enol (E^*) and keto (K^*) tautomers of SA at the S_1 state. The atom numbering used in this work is also depicted.

toward the *cis*-keto structure in the same excited electronic state.[31] Such a mechanism has been also found in a recent quantum dynamics study of the ESIPT process in the related Schiff bases salicylidene methylamine, a simplified model of the SA that has a methyl substituent instead of a phenyl group in the nitrogen atom.[32]

The processes that follow ESIPT and eventually led to the formation of the photochromic transient are also unclear. The initially formed *cis*-keto structure decays in times that range between 1.5 and 8.5 ps depending on the wavelength used for the photoexcitation.[29–31] The fact that the longer time is found for the higher excitation wavelengths (the less energetic ones) led Okabe *et al.*[30] to conclude that some energy barriers were implied in this process that were believed to involve a *cis/trans* isomerization of the keto tautomer to finally obtain the photochromic transient, expected to be also some form of *trans*-keto structure. Additionally, there is a fastest time-decay component of just a few hundreds of femtoseconds that is usually attributed to an internal vibrational relaxation (IVR) of the hot *cis*-keto initially obtained. Some authors[21] assume that this IVR also involves the *cis/trans* isomerization. Some works also find a residual and much longer time decay for the *cis*-keto isomer that has no clear assignation.[29,30] Involvement of a higher excited singlet state or a triplet state has been tentatively proposed.[30] Finally, it has also been observed that ESIPT may compete with another ultrafast nonradiative process that Okabe *et al.*[30] assigned to an IC of the initially obtained (π, π^*) excited state to a more stable (n, π^*) state.

Curiously enough, not so many theoretical works have been devoted to SA and its photochemistry.[16,20,24,25,27,33] Among these works, only the one by Zgierski and Grabowska[33] dealt with the dynamics of the photochemical processes and performed localization of stationary points on the ground and excited electronic states of SA using *ab initio* techniques [Hartree–Fock for the ground state and configuration interaction single (CIS) for the excited states]. The results of Zgierski and Grabowska showed that the enol and keto minima are nonplanar structures in the ground electronic state. In the first singlet excited state the more stable minimum of the enol is identified as a strongly twisted (n, π^*) state. Because the first allowed electronic transition leads to a (π, π^*) excited state, an IC takes place between (π, π^*) and the most stable (n, π^*). Conversely, in the *cis*-keto side the more stable excited state structure is a planar (π, π^*) geometry with the twisted (n, π^*) minimum lying ~ 3 kcal mol^{-1} higher. As for the *trans*-keto tautomer, it is also slightly nonplanar and higher in energy (4.8 kcal mol^{-1}) with respect to the *cis*-keto minimum. The ESIPT reaction is only possible between the planar (π, π^*) enol and *cis*-keto

structures and has to surpass an energy barrier of 7.2 kcal mol^{-1} from the minimum of the (π, π^*) enol tautomer. Zgierski and Grabowska analyzed the dynamics of the ESIPT process using the instanton method[34] that gives crude estimations of ~ 1.2 and ~ 21 ps for the hydrogen and deuterium transfers, respectively. As CIS is known to overestimate ESIPT barriers,[35] energies were recalculated using the more reliable time dependent-density functional theory (TDDFT) method that lead to a much lower barrier of 3.2 kcal mol^{-1}. Rescaling the energy barrier to 5.7 kcal mol^{-1} leads to instanton transfer rates of 220 fs and 2.7 ps for hydrogen and deuterium transfers, respectively, believed to be of the same order of the experimental measurements.

In this work we propose a quantum electronic study of the SA in both the ground (S_0) and first singlet excited (S_1) electronic states. Using the DFT (S_0) and TDDFT (S_1) methodologies we will locate all the stationary points (minima and transition-state structures) in both potential energy surfaces (PESs). Previous studies[36–42] of a myriad of ESIPT processes revealed that IC through CIs may play a key role in the whole photochemistry of these systems. For this reason, we will carefully look for and analyze the regions where CIs are likely expected. Our full (but static) electronic calculations will be completed by a comprehensive quantum dynamics study of the different processes that may take place in the excited S_1 state following vertical electronic excitation of the ground state enol tautomer. In particular we will carefully analyze the ESIPT dynamics and the competing relaxation channel from the enol tautomer in S_1 from the dynamical point of view.

II. METHOD OF CALCULATION

A. Electronic-structure calculations

Electronic DFT based methods have been used to explore the topology of the ground (S_0) and first (π, π^*) singlet excited (S_1) electronic states. DFT and TDDFT[43,44] optimizations have been performed for the S_0 and S_1 states, respectively. TDDFT has been successfully used to study other related ESIPT systems.[32,45,46] The three parameter hybrid functional of Becke with the correlation functional of Lee, Yang, and Parr[47,48] has been chosen. The TURBOMOLE program (version 5.4),[49,50] which implements analytical gradients at the TDDFT level,[49,51] has been used to perform the TDDFT calculations. In fact, TDDFT is known to always give very reliable results provided that the excited state is not of a charge-transfer type.[52–61] In that case TDDFT grossly underestimates the excitation energy (this fact coming from the unability of pure DFT methods to properly describe long range exchange effects). We have verified that in our system the photoactive state is not of a charge-transfer nature so that TDDFT should lead to decent results.

Multireference complete active space self-consistent field[62] (CASSCF) and CASSCF at the second-order perturbation theory[62] (CASPT2) calculations have been carried out with the MOLCAS program (Version 6.4).[63] These calculations have been carried out with an active space of ten electrons and ten molecular orbitals. The description of the nature of

the active space will be given in Sec. III when needed. We note that this active space is probably not large enough to correctly describe the whole PES but it has been used just to analyze the presence of CIs between the S_0 and S_1 states. A much larger active space would be necessary to compare the different regions of the PES.

An approximation to the geometry and energy of the CI has been obtained minimizing the energy of the S_1 state using TDDFT, while monitoring its excitation energy. The optimization was manually stopped when the excitation energy was smaller than 3 kcal mol^{-1}. Given the intrinsic multiconfigurational character of the CI region, it is not possible to carry out an exact localization of the minimum energy crossing point (MECP) using the TDDFT method. However, it has been recently proven that a monoconfigurational method may be used to roughly determine such points by searching for a geometry where the energy difference between the two implied states is fairly low.[64] Of course, such a procedure may lead to unphysical results so that it is compulsory to verify and refine the obtained results through the use of a multiconfigurational method. Then we have also localized CIs at the CASSCF level through minimization of the absolute value of the energy difference between the states that cross with the added condition that the energy of the state is the lowest possible that satisfies the first condition. Single point CASPT2 calculations at the final geometries were done to take into account dynamical correlations effects.

For all the DFT/TDDFT calculations, the 6-31G(d,p) (Refs. 65 and 66) basis has been used for the hydrogen and carbon atoms, while additional diffuse functions [6-31G+(d,p) basis][65,66] have been added to the oxygen and nitrogen atoms. For the CASSCF/CASPT2 calculations, the cc-pVDZ (Ref. 67) basis set has been employed for all the atoms.

B. Quantum dynamics calculations

The method chosen to determine the time scale of the processes in the excited state is wave packet propagation. In order to simulate the experimental setup an appropriate initial quantum state of the system is needed ($|\psi_0\rangle$), and is placed in the Franck–Condon region of the excited state, where its time evolution is followed and analyzed. Given that the ground vibrational state is the most populated in S_0 if thermal equilibrium is assumed, the photoexcitation process is simulated by selecting, as initial state, the ground vibrational state of the ground electronic state. This state is promoted to the Franck–Condon region of S_1 to simulate photoexcitation. However, $|\psi_0\rangle$ is not a stationary state of S_1 and to determine its time evolution, the time-dependent Schrödinger equation must be solved,

$$i\hbar \frac{d}{dt}|\psi(t)\rangle = \hat{H}|\psi(t)\rangle. \tag{1}$$

Because the Hamiltonian is time independent, this is equivalent to

$$|\psi(t)\rangle = e^{-i\hat{H}t/\hbar}|\psi_0\rangle, \tag{2}$$

where

$$\hat{H} = \hat{T} + \hat{V}^{S_1}(\mathbf{q}) \tag{3}$$

is the Hamiltonian (total energy) operator for the photoactive state, and $\mathbf{q}$ is a vector describing the coordinates upon which the PES is defined. As will be explained later, we have selected a unique collective isoinertial coordinate to describe the processes in the excited state. To solve Eq. (2) a standard split-time propagator scheme has been used.[68,69] The propagation proceeds by applying a split-operator propagator over a short-time interval Δt,

$$e^{-i\hat{H}t/\hbar} \approx e^{-i\hat{V}\Delta t/2\hbar} e^{-i\hat{T}\Delta t/\hbar} e^{-i\hat{V}\Delta t/2\hbar}. \tag{4}$$

So, during each time step the potential energy propagator is initially applied for half a time step, it is followed by the kinetic energy propagator for a full time step, and finally, the potential energy propagator is applied again for the remaining half a time step. The split-operator scheme has to be applied in small time steps because the kinetic and potential energy operators do not commute.

Fast-Fourier transform (FFT) was employed to transform the wave packet from position to momentum representations and vice versa in between any two time propagators in Eq. (4). The size of the FFT grid was of $2^9=512$ points and the time step used was of 1 atu (1 atu=2.419×10^{-17} s). The quality of the simulations was monitored by measuring the norm of $|\psi\rangle$, which was preserved to within 0.5%. The eigenvalues and eigenvectors of the S_0 Hamiltonian have been obtained through diagonalization of its matrix representation in an appropriate basis. The generic discrete variable representation (DVR) method proposed some time ago by Colbert and Miller was used to this end.[70]

III. RESULTS AND DISCUSSION

As in Sec. II we will divide the main results section into two parts: the first devoted to analyze the purely electronic-structure calculations and the second one where the previous electronic results are used to perform nuclear dynamics simulations of the ESIPT process using the methodology outlined in Sec. II.

A. Electronic-structure calculations

As explained in Sec. I, the only previous *ab initio* work was published by Zgierski and Grabowska[33] using the Hartree–Fock method in the ground electronic state (S_0) and the CISs method in the first singlet excited electronic state (S_1). Energies in S_1 were recalculated performing TDDFT single-point calculation at the CIS optimized geometries. For that reason our first task in this paper has been the recalculation of the relevant geometries using DFT in S_0 and the corresponding TDDFT method in S_1 also optimizing the geometries. The stationary points in the S_0 state have been localized by full minimization and characterized at the DFT level of calculation, while only the zeroth-order stationary points in the S_1 state have been directly located at the TDDFT level. At present, to characterize stationary points in the TDDFT scheme, numerical second derivatives must be computed (due to the unavailability of analytic second derivatives), which is a fairly expensive calculation. Instead,

TABLE I. DFT ground state relative energies (REs) referred to the C_1 enol form, torsional frequencies (ω_T) of the planar (C_S) and nonplanar (C_1) forms of the SA, and frequencies corresponding to the reaction coordinate for the proton transfer process (ω_R). For the C_1 structures the value of the torsional angle around the N_1–C_6 bond (see Scheme 1 for atom numbering) is also presented.

Structure	RE (kcal mol^{-1})	(ω_T) (cm^{-1})	ω_R (cm^{-1})	Torsional angle (deg)
enol, C_S	0.75	47i	⋯	⋯
cis-keto, C_S	4.95	12i	⋯	⋯
trans-keto, C_S	15.94	6i	⋯	⋯
TS (enol→*cis*-keto), C_S [a]	6.03	36i	1029i	⋯
enol, C_1	0.00	42	⋯	36
cis-keto, C_1	4.96	27	⋯	16
trans-keto, C_1	15.96	22	⋯	13
TS (enol→*cis*-keto), C_1	5.92	27	986i	22

[a]Within the C_s symmetry, this corresponds to a second-order saddle point.

a relaxed potential energy profile for the proton transfer has been computed using as a reaction coordinate the distance between the O_1–H_1 bond (see Scheme 1 for atom numbering).

The DFT calculations for the planar structures of SA in S_0 predict the enol form to be more stable, with the *cis*-keto form being 4.20 kcal mol^{-1} higher in energy. As expected, the enol-keto tautomerization leads to a large rearrangement of bond lengths of the phenolic (keto) ring, reflecting a loss of aromaticity upon proton transfer. The *trans*-keto form, in which the hydrogen bond is broken, lies, as expected, higher in energy than the *cis*-keto, 15.19 kcal mol^{-1} above the enol form. However, the true enol and keto minima are nonplanar structures in the ground electronic state. The transition state for the proton transfer process has also been located. Table I shows the relative potential energies (referred to the enol form) and the calculated torsional frequencies of all optimized C_S and C_1 SA tautomers and the transition-state structure for the proton transfer process.

According to these results, the stable ground state geometries are achieved by twisting the anilino ring by 36°, 16°, and 13° for the enol, *cis*-keto, and *trans*-keto tautomers, respectively. This out-of-plane distortion hardly affects any bond lengths and, as seen in Table I, brings an energy gain of less than 1 kcal mol^{-1} in all three cases, therefore the relative stability between the three tautomers is not altered when C_S symmetry is broken. All these results agree with those previously published by Zgierski and Grabowska.[33]

As mentioned in Sec. I, the experimental absorption spectrum has a band with a maximum at 344 nm (Ref. 14) (3.60 eV). We have theoretically evaluated this energy by single energy point calculation from the nonplanar enol minimum in S_0 at the TDDFT level of theory. The calculated vertical excitation energy is 3.66 eV (339 nm), which is in reasonable agreement with the experimental value. In fact, it is now well known that the TDDFT (Ref. 44) level provides a very good description for the excitation energy of valence-excited (π,π^*) states.[71] Also the transient absorption band of the nonplanar *trans*-keto structure, assumed to be transient
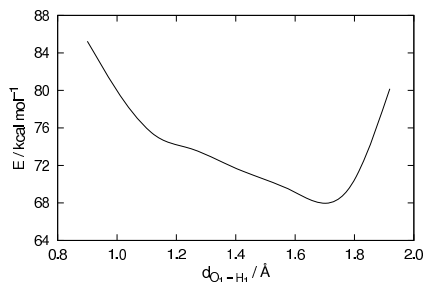

FIG. 1. TDDFT proton transfer reaction profile relaxed along the O_1–H_1 distance for the first (π,π^*) singlet excited electronic state. The energy origin is the energy of the DFT-optimized enol form in S_0.

species, is calculated at 439 nm, whereas the experimental value is 474 nm.[29]

To verify the goodness of the TDDFT description of the enol and *trans*-keto tautomers in the excited state, single-point CASSCF/CASPT2 calculations have been performed on the DFT nonplanar enol and *trans*-keto minima. As mentioned in Sec. II, an active space of ten electrons and ten orbitals has been used to this end. This active space includes the four highest a'' and the highest a' molecular orbitals as occupied orbitals, and the four lowest a'' and the lowest a' molecular orbitals as unoccupied orbitals. In this way, excitation wavelengths of 342 and 445 nm have been obtained at the CASPT2 level of theory for the enol and *trans*-keto tautomers, respectively. These results validate the active space chosen and also provide support to the TDDFT results.

The TDDFT exploration of the S_1 state is quite different when compared to the DFT results obtained in S_0, and with the corresponding CIS results published by Zgierski and Grabowska.[33] All the attempts to locate a TDDFT minimum in the enol region reverted to the *cis*-keto tautomer. This suggests a barrierless ESIPT process, which involves the absence of a transition-state structure. A set of relaxed reaction coordinate calculations was carried out varying the O_1–H_1 distance and allowing the rest of the geometry to relax and attain minimum energy. The reaction profile obtained, depicted in Fig. 1, confirms that the ESIPT is indeed barrierless at this level of theory. A similar result was obtained for the closely related salicylidene methylamine molecule (SMA),[32] where the nitrogen atom has a methyl substituent instead of a phenyl group. In contrast to what was observed in S_0, the *cis*-keto does not present a more stable structure when twisting the aniline ring, and only exists as a minimum when confined to remain in C_S. In addition to this, the *trans*-keto tautomer only presents an energy minima with a slight twisting not of the aniline but of the phenyl ring by 14°.

The present discussion on the topological features of the S_0 and S_1 electronic states of SA (a barrierless ESIPT process) would point toward an ultrafast time scale of the proton transfer process, implying a ballistic motion of the transferred proton. In a previous work[32] we have described a similar mechanism for a simplified model of the SA, the SMA molecule. However, it has been reported in several
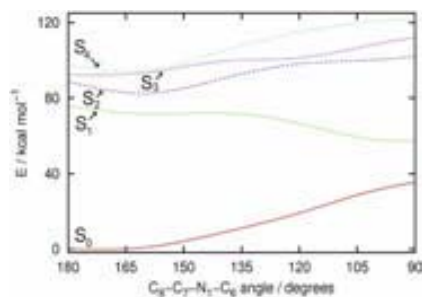
FIG. 2. (Color online) S_0-relaxed DFT potential energy profile along the $C_8-C_7-N_1-C_6$ dihedral angle. Energy origin is the energy of the S_0 minimum energy planar enol. TDDFT energies for the excited states represent vertical transitions from the S_0-relaxed geometries.

works[19–21,25,30] that different photochromic processes may occur before and after the ESIPT process in SA, and fast depopulations of the enol and *cis*-keto tautomers in the S_1 state have been experimentally detected. As no evidences of such processes for SMA have been reported experimentally, a simple ballistic motion mechanism might not be suitable for SA. In that context, in order to get more insight on the photochemistry of SA, a major point of interest is the likely presence of other competitive processes. The experimental work of Okabe *et al.*[30] pointed to the presence of two ICs. According to Fig. 7 in Ref. 30, the first IC (IC1) would take place from the excited (π, π^*) enol to a (n, π^*) state, and ulterior nonradiative decay to S_0. The process of depopulation of the excited (π, π^*) enol due to IC lies under 500 fs. The second IC (IC2) would occur just after the ESIPT process, from the excited (π, π^*) *cis*-keto again to a (n, π^*) state that would later revert to a vibrationally hot *trans*-keto tautomer in S_0 within a larger time scale ($\sim$2 ps).

According to the theoretical study of Zgierski and Grabowska,[33] the excited (π, π^*) planar unstable enol conformer can undergo IC to a highly nonplanar (n, π^*) state through rotation along the C_7-N_1 bond. In this conformation, intramolecular proton transfer is virtually impossible, and thus it would decay to S_0. Figure 2 depicts a ground electronic state relaxed TDDFT potential energy profile along the rotation of the C_7-N_1 bond of the enol form, showing the energy of the electronic ground state and the energy of the four lowest singlet excited states. At the initial planar structure, the lowest (n, π^*) state corresponds to the third excited singlet state (S_3), which lies $\sim$15.0 kcal mol^{-1} above the Franck–Condon excitation point, and thus it is energetically unreachable. At 20°, there is a crossing between the S_3 (n, π^*) and a S_4 (π, π^*) state, where the nature of both states is exchanged. The lowest (n, π^*) state remains the fourth excited state along the rest of the energy profile and does not cross with the S_1 state, which is always pure (π, π^*). However, at largely twisted angles ($\sim$80°–90°) an approach between the S_0 and S_1 states is observed with an energy difference of less than 20.0 kcal mol^{-1} at the final 90° calculation. In light of this not too large energy gap between these states, we considered the possibility of the

existence of a CI corresponding to a twisted conformation of the enol form, which would be the reason behind the internal conversion mechanism IC1.

As explained in Sec. II, the area of the CI has been approximately located by minimizing the energy of the S_1 state, and monitoring its excitation TDDFT energy, until the excitation energy fell under 3 kcal mol^{-1}. From this calculation arises a point with an energy difference between both states of 2.67 kcal mol^{-1}. The lowest energy of the quasidegenerate pair raises 51.62 kcal mol^{-1} above the S_0 enol minimum. The geometry of this point is characterized by a $C_8-C_7-N_1-C_6$ torsional angle of 92° and a C_7-N_1 bond distance of 1.37 Å.

Additionally, we carried out the CASSCF/CASPT2 search of a MECP between the S_0 and S_1 states in the region of the twisted enol tautomer, obtaining a point with an energy difference between both states less than 0.2 kcal mol^{-1}. Now, the energy of this point with respect to the S_0 enol minimum at the CASSCF/CASPT2 level is 48.03 kcal mol^{-1}. The geometry of this point is quite similar to the one obtained at the TDDFT level, with a $C_8-C_7-N_1-C_6$ torsional angle of 91° and a C_7-N_1 bond distance of 1.36 Å. The marked similarity of the TDDFT and CASSCF/CASPT2 results in the CI region further validates the TDDFT method to analyze the whole PES. A similar result has been previously stated in a related photochemical process.[72]

The transit through the CI just described might bring the system to S_0. Should the system achieve this with a change in the diabatic state, this would eventually lead—with increasing values of the $C_8-C_7-N_1-C_6$ torsional angle—to the enol minimum in S_0, closing the photocycle. However, the system could *also* remain in the same diabatic state. For the sake of completeness, we have explored this possibility and have located and characterized yet another minimum energy structure in S_0 at small $C_8-C_7-N_1-C_6$ torsional values (7.4°), in which the phenyl ring ($C_{13}-C_8-C_7-N_1$ torsional angle) is rotated 33.7° in order to avoid steric hindrances. This structure lies 15.15 kcal mol^{-1} above the C_S enol structure.

The second IC in SA (IC2) is proposed to occur in the S_1 (π, π^*) state of the planar *cis*-keto tautomer, just after the ESIPT process. As hinted by the *ab initio* calculations of Zgierski and Grabowska,[33] the lowest (n, π^*) state of the planar *cis*-keto form lies higher in energy than the S_1 (π, π^*) state, but it becomes significantly stabilized by a twist of the phenyl ring that becomes almost perpendicular to the aniline ring. Being this twisted conformation a favorable one to initiate the *cis-trans* isomerization process, the (n, π^*) state of the twisted *cis*-keto form represents an effective depopulation channel toward the *trans*-keto form. As mentioned before, our TDDFT calculations did not locate a stable C_1 *cis*-keto form when breaking the C_S symmetry, neither by the twisting of the aniline nor the phenyl rings. The planar S_1 (π, π^*) state of the *cis*-keto tautomer is unstable with respect to the rotation leading to the *cis-trans* isomerization. In order to give some explanation of the observed depopulation channel of the excited *cis*-keto form, we have proceeded in a

similar fashion as previously explained for the twisted enol conformation. In this way we have searched a second MECP between S_0 and S_1 in the region of the twisted *cis*-keto tautomer along the C_{13}–C_8–C_7–N_1 dihedral angle, which corresponds to the *cis-trans* isomerization process. We have found a TDDFT geometry, lying 56.64 kcal mol^{-1} above the S_0 enol minimum, with an energy difference between both states of 2.88 kcal mol^{-1}. This point presents a C_8–C_7–N_1–C_6 torsional angle of 90° and a C_7–N_1 bond distance of 1.46 Å. In turn, a CASSCF/CASPT2 CI geometry has also been found, lying 56.35 kcal mol^{-1} above the S_0 enol minimum, with an energy difference between both states less than 0.2 kcal mol^{-1}. This point presents a C_8–C_7–N_1–C_6 torsional angle of 89° and a C_7–N_1 bond distance of 1.47 Å.

This geometry corresponds to a twisting angle half way on the *cis-trans* isomerization process. The presence of a CI between S_0 and S_1 in the twisted *cis*-keto region may have an important role in the depopulation of the excited *cis*-keto form through internal conversion IC2, and is also consistent with the absence of a C_1 *cis*-keto energy minimum in S_1 as explained before. A complete list of the Cartesian coordinates of all the relevant geometries analyzed here (minima, transition states and CIs) is supplied as a supplemental material.[73]

B. Molecular dynamics calculations

Experimental data available on the photodynamics of SA include experimental estimates for the duration of the ESIPT process, as well as for some IC process starting right after photoexcitation and depleting also the enol species in the excited state—a competitive process of the former. Thus, the ESIPT process has been measured to occur faster than 750 fs by Otsubo *et al.*,[25] and more recent measurements by Ziółek *et al.*[29] and Rodríguez-Córdoba *et al.*[31] brought this limit down to 50 fs (at the experimental resolution limit). The electronic-structure study presented in Sec. III A provided a reasonable picture upon which to interpret the experimental findings, and indeed, a clear candidate to the IC process described by Okabe *et al.*[30] (IC1) in the form of a CI connecting the ground and photoactive states in the enol region. It would be useful to provide also a reasonable theoretical estimate of the decay times of the excited enol form to compare to experiment. This we will do in this section by employing a simple but sufficient model based on quantum dynamics, using wave packet propagation as dynamical tool.

For any kind of dynamical study it is a prerequisite to obtain a detailed knowledge of the forces acting on the atoms, in this case the PESs of the electronic states involved. The processes leading to the disappearance of the enol form, namely, the ESIPT and the IC processes, are multidimensional in nature (i.e., they involve motion of more than one atom, or more precisely, more than a single coordinate is needed to describe them: for the proton transfer at least the proton position and the distance between donor and acceptor atoms must be accounted for, while IC1 includes at the very least the torsion along the C_8–C_7–N_1–C_6 dihedral angle). Besides, the ESIPT and IC processes just described occur

competitively as they start off the same reactant so that they ought to be considered at the same time. At present, building an analytical representation of the PESs of the ground and photoactive states simultaneously, that is sufficiently detailed and includes all relevant degrees of freedom, is still a daunting task and modeling is needed. To this end, let us analyze the topographical features found so far for the ESIPT and IC1 processes, to tailor a reasonable methodology to study the dynamics of the system. The ESIPT process has been described as ultrafast ($\tau_{ESIPT} < 50$ fs) and, as seen in Sec. III A (see Fig. 1), takes place along a purely downhill potential energy profile which lacks a saddle point, and results in a potential energy loss of about 8 kcal mol^{-1}. It seems reasonable to assume that this process will involve essentially the motion of the proton, with maybe a certain degree of motion of the donor and acceptor atoms, while the rest of the molecule remains approximately static for times substantially longer than those required for the products of the ESIPT to form. As for IC1, experimental data available also describe it as very fast. According to Ref. 30 the whole decaying process lasts 3.3 ps, whereas the time needed to reach the CI region of the PES is estimated to be within 500 fs. The results presented in Sec. III A reveal that this process involves a CI between S_0 and S_1. The potential energy profile on S_1 on the surroundings of the Franck–Condon point (see Fig. 2) suggests a steep downhill monotonous potential energy profile, much more pronounced in fact than that of the ESIPT. Besides, motion along this potential energy profile must be almost purely the torsion of the C_8–C_7–N_1–C_6 dihedral angle from 180° to about 90° until the CI region is reached. Thus, it is reasonable that this motion should be very fast, except for the pronounced inertial effect due to the large mass of the atoms involved (because almost all atoms move).

Thus, the potential energy profiles found in Sec. III A agree, in principle, with the experimental observations regarding the decay times of the enol species in the photoactive state. It is nevertheless true that both processes occur at the same time after photoexcitation and should to be considered simultaneously. Interference between both processes could take on two different shapes: effects on the branching ratio between both reaction channels after photoexcitation and effects caused in a given channel due to interference from density coming from the other reaction channel once the wave packet has reached the latter channel's end and has been reflected. However, because (1) both are energetically strictly downhill processes, (2) both have been described as very fast, and most important (3) experimental data are obtained from the decay of the photoexcited enol form of SA (the Franck–Condon species), we think it is reasonable to study both processes separately, obtaining the rate at which the population of photoexcited enol species disappears through each process without considering the presence of the other. Of course, by proceeding in this way a reasonable estimate can be obtained for the decay times, τ_{ESIPT} and τ_{IC}, but not on the branching ratio among both competitive processes.
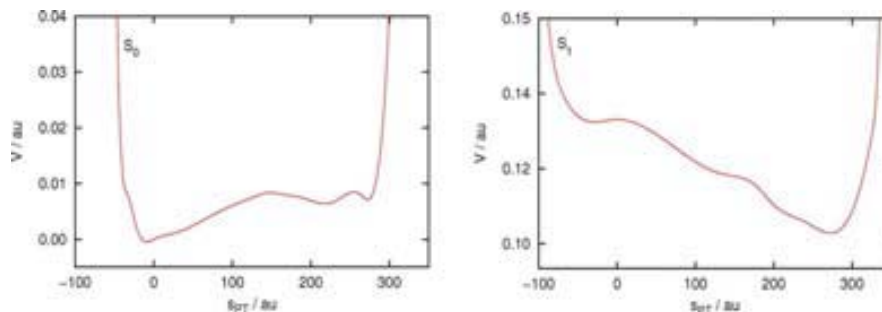
FIG. 3. (Color online) DFT and TDDFT relaxed potential energy profiles for the proton transfer in S_0 (left) and S_1 (right), respectively. Potential energy values in the y-axis are referred to the energy of the C_S cis-enol minimum in S_0 and shown in atomic units. The abscissa values correspond to arc-length distances in isoinertial coordinates of any given structure to that of the C_S cis-enol minimum in S_0 (for the ground state, left) and to that of the C_S Franck–Condon structure in S_1 (right).

1. Dynamical study of the ESIPT process

The ESIPT process described herein so far for SA is very similar to that studied recently by us occurring in 1-hydroxy-2-acetonaphtone.[74] In the present case not even a small potential energy barrier exists on the photoactive electronic state between enol and cis-keto forms. Accordingly we feel justified in using the same dynamical approach, which we summarize here. In essence, a monodimensional (1D) approach has been used to represent appropriately the main characteristics of the ESIPT process. First, relaxed potential energy profiles have been built for S_0 and S_1 using restrained energy minimizations at different values of the O–H distance and covering the full range of distances going from reactants to products of the proton transfer. Next, the distance in an isoinertial coordinate s_{PT} (for "proton transfer") between any two consecutive geometries in this profile has been calculated, assigning the value $s_{PT}=0$ to the geometries of the points, where the O–H distances match that of the potential energy minimum in S_0 (1.0 Å). The rest of the geometries are assigned s_{PT} values that represent the isoinertial arc-length distance in configurational space from that geometry to the minimum of potential energy (in S_0) or to the Franck–Condon structure (in S_1). Because of the nature of the process, most of the changes in the values of s_{PT} along this profile are originated by displacement of the proton, but due to the fact that the geometries have been computed using constrained optimization of all parameters except the O–H distance, all atoms have moved and thus their contribution is contained in the variation of s_{PT}. We have used this approach to represent processes dynamically in a simplified way before with success.[74–78] Figure 3 displays the relaxed potential energy profiles describing the proton transfer in the ground electronic and photoactive states as a function of the isoinertial coordinate s_{PT}. As defined, values of s_{PT} close to zero represent structures very similar to the reactant species, whereas large positive values of s_{PT} identify structures close to products (i.e., cis-keto structures).

Having defined a set of potential energy profiles and a single coordinate value to represent the extent of the ESIPT process, quantum dynamics on this potential energy profile is possible. As explained in Sec. II, an initial state is needed to start the integration of the time-dependent Schrödinger equation, Eq. (1). This initial state, as mentioned, is obtained through diagonalization of the matrix representation of the Hamiltonian of S_0 (in atomic units),

$$\hat{H}^{S_0} = -\frac{1}{2}\frac{d^2}{ds_{PT}^2} + V^{S_0}(s_{PT}), \tag{5}$$

to yield the ground vibrational state as a function of the ESIPT coordinate s_{PT}. Notice that the mass is missing from the kinetic energy term, as it is included in the definition of the isoinertial coordinate s_{PT}. Given that in our approach we study now only the ESIPT process, the s_{PT} coordinate represents only geometrical transformations in the process enol to cis-keto, the ground vibrational state describes mainly motion of the proton relative to the donor and acceptor atoms and has accordingly no information about the IC process. Thus, we label this initial state as $|\psi_0(s_{PT})\rangle$. The photoexcitation process is simply simulated by promoting $|\psi_0(s_{PT})\rangle$ to S_1. This is possible and meaningful because the choice for $s_{PT}=0$ is the same for both electronic states, even though for values of s_{PT} far from zero, it is also true that both 1D paths could visit areas of configurational space that could be increasingly diverging, as s_{PT} departs from zero. $|\psi_0(s_{PT})\rangle$ is an eigenstate of the ground electronic state Hamiltonian, but not of the excited state Hamiltonian, where its time evolution is obtained solving Eq. (2) using the FFT. The excited state dynamics has been followed for 1 ps.

We are interested in the decay time along this reaction channel. Experimentally, the fluorescence response signal obtained for the enol form has been fitted to a multiexponential function, usually of the form

$$I = \sum_i A_i e^{-t/\tau_i}, \tag{6}$$

where τ_i is the decay time of reaction (or deactivation) channel i, and A_i provide information on the branching ratio for each reaction (or deactivation) channel. As such, τ_{ESIPT} represents the time needed to cause a decrease of signal to $1/e$ of its initial value, through activity of the ESIPT channel. The autocorrelation function $\langle \psi(0)|\psi(t)\rangle$ can be used to this end, as it represents the overlap of the wave packet at any
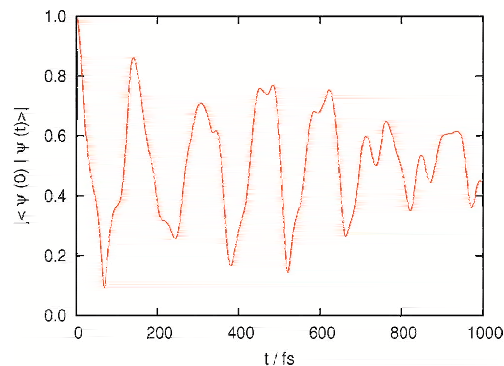
FIG. 4. (Color online) Modulus of the autocorrelation function represented as a function of time for the dynamical simulation of the ESIPT in S_1.

FIG. 5. (Color online) DFT and TDDFT relaxed potential energy profiles for the torsion of the C_8–C_7–N_1–C_6 dihedral angle in S_0 (solid lines) and S_1 (dashed lines), respectively. Potential energy values in the *y*-axis are referred to the energy of the C_S enol minimum in S_0 and shown in atomic units. The abscissa values correspond to isoinertial arc-length distance of any given structure to that of the C_S cis-enol minimum in S_0 (left) and C_S Franck–Condon structure in S_1 (right).

time with itself at $t=0$. Thus, according for instance to Sakurai,[79] the autocorrelation function (also known as correlation amplitude) provides a quantitative measure of the "resemblance" between the state kets at different times. When the modulus of the autocorrelation function goes to 1, this means that the wave packet is physically in the same region of space where it was originally and approximately with the same shape, whereas when the modulus of the autocorrelation function goes to zero, it means that the wave packet *has moved away* from its starting point. The modulus of the autocorrelation function is depicted in Fig. 4.

The analysis of the autocorrelation function in Fig. 4 reveals a certain periodic behavior in which the function goes through maxima—representing partial regeneration of the initial wave packet—every 150 fs approximately. Finally, the value of t at which the autocorrelation function goes down to $1/e$ is 49.6 fs, which can be accepted as our estimate for τ_{ESIPT}, in good agreement with experimental data available. This value is similar to values theoretically proposed for barrierless[32] or almost barrierless[74] ESIPT processes.

Before continuing to the next dynamical aspect of the complete process, it is necessary to remark that the pronounced periodicity observed in Fig. 4 would not likely be found experimentally to the same extent. At large t values the actual system would have seen other degrees of freedom (i.e., vibrations) activated because they must be coupled to the proton motion. Thus, the energy content of the degrees of freedom that have been activated would increase, obtaining their energy from the proton motion, in our case represented by the s_{PT} coordinate. In actuality one should expect these recurrences to die out much faster than in our simulation and the system to finally stabilize after some time in the products' (*cis*-keto) region, that is, regions with large s_{PT}.

2. Dynamical study of the IC1 process

Finally, we turn our attention to determining, on theoretical grounds, an estimate of the time it takes to depopulate of photoexcited wave packet the Franck–Condon area of S_1 toward the IC1 channel region. The potential energy landscape
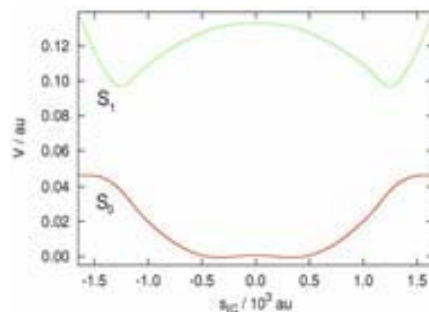
for the IC1 process in the enol area of S_1 shows a very steep downhill profile, and as seen in Fig. 2 it is the torsion C_8–C_7–N_1–C_6 that is the main geometrical parameter involved in such energy decrease. Given that this torsion is the main character in the IC1 channel, it seems reasonable to approximate this process again with a 1D process as done in the ESIPT case. Hence, we have now built another relaxed potential energy profile for S_0 and S_1 using constrained energy minimizations at different values of the C_8–C_7–N_1–C_6 dihedral angle, covering all values from 180° (meaning planar structure) to values of about 90°, where the CI is found. Because of the symmetry of the molecule, the potential must be symmetrical with respect to the dihedral value of 180°, and has been replicated manually. As before, the isoinertial arc-length distance has been computed, assigning the zero value to the C_S enol structure. At this point, we highlight that this isoinertial coordinate represents an entirely different path in configurational space than s_{PT} did in the dynamical study of the ESIPT above, and to emphasize this, we choose to name it differently (s_{IC1}, for IC1). As before, the s_{IC1} value at a point in the path reflects the displacements of all atoms along the IC1 channel, that is to say, the amount of geometrical distortion experienced upon twisting of the C_8–C_7–N_1–C_6 dihedral angle. The potential energy profiles obtained are depicted in Fig. 5 and deserve some analysis.

The abscissa values in Fig. 5 are sensibly larger than those in Fig. 3. This is the natural consequence of the isoinertial character of the s_{PT} and s_{IC1} coordinates, and that in the IC channel what actually happens is a substantial amount of heavy atom motion. Another relevant point to highlight is the presence of a tiny maximum at $s_{IC1}=0$ in the electronic ground state. Actually, $s_{IC1}=0$ corresponds to the structure with the smallest energy that lies completely in a plane, and as mentioned in Sec. III A of this paper, such structure is not a minimum, but a transition-state structure. The system can see its potential energy slightly lowered (by -0.75 kcal mol^{-1}) upon twisting of the N_1–C_6 bond, which is permitted in this profile.
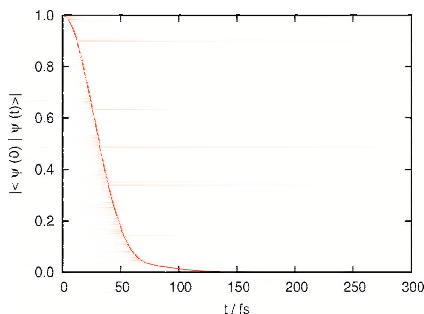
FIG. 6. (Color online) Modulus of the autocorrelation function represented as a function of time for the dynamical simulation of the torsion of the $C_8-C_7-N_1-C_6$ dihedral angle in S_1.
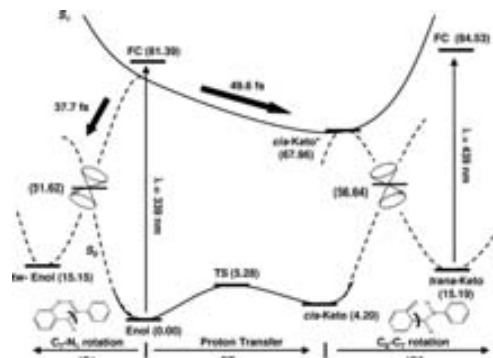

FIG. 7. Model for the photochemistry of SA as inferred from the electronic structure and dynamical results obtained in this work. DFT (S_0) and TDDFT (S_1) energies (in kcal mol^{-1}) are referred to the C_S enol in S_0. Solid lines represent reaction paths that maintain the planar (C_S) symmetry whereas out-of-plane reaction paths are indicated by dashed lines. A double cone symbol is posted on the regions of the CIs between S_0 and S_1. The arrows at the foot of the figure indicate the processes that occur along the paths. The times corresponding to the ESIPT process and the competing relaxation channel from the enol tautomer in S_1 are also depicted. For atom numbering, see Scheme 1.

Yet the point deserving more attention is the S_1 potential energy profile. A clear strongly downhill trend is seen around $s_{IC1}=0$ and it is likely that this repulsive component is going to determine the short-time dynamics in this channel. However, Fig. 5 shows clearly that this decrease turns into a sudden energy increase for values $|s_{IC1}| \geq 1.20 \times 10^3$ a.u.. At these values of s the $C_8-C_7-N_1-C_6$ dihedral angle is bent close to 90° so this section of the graph represents points neighboring the CI. Note that as we are optimizing the two electronic states separately, we are not truly arriving at the CI point so that now there is a relatively large energy difference between both states at the CI region of $\sim$30 kcal mol^{-1}. In the S_1 profile of Fig. 5, points with $s_{IC1}>1.20 \times 10^3$ a.u. and $s_{IC1}<-1.20 \times 10^3$ a.u. are *on a different diabatic state* than those with -1.20×10^3 a.u.$<s_{IC1}<1.20 \times 10^3$ a.u. Definitely, a comprehensive dynamical treatment of this nonadiabatic system should be done through diabatization of the S_0 and S_1 adiabats and quantification of the couplings between the diabats. Then, an outcome of the simulation would be also the time evolution of the ground and excited state populations. However, we have no experimental data regarding this latter issue; we are rather interested in knowing *how long it takes for the wavepacket to leave the Franck–Condon area in S_1*, for this is the magnitude measured by τ_{IC}. Given the repulsive nature of the S_1 potential energy curve, we assume that when the wave packet reaches the neighborhood of the CI—which is where the dynamics would turn inaccurate—it would be long gone from the Franck–Condon area. Hence, a dynamical simulation on the sector of the S_1 adiabat that is comprised between $|s_{IC1}| \leq 1.20 \times 10^3$ a.u. should provide a reasonable estimate of τ_{IC1}.

The simulation is carried out analogously as in the ESIPT case, determining first the ground vibrational state of S_0 in terms of the IC1 isoinertial coordinate s_{IC1}, and then employing the FFT approach to integrate the time-dependent Schrödinger equation. In this case, the simulation has only been integrated until $t=300$ fs. Figure 6 shows the modulus of the autocorrelation function for the dynamics in S_1. As mentioned before, the autocorrelation function provides a quantitative measure of the resemblance between the state kets at different times.[79] It is surprising how quickly the autocorrelation function goes to zero—actually faster than for

the ESIPT process—even though there is heavy atom motion to a much larger extent. This must be a consequence of the marked downhill character of the S_1 potential energy profile. Trying to establish a value for τ_{IC1} based on the time it takes to the modulus of the autocorrelation function to drop to $1/e$ of its value at $t=0$ yields a theoretical estimate of 37.7 fs for τ_{IC1}, well below the experimental estimate.

Finally, we want to clarify why a dynamical simulation of the IC2 process has not been undertaken. While it is true that enough data have been obtained to enable a 1D dynamical approach of quality analogous to that of the IC1 process, it is nonetheless true that an initial state for the dynamical study of the second IC process cannot be obtained so easily. Experimentally, the second IC starts off where the ESIPT ends. Our ESIPT simulation is reasonable and thus we have such a final state for $|\psi_{ESIPT}\rangle$ but one needs to remember that this state is projected onto s_{PT}, that is, a 1D path that contains mainly $O-H \cdots N$ motion and no displacements along $C_{13}-C_8-C_7-N_1$. Thus, if we name the path for the second IC s_{IC2}, one can say that s_{IC2} and s_{PT} are orthonormal. Thus $\Psi(s_{PT})$ has no information at any time on the density along the second IC channel and cannot be used as starting state for the dynamics. To obtain an estimate of τ_{IC2} one should do dynamics on, at least, a two-dimensional surface which simultaneously represented the energy landscape along s_{IC2} and s_{PT}, which lies beyond the scope of this work.

IV. CONCLUSIONS

Finally, we are able to discuss the expected photochemistry of SA. To do so we have devised a "full picture" of the energy variations along the different molecular motions that will likely play a role. Figure 7 depicts such a picture in a very schematic way. As the real photochemistry of SA involves the participation of reaction coordinates of different

nature, we have used in Fig. 7 solid lines for the reaction paths that maintain the planar symmetry (i.e., the ESIPT) and dashed lines for the out-of-plane reaction paths.

Radiation of suitable energy (339 nm according to our best calculations) places the enol tautomer in the first singlet excited electronic state S_1. After electronic excitation, the molecule is no longer a minimum energy structure but is in a very unstable conformation that may relax to an energy minimum. However, according to our TDDFT calculations, such an energy minimum in the enol region does not exist in S_1, and thus the photoexcited enol molecules may evolve rapidly. The evolution of the system in S_1 may occur through two different channels: ESIPT and IC1.

An ESIPT process may happen to form the excited *cis*-keto* tautomer. Due to the ultrafast nature of the process, thinking that the proton transfer process will take place in the C_S symmetry is a reasonable approximation. However, the planar *cis*-keto* tautomer is not a stable structure in S_1 and may undergo out-of-plane torsions to gain some energy stability. This ESIPT has been simulated too occur within 49.6 fs. Later, the torsion that leads to the *cis-trans* isomerization process (through the C_8–C_7 bond, process IC2) is connected to a CI between S_0 and S_1. At this point, the *cis*-keto* molecules may deactivate to S_0 to form either the *trans*-keto as the final photoproduct or the *cis*-keto minimum where, due to the very low reverse proton transfer energy barrier, would form again the enol tautomer, closing the photochemical cycle and allowing a new photoactivation to start again the process.

A second deactivation path, which is competitive with the ESIPT, is open for the enol* molecules (IC1). By a twisting around the C_7–N_1 bond up to a point where the proton transfer process is virtually impossible, a second CI between S_0 and S_1 is reached. The quantum dynamical simulation of the deactivation channel IC1 revealed a decay time of 37.7 fs to leave the excited enol* region. Transit through this CI will bring the system to S_0, either by staying in the same diabatic state (bringing the system to the enol minimum in S_0, closing the photocycle) or by changing the diabatic state. In the latter case a stable minimum corresponding to a strongly twisted enol (indicated as tw-enol in Fig. 7) conformation lying 15.15 kcal mol^{-1} above the C_S enol structure in S_0 would be assumed.

ACKNOWLEDGMENTS

[1] H. Bouas-Laurent and H. Dürr, Pure Appl. Chem. **73**, 639 (2001).
[2] R. Exelby and R. Grinter, Chem. Rev. (Washington, D.C.) **65**, 247 (1965).
[3] A. Senier and F. G. Shepheard, J. Chem. Soc. **95**, 1943 (1909).
[4] *Photochromism*, edited by G. H. Brown (Wiley Interscience, New York, 1971).
[5] S. Kawamura, T. Tsutsui, S. Saito, Y. Murao, and K. Kina, J. Am. Chem.
Soc. **110**, 509 (1988).
[6] *Photochromism: Molecules and Systems*, edited by H. Dürr and H. Bouas-Laurent (Elsevier, Amsterdam, 1990).
[7] P. F. Barbara, L. E. Brus, and P. M. Rentzepis, J. Am. Chem. Soc. **102**, 5631 (1980).
[8] P. T. Chou, Y. C. Chen, W. S. Yu, Y. H. Chou, C. Y. Wei, and Y. M. Cheng, J. Phys. Chem. A **105**, 1731 (2001).
[9] E. T. J. Nibbering and T. Elsaesser, Chem. Rev. (Washington, D.C.) **104**, 1887 (2004) (and references therein).
[10] Phys. Chem. Chem. Phys. **102**, 289 (1998), special issue on *Hydrogen Transfer: Experiment and Theory*.
[11] M. D. Cohen, G. M. Schmidt, and S. J. Flavian, J. Chem. Soc. 2041 (1964).
[12] T. Sekikawa, T. Kobayashi, and T. Inabe, J. Phys. Chem. A **101**, 644 (1997).
[13] T. Rosenfeld, M. Ottolenghi, and A. Y. Meyer, Mol. Photochem. **5**, 39 (1973).
[14] P. F. Barbara, P. M. Rentzepis, and L. E. Brus, J. Am. Chem. Soc. **102**, 2786 (1980).
[15] K. Kownacki, L. Kaczmarek, and A. Grabowska, Chem. Phys. Lett. **210**, 373 (1993).
[16] K. Kownacki, A. Mordzinski, R. Wilbrandt, and A. Grabowska, Chem. Phys. Lett. **227**, 270 (1994).
[17] A. Grabowska and K. Kownacki, Acta Phys. Pol. A **88**, 1081 (1995).
[18] M. I. Knyazhansky, A. V. Metelitsa, A. Ya. Bushkov, and S. M. Aldoshin, J. Photochem. Photobiol., A **97**, 121 (1996).
[19] S. Mitra and N. Tamai, Chem. Phys. Lett. **282**, 391 (1998).
[20] S. Mitra and N. Tamai, Chem. Phys. **246**, 463 (1999).
[21] S. Mitra and N. Tamai, Phys. Chem. Chem. Phys. **5**, 4647 (2003).
[22] K. Ogawa, J. Harada, T. Fujiwara, and S. Yoshida, J. Phys. Chem. A **105**, 3425 (2001).
[23] V. Vargas and L. Amigo, J. Chem. Soc., Perkin Trans. 2 **2001**, 1124.
[24] M. I. Knyazhansky, A. V. Metelitsa, M. E. Kletskii, A. A. Millov, and S. O. Besugliy, J. Mol. Struct. **526**, 65 (2000).
[25] N. Otsubo, Ch. Okabe, H. Mori, K. Sakota, K. Amimoto, T. Kawato, and H. Sekiya, J. Photochem. Photobiol., A **154**, 33 (2002).
[26] V. Vargas, J. Phys. Chem. A **108**, 281 (2004).
[27] M. E. Kletskii, A. A. Millov, A. V. Metelitsa, and M. Knyazhansky, J. Photochem. Photobiol., A **110**, 267 (1997).
[28] M. Ziółek, J. Kubicki, A. Maciejewski, R. Naskręcki, and A. Grabowska, Chem. Phys. Lett. **369**, 80 (2003).
[29] M. Ziółek, J. Kubicki, A. Maciejewski, R. Naskręcki, and A. Grabowska, Phys. Chem. Chem. Phys. **6**, 4682 (2004).
[30] Ch. Okabe, T. Nakabayashi, Y. Inokuchi, N. Nishi, and H. Sekiya, J. Chem. Phys. **121**, 9436 (2004).
[31] W. Rodríguez-Córdoba, J. S. Zugazagoitia, E. Collado-Fregoso, and J. Peon, J. Phys. Chem. A **111**, 6241 (2007).
[32] J. M. Ortiz-Sánchez, R. Gelabert, M. Moreno, and J. M. Lluch, J. Phys. Chem. A **110**, 4649 (2006).
[33] M. Z. Zgierski and A. Grabowska, J. Chem. Phys. **112**, 6329 (2000).
[34] W. Siebrand, Z. Smedarchina, M. Z. Zgierski, and A. Fernández-Ramos, Int. Rev. Phys. Chem. **18**, 5 (1999).
[35] O. Vendrell, M. Moreno, and J. M. Lluch, J. Chem. Phys. **117**, 7525 (2002).
[36] M. J. Paterson, M. A. Robb, L. Blancafort, and A. D. DeBellis, J. Am. Chem. Soc. **126**, 2912 (2004).
[37] A. L. Sobolewski, W. Domcke, and C. Hättig, J. Phys. Chem. A **110**, 6301 (2006).
[38] A. L. Sobolewski and W. Domcke, Phys. Chem. Chem. Phys. **8**, 3410 (2006).
[39] J. D. Coe, B. G. Levine, and T. J. Martinez, J. Phys. Chem. A **111**, 11302 (2007).
[40] A. L. Sobolewski and W. Domcke, J. Phys. Chem. A **111**, 11725 (2007).
[41] Y. Nosenko, G. Wiosna-Sałyga, M. Kunitski, I. Petkova, A. Singh, W. J. Buma, R. P. Thummel, B. Brutschy, and J. Waluk, Angew. Chem., Int. Ed. **47**, 6037 (2008).
[42] A. Migani, L. Blancafort, M. A. Robb, and A. D. DeBellis, J. Am. Chem. Soc. **130**, 6932 (2008).
[43] R. Bauernschmitt and R. Ahlrichs, Chem. Phys. Lett. **256**, 454 (1996).
[44] A. Dreuw and M. Head-Gordon, Chem. Rev. (Washington, D.C.) **105**, 4009 (2005).
[45] A. L. Sobolewski and W. Domcke, Phys. Chem. Chem. Phys. **1**, 3065 (1999).
[46] A. J. A. Aquino, H. Lischka, and C. Hattig, J. Phys. Chem. A **109**, 3201

(2005).

[47] A. D. Becke, J. Chem. Phys. **98**, 5648 (1993).

[48] C. T. Lee, W. T. Yang, and R. G. Parr, Phys. Rev. B **37**, 785 (1988).

[49] F. Furche and R. Ahlrichs, J. Chem. Phys. **117**, 7433 (2002).

[50] R. Ahlrichs, M. Bär, M. Haser, H. Horn, and C. Kolmel, Chem. Phys. Lett. **162**, 165 (1989).

[51] C. Van Caillie and R. D. Amos, Chem. Phys. Lett. **317**, 159 (2000).

[52] L. Serrano-Andrés and M. Merchán, J. Mol. Struct.: THEOCHEM **729**, 99 (2005).

[53] R. Gelabert, M. Moreno, and J. M. Lluch, J. Phys. Chem. A **110**, 1145 (2006).

[54] M. J. G. Peach, P. Benfield, T. Helgaker, and D. Tozer, J. Chem. Phys. **128**, 044118 (2008).

[55] M.-S. Liao, Y. Lu, and S. Scheiner, J. Comput. Chem. **24**, 623 (2003).

[56] A. L. Sobolewski and W. Domcke, Chem. Phys. **294**, 73 (2003).

[57] A. Dreuw and M. Head Gordon, J. Am. Chem. Soc. **126**, 4007 (2004).

[58] S. Anand and H. B. Schegel, Mol. Phys. **104**, 933 (2006).

[59] E. Fabiano, F. Della Sala, G. Barbarella, S. Lattante, M. Ani, G. Sotgiu, C. Hättig, R. Cingolani, and G. Gigli, J. Phys. Chem. B **110**, 18651 (2006).

[60] E. Perpete, J. Preat, J.-M. Andre, and D. Jacquemin, J. Phys. Chem. A **110**, 5629 (2006).

[61] X. Xu, Z. Cao, and Q. Zhang, J. Phys. Chem. A **110**, 1740 (2006).

[62] K. Andersson, P.-Å. Malmqvist, and B. O. Roos, J. Chem. Phys. **96**, 1218 (1992).

[63] K. Andersson, M. Barysz, A. Bernhardsson, M. R. A. Blomberg, Y. Carissan, D. L. Cooper, M. P. Fülscher, L. Gagliardi, C. de Graaf, B. A.

Hess *et al.*, *Molcas, Version 6.2* (Lund University, Sweden, 2000).

[64] K. Sadeghian and M. Schütz, J. Am. Chem. Soc. **129**, 4068 (2007).

[65] P. C. Hariharan and J. A. Pople, Theor. Chim. Acta **28**, 213 (1973).

[66] M. M. Francl, W. J. Pietro, W. J. Hehre, J. S. Binkley, M. S. Gordon, D. J. Defrees, and J. A. Pople, J. Chem. Phys. **77**, 3654 (1982).

[67] T. H. Dunning, Jr., J. Chem. Phys. **90**, 1007 (1989).

[68] M. D. Feit and J. A. Steiger, J. Comput. Phys. **47**, 412 (1982).

[69] R. Kosloff, J. Phys. Chem. **92**, 2087 (1988).

[70] D. T. Colbert and W. H. Miller, J. Chem. Phys. **96**, 1982 (1992).

[71] M. Dierksen and S. Grimme, J. Phys. Chem. A **108**, 10225 (2004).

[72] S. Fantacci, A. Migani, and M. Olivucci, J. Phys. Chem. A **108**, 1208 (2004).

[73] See EPAPS document No. E-JCPSA6-129-004847 for a full list of the Cartesian coordinates of all the relevant points localized along both the ground and first singlet excited electronic states using the method of calculation described in Sec. II A. For more information on EPAPS, see http://www.aip.org/pubservs/epaps.html.

[74] J. M. Ortiz-Sánchez, R. Gelabert, M. Moreno, and J. M. Lluch, J. Chem. Phys. **127**, 084318 (2007).

[75] R. Gelabert, M. Moreno, J. M. Lluch, A. Lledós, V. Pons, and D. M. Heinekey, J. Am. Chem. Soc. **126**, 8813 (2004).

[76] R. Gelabert, M. Moreno, J. M. Lluch, and A. Lledós, Organometallics **16**, 3805 (1997).

[77] M. Garcia-Viloca, R. Gelabert, A. González-Lafont, M. Moreno, and J. M. Lluch, J. Phys. Chem. A **101**, 8727 (1997).

[78] M. Garcia-Viloca, R. Gelabert, A. González-Lafont, M. Moreno, and J. M. Lluch, J. Am. Chem. Soc. **120**, 10203 (1998).

[79] J. J. Sakurai, in *Modern Quantum Mechanics*, revised ed., edited by S. F. Tuan (Addison-Wesley, New York, 1994).